Central nervous system melanoma metastasis.
Experimental studies on pathogenesis, diagnosis and therapy.

een wetenschappelijke proeve op het gebied van de
Medische Wetenschappen

Proefschrift

ter verkrijging van de graad van doctor aan de Radboud Universiteit Nijmegen,
op gezag van de Rector Magnificus prof. dr. C.W.P.M. Blom,
volgens besluit van het college van Decanen in het openbaar te verdedigen op
maandag 10 april 2006 des namiddags om 13.30 uur precies

door

Benno Küsters

geboren op 29 oktober 1970 te Dülmen (Duitsland)

Promotor:
Prof. dr. D.J. Ruiter

Co-promotores:
Dr. R.M.W. de Waal
Dr. P. Wesseling

Manuscript commissie:
Prof. dr. G. J. Adema
Prof. dr. W. J. Oyen
Dr. J. M. Kros (Erasmus Medical Center, Rotterdam)

The research described in this thesis was financially supported by the AGIKO-fellowships for B. Küsters from the NWO (Netherlands Organisation for Scientific Research; grant number NWO 920-03-149) and from the Dutch Cancer Society (grant number KUN 2001-2399).

ISBN-10: 90-9020389-3
ISBN-13: 978-90-9020389-8

für meine Eltern

voor Heidi

Contents

Chapter 1

Introduction

Cancer is still one of the most frequent causes of morbidity and mortality in Western countries. Although today part of the cancer patients may be cured using novel therapeutics (chemotherapy etc.), in many cases, except for hematological malignancies, surgical resection of the primary tumor still remains the main option. Once a tumor has disseminated to other organs, in the majority of the cases it is impossible to cure the patient. In such cases, chemotherapy and radiotherapy are frequently used as additional therapeutic regimens. Animal models have been of utmost importance for gaining insight into the biology of tumor growth and metastasis: the patho-physiological steps of tumor growth and metastasis can be studied under defined laboratory conditions, which is for ethical reasons impossible in human beings[1]. The experimental setting also allows the development of new therapies and diagnostic tools. Although many theories and hypotheses on the mechanisms of tumor growth and dissemination are up to now based on tumor models [2], it is important to realize that such models are not necessarily valid for the different malignancies. Nevertheless, such models do offer the possibility to elucidate processes that are incompletely understood.

In this thesis, studies on human melanoma cell lines in nude mouse xenograft models and mechanisms of development and growth of metastases are described with a focus on tumor angiogenesis. In these studies, preclinical data on diagnostic (radiological) and therapeutical (anti-angiogenic) interventions are presented and discussed. As melanoma is a highly malignant type of cancer, it is easy to transplant it in animals. Although the characteristics of only one type of malignancy are described here, many of the results and conclusions may also be extrapolated to other types of malignancies in patients, because these characteristics described are frequently mirrored in human tumor material.

Human melanoma

Melanoma is known as one of the most aggressive tumors in humans. The tumor originates from melanocytes that are derived from the neural crest. Although most melanomas arise in the skin, they may also arise in mucosal surfaces or at other sites to which neural crest cells have migrated. The incidence of melanoma has been steadily increasing over the past years, making it a serious problem for healthcare systems in several countries, e.g. Australia, Canada and the USA (www.cancer.gov).

Fortunately, most melanomas are detected early and are excised as thin lesions. At this stage the probability of tumor dissemination is low. Most patients with a thin melanoma are therefore cured by excision of the lesion with an adequate tumor-free margin[3,4].
A more serious oncological problem are larger sized (thick) melanoma lesions: these tumors tend to spread via lymphogenous and hematogenous routes. The chances of curing such a patient are low.
Frequent sites of distant metastasis are the lungs, the liver and the brain; moreover, it is the distant metastases that are fatal for the patients. The high affinity of melanoma to metastasize to the central nervous system (CNS) may be due to its neuroectodermal origin: the micro-environmental conditions in the brain harbouring (a cocktail of) CNS-specific growth factors may facilitate the growth of melanoma cells[5].

Central nervous system metastasis

The incidence of CNS metastasis in patients with melanoma ranges from 10% to 40% in clinical studies, while in autopsy series CNS involvement was identified in up to two thirds of the patients with metastatic melanoma[6]. This means that among cancer patients with advanced (disseminated) disease, melanoma patients have a high-risk for developing CNS metastasis[7].
This site of metastasis is life threatening for the patient. In a large series with more than 700 melanoma patients with brain metastases, the median overall survival was 3.8 months[7,8].
Brain metastases in general are difficult to treat[6] because of anatomical and physiological reasons: surgical excision is often limited to solitary lesions at locations that allow surgical intervention and do not involve vital areas of the brain. Radiation dose is limited because of vulnerability of the CNS for irradiation. Chemotherapy efficiency is limited as melanoma is relatively insensitive to cytotoxic agents. Furthermore, the blood-brain barrier may prevent adequate delivery of some of the cytotoxic agents to the brain parenchyma.
The CNS consists of parenchyma with neuronal and glial cells, and a delicate branched network of brain microvessels is present that is characterized by a specific vascular-astrocytic functional unit, representing the blood-brain barrier. The CNS is surrounded by the meninges (pachymeninx (dura mater) and leptomeninges). In cancer patients metastases occur both in the meninges and the brain parenchyma.

Angiogenesis

Angiogenesis is the formation of a neovascular bed in physiological (e.g. embryogenesis, menstrual cycle) and pathological conditions[9] (e.g. wound healing). Angiogenesis is now for more than two decades a major focus of interest in the field of oncology. Judah Folkman postulated that growth of a tumor beyond a certain size (1-2 mm^3) depends on the formation of new blood vessels. Such vessels facilitate the supply of oxygen and nutritients to the tumor[10]. This hypothesis seems straight forward, as healthy normal tissue also depends on a vasculature, which is the result of physiological angiogenesis during organogenesis[11]. Therefore, the hypothesis of Folkman provided a dogmatic view for the scientists working in the field of tumor angiogenesis.

To date there is abundant data that angiogenesis occurs in human tumors[12,13]. Studies in animal models have shown that tumor-induced angiogenesis is essential for tumor growth, as inhibition of angiogenesis resulted in diminished tumor growth rates in such models[12-15].

Physiological angiogenesis is a tightly regulated multistep process. Only tumors that have the repertoire to induce the full program of angiogensis will be vascularized by functional, mature vessels. The most prominent and most potent angiogenic factor is vascular endothelial growth factor (VEGF)[16]. This factor is also known as vascular permeability factor (VPF) [17] because of its potency to induce vascular leakage. It is a secreted protein and occurs as different isoforms. The human isoforms described to date consist of 121, 144, 165, 189 and 206 amino acids[18]; three well characterized murine counterparts lack one amino acid resulting in sequences of 120, 164, 188 amino acids[19]. VEGF acts via VEGF-receptors: VEGFR1, VEGFR2 and VEGFR3. Among these, VEGFR2 plays a crucial role in the induction of angiogenesis, whereas the role of VEGFR1 and VEGFR3 in the process of angiogenesis is not fully clear yet [20]. VEGFR3 is thought to be involved in lymphangiogenesis[21]. Besides these VEGF receptors, there are co-receptors that bind to VEGF and may enhance VEGF signalling. Neuropilin-1 is such a co-receptor[22]. The different VEGF-isoforms were found to have a different impact in vascular patterning in physiological and tumor angiogenesis because of a different capacity to induce co-signalling via such associated receptors[23].

Metastasis

Tumor dissemination in cancer patients usually results (sooner or later) in death of these patients. The current concept of tumor growth and dissemination may be briefly described as follows: a tumor grows to a macroscopically relevant size. The induction of angiogenesis is

crucial for this growth. During this process, tumor cells may gain the capacity to migrate and penetrate blood- and lymph vessels. Such tumor cells may reach distant organs or lymph nodes via the blood stream or lymphatic drainage and can develop into larger metastatic lesions if they again succeed to induce angiogenesis.

This cascade is thought to represent a micro-evolutionary process in which tumor cells are selected by acquiring the capacity to induce angiogenesis, to migrate and invade vessels, to adhere in vessels of distant organs and to develop there into metastases[2,24-26]. In Darwinian terms: survival of the most malignant species with optimal fitness to perform the different steps just mentioned. In this context, different tumor subclones may preferentially metastasize to different organs because of varying microenvironmental conditions. Examples of such microenvironmental factors are the presence of certain adhesion molecules in the local vasculature and parenchyma, and the presence of local growth factors at these sites. This idea is in fact based on the 'seed and soil' hypothesis described by Paget more than 100 years ago[27]. More recently, Fidler and co-workers substantially contributed to the unravelling of these mechanisms and promoted Paget's hypothesis[26].

It is generally accepted that increased angiogenesis correlates with an increased metastatic potential[15]. Theoretically angiogenesis facilitates different *pro-metastatic* conditions in the process of dissemination:

- increase in the tumor mass, enhancing the probability of a spontaneously developed tumor subclone that is able to leave the tumor via (blood) vessel invasion.
- increase in the vessel density, resulting in a higher chance that migratory tumor cells encounter and invade vessels and leave the tumor.

Furthermore, a disseminated tumor cell with an angiogenic phenotype has a higher probability to develop into a larger, clinically relevant metastasis.

Animal models

Animal models were essential for developing the above-mentioned theories on angiogenesis and metastasis. They allowed investigation of the influence of defined factors on tumor biology and behavior. A major part of oncological research is performed in mice and rats. Mice are especially suitable and used for several reasons: they are small, highly reproductive animals with extensively characterized different strains (the 'Drosophila' for oncological research). Furthermore, mice are easy to handle, they are less expensive than rats, and their housing is easy as well.

Tumor animal models can be divided into syngenic and xenogenic models. In syngenic models, tumors are studied that develop from the animal tissue itself because of exogenous (e.g. radiation, etc.) or endogenous (e.g. tumor oncogene mutation) influence in the animal. Another syngenic model is the transplantation of a tumor cell line derived from the animal strain studied. Xenograft models, on the other hand, are models in which tumor cells from a different species are introduced into animals (e.g. human tumor cells into mice).
Based on the site of tumor growth in animals the models can be classified orthotopic versus heterotopic. For example human astrocytic brain tumors studied in the mouse brain parenchyma are orthotopic models. However, heterotopic brain tumor models in which astrocytic tumor cells are inoculated into the subcutaneous space in mice are also used.
The relevance of data from animal experiments for the understanding of the tumor biology depends on the exact model that is used. The micro-environmental circumstances between subcutaneous space and brain parenchyma are very different.
For simulation of metastasis, there are also different model types:
- direct tumor cell inoculation into the organ of interest (e.g. transcranial (through skin and skull) inoculation of tumor cells into the brain parenchyma).
- colonization models: tumor cells are inoculated into the blood stream proximal to the organ of interest (e.g. internal carotid artery injection to induce CNS metastasis).
- spontaneous metastasis: a primary (e.g. subcutaneous) tumor is inoculated into the animal and distant organs are examined for metastatic deposits after a period of tumor growth.
Again Fidler and co-workers did pioneering work on this aspect of basic oncology: they developed different orthotopic tumor models, closely mimicking the human situation[28] in order to prevent a situation that 'mice tell lies'.

Additional questions

The concepts of angiogenesis and metastasis mentioned above are clear, comprehensive and in line with the paradigm of evolution in all kind of processes in (medical) biology. However, these concepts may be somewhat oversimplified.

Angiogenesis:

Are all tumors really angiogenesis dependent? Astrocytic brain tumors, for example, are characterized by highly infiltrative growth[29]. Tumor cell infiltration is an essential criterion for neoplastic malignancy. There is a dilemma here: if malignant tumors infiltrate normal

healthy tissue, why is angiogenesis necessary? Are pre-existent vessels not enough to sustain tumor growth, especially in a highly vascularized organ as the brain?
The initially promising results of anti-angiogenic therapy in animal models could so far not be reproduced in human patient trials. What is the reason for the discrepancy between data from animal models and that from patient trials? How valid are the tested models, what are the limitations of extrapolating animal data to patients? Are there valid (diagnostic) parameters for detecting angiogenesis in mice and men?

Metastasis:
There is no clear-cut correlation between circulating single tumor cells and metastasis[30], showing that pure intravascular tumor load of single tumor cells is not the rate limiting factor in metastasis. Is metastasis always a phenomenon of survival of the fittest, i.e. a clonal selection at single cell level? Interestingly, in the experience of a pathologist tumor emboli, rather than single cells are frequently seen in the vasculature of the primary tumor and in the vessels at the site of metastases. Are multicellular tumor (tissue) fragments rather than single tumor cells involved in metastasis? If so, the pattern of metastasis of these fragments could be more dependent on anatomical/mechanical circumstances. What is exactly the contribution of mechanical conditions and what of 'biochemistry' (adhesion molecules etc.) to the site of metastasis?

General outline of the thesis:

This thesis describes different aspects of angiogenesis and metastasis in nude mice human melanoma xenograft models and deals with different unanswered questions, controversial hypotheses and translation of experimental data to the human situation.

In chapter 2 the development of a human melanoma metastasis xenograft model in nude mice brains (orthotopic colonization model) is described. Different patterns of metastasis to the CNS are encountered and the role of the $\alpha_v\beta_3$ integrin expression in tumor cells and the impact of tumor cell clusters versus single tumor cells in this process are investigated.

In chapter 3 a possible mechanism of metastatic growth of human melanoma in the model described in chapter 2 is presented: vascular co-option - no need for an angiogenic switch. The role of VEGF secretion in this situation is also demonstrated.

The clinical, especially diagnostic impact of the model described in chapter 3 is presented in chapter 4: growth patterns of metastases have direct consequences for their appearance in contrast-enhanced MRI. A new iron oxide based contrast agent is compared with gadolinium diethylenetriaminepenta-acetic acid (Gd-DTPA) and potential advantages of this agent are investigated.

The role of the three most frequent VEGF-isoforms in metastatic growth is described in chapter 5: differences in the morphology of tumor vascularization and their radiological consequences are presented.

Experimental anti-angiogenic therapy in the brain metastasis model is investigated in studies described in chapter 6: ZD 6474 is a small compound inhibiting the VEGF receptor-signalling pathway; therapeutical and radiological consequences of this treatment are presented.

In chapter 7 a new concept on spontaneous formation of metastasis is introduced. The colonization model described in chapters 2-6 is compared with the development of spontaneous metastasis from the subcutaneous space.

Finally, a summarizing discussion and future perspectives are presented in chapter 8.

References

1. Holland, E. C. Mouse models of human cancer as tools in drug development. Cancer Cell, *6*: 197-198, 2004.
2. Fidler, I. J. Critical determinants of cancer metastasis: rationale for therapy. Cancer Chemother.Pharmacol., *43 Suppl*: S3-10, 1999.
3. Ruiter, D. J., Spatz, A., van den Oord, J. J., and Cook, M. G. Pathologic staging of melanoma. Semin.Oncol., *29*: 370-381, 2002.

4. Ruiter, D. J. Clinical and pathologic diagnosis, staging and prognostic factors of melanoma and management of primary disease. Curr.Opin.Oncol., *4*: 357-367, 1992.
5. Nicolson, G. L. and Menter, D. G. Trophic factors and central nervous system metastasis. Cancer Metastasis Rev., *14*: 303-321, 1995.
6. Bafaloukos, D. and Gogas, H. The treatment of brain metastases in melanoma patients. Cancer Treat.Rev., *30*: 515-520, 2004.
7. Sampson, J. H., Carter, J. H., Jr., Friedman, A. H., and Seigler, H. F. Demographics, prognosis, and therapy in 702 patients with brain metastases from malignant melanoma. J.Neurosurg., *88*: 11-20, 1998.
8. Schouten, L. J., Rutten, J., Huveneers, H. A., and Twijnstra, A. Incidence of brain metastases in a cohort of patients with carcinoma of the breast, colon, kidney, and lung and melanoma. Cancer, *94*: 2698-2705, 2002.
9. Risau, W. Mechanisms of angiogenesis. Nature, *386*: 671-674, 1997.
10. Folkman, J. What is the evidence that tumors are angiogenesis dependent? J.Natl.Cancer Inst., *82*: 4-6, 1990.
11. Denekamp, J. The tumour microcirculation as a target in cancer therapy: a clearer perspective. Eur.J.Clin.Invest, *29*: 733-736, 1999.
12. Thorpe, P. E. Vascular targeting agents as cancer therapeutics. Clin.Cancer Res., *10*: 415-427, 2004.
13. Cao, Y. Antiangiogenic cancer therapy. Semin.Cancer Biol., *14*: 139-145, 2004.
14. Feron, O. Targeting the tumor vascular compartment to improve conventional cancer therapy. Trends Pharmacol.Sci., *25*: 536-542, 2004.
15. Ellis, L. M. and Fidler, I. J. Angiogenesis and metastasis. Eur.J.Cancer, *32A*: 2451-2460, 1996.
16. Ferrara, N. Timeline: VEGF and the quest for tumour angiogenesis factors. Nat.Rev.Cancer, *2*: 795-803, 2002.
17. Dvorak, H. F. Vascular permeability factor/vascular endothelial growth factor: a critical cytokine in tumor angiogenesis and a potential target for diagnosis and therapy. J.Clin.Oncol., *20*: 4368-4380, 2002.
18. Robinson, C. J. and Stringer, S. E. The splice variants of vascular endothelial growth factor (VEGF) and their receptors. J.Cell Sci., *114*: 853-865, 2001.
19. Carmeliet, P., Ng, Y. S., Nuyens, D., Theilmeier, G., Brusselmans, K., Cornelissen, I., Ehler, E., Kakkar, V. V., Stalmans, I., Mattot, V., Perriard, J. C., Dewerchin, M., Flameng, W., Nagy, A., Lupu, F., Moons, L., Collen, D., D'Amore, P. A., and Shima, D. T. Impaired myocardial angiogenesis and ischemic cardiomyopathy in mice lacking the vascular endothelial growth factor isoforms VEGF164 and VEGF188. Nat.Med., *5*: 495-502, 1999.
20. Claesson-Welsh, L. Signal transduction by vascular endothelial growth factor receptors. Biochem.Soc.Trans., *31*: 20-24, 2003.

21. Clarijs, R., Ruiter, D. J., and de Waal, R. M. Lymphangiogenesis in malignant tumours: Does it occur? J.Pathol., *193*: 143-146, 2001.
22. Neufeld, G., Cohen, T., Shraga, N., Lange, T., Kessler, O., and Herzog, Y. The neuropilins: multifunctional semaphorin and VEGF receptors that modulate axon guidance and angiogenesis. Trends Cardiovasc.Med., *12*: 13-19, 2002.
23. Grunstein, J., Masbad, J. J., Hickey, R., Giordano, F., and Johnson, R. S. Isoforms of vascular endothelial growth factor act in a coordinate fashion To recruit and expand tumor vasculature. Mol.Cell Biol., *20*: 7282-7291, 2000.
24. Gassmann, P., Enns, A., and Haier, J. Role of tumor cell adhesion and migration in organ-specific metastasis formation. Onkologie., *27*: 577-582, 2004.
25. Fidler, I. J. and Talmadge, J. E. Evidence that intravenously derived murine pulmonary melanoma metastases can originate from the expansion of a single tumor cell. Cancer Res., *46*: 5167-5171, 1986.
26. Fidler, I. J. The pathogenesis of cancer metastasis: the 'seed and soil' hypothesis revisited. Nat.Rev.Cancer, *3*: 453-458, 2003.
27. Paget, S. The distribution of secondary growths in cancer of the breast. *Lancet* **1**, 571-573 (1889).
28. Killion, J. J., Radinsky, R., and Fidler, I. J. Orthotopic models are necessary to predict therapy of transplantable tumors in mice. Cancer Metastasis Rev., *17*: 279-284, 1998.
29. Wesseling, P., Ruiter, D. J., and Burger, P. C. Angiogenesis in brain tumors; pathobiological and clinical aspects. J.Neurooncol., *32*: 253-265, 1997.
30. Vlems, F. A., Ruers, T. J., Punt, C. J., Wobbes, T., and van Muijen, G. N. Relevance of disseminated tumour cells in blood and bone marrow of patients with solid epithelial tumours in perspective. Eur.J.Surg.Oncol., *29*: 289-302, 2003.

Chapter 2

The pattern of metastasis of human melanoma to the central nervous system is not influenced by integrin $\alpha_v\beta_3$ expression

Benno Küsters
Johan R Westphal
Debby Smits
Dirk J Ruiter
Pieter Wesseling
Ulrich Keilholz
Robert M W de Waal

Int J Cancer 2001, 92:176-180

Abstract

We investigated the effect of integrin αvβ3 expression on the metastatic pattern of human melanoma cells in the central nervous system (CNS). For this purpose, we developed a hematogenous CNS melanoma metastasis model in nude mice using a modified internal carotid artery infusion technique. This protocol revealed 2 different patterns of CNS metastasis. The integrin αvβ3-expressing melanoma lines Mel57 and Zkr nearly exclusively produced metastases in the brain parenchyma, whereas cells of the BLM and MV3 lines, devoid of integrin αvβ3 expression, preferentially metastasized to dura mater and leptomeninges. Treatment with hyaluronidase to obtain single BLM cell suspensions did not influence the metastatic pattern, indicating that this was not simply the result of entrapment of tumor cell aggregates in large-sized leptomeningeal vessels. The role of integrin αvβ3 expression in the process of metastasis was tested by transfection of BLM, but did not lead to an altered pattern of metastasis. We did observe, however, slower growth of the transfected tumors, although the in vitro growth rate was unaltered, indicating a reduction in tumorigenicity. We conclude from our findings that CNS metastasis of melanoma cells in the mouse xenograft model occurs in at least 2 different but very reproducible patterns. Although it is predicted that adhesion of tumor cells to endothelial cells plays a role in this phenomenon, tumor cell integrin αvβ3 expression per se does not explain the difference in metastatic behavior in the CNS. We assume that other, as yet unknown factors, must be involved

Introduction

The capacity of tumors, including malignant melanoma, to form central nervous system metastases is an increasing problem in clinical oncology [1]. The special biology of the CNS blood-brain barrier (BBB), that is impermeable for a number of therapeutics, together with the vulnerability of the brain for irradiation and surgery, form main obstacles for treatment. Since it is unclear why some tumors preferentially metastasize to the CNS, investigation of the molecular mechanisms involved is needed. Various molecules may be involved, because different CNS compartments show differences in vascularity, extracellular matrix (ECM) composition [2], immune surveillance[3] and growth factor expression [4]. Interestingly, dura mater and leptomeninges contain almost the same ECM components as most peripheral organs and their vessels do not form a tight BBB. The ECM of the brain parenchyma on the other hand, is completely different from that found in the meninges [5] and other parts of the human body. Recently, it was proposed that integrins expressed on the tumor cell membrane play a dominant role in determining the site of metastasis [6-8]. In particular, the integrin αvβ3 was assumed to facilitate melanoma metastasis in general [9-14]. Besides mediating adhesion to ECM components [5-6], intercellular adhesion via this integrin between tumor cells and, e.g. capillary endothelial cells, may play a role as well [8,15-16].

To test whether integrin αvβ3 expression is involved in determining the metastatic behavior to the CNS, we developed a model of hematogenous metastasis formation in the CNS of nude mice by modification of a previously described internal carotid artery tumor cell injection technique [17]. We used melanoma cell lines with metastatic behavior in nude mice, and with differences in integrin αvβ3 expression [18-19].

Finally, we investigated whether the metastatic pattern of an integrin αvβ3-negative melanoma cell line was changed by introduction of expression of this molecule via gene transfection.

Materials and Methods

Mice

Specific pathogen-free (SPF) male, 6 to 8 weeks old BALB/c nu/nu mice weighing 18-25g were purchased from the central university animal facility. A maximum of 5 mice were housed per cage under SPF conditions (temperature 20-24°C; relative humidity 50-60%; 15 air changes per hour; light-dark periods 14hr/10hr). Water and food (RMH, Hope Farms, The Netherlands) were available to the animals ad libitum.

Cell lines

Melanoma cell lines included: Mel57 and Zkr, the latter derived from a melanoma brain metastasis (αvβ3 positive) and BLM(20) and MV3 [21], both lacking integrin αvβ3 expression (18-19). All cell lines were cultured in Dulbeccos Modified Eagles Medium (DMEM), supplemented with 10% fetal calf serum (FCS), streptomycin, penicillin and glutamate at 37°C. Cultures were free of Mycoplasmata.

Microsurgical injection procedure

For tumor cell injection cell cultures were trypsinized (trypsin 0.125%; EDTA 0.1% and glucose 0.1%) and cell suspensions were counted on a Coulter counter. Cells were washed and resuspended in phospate-buffered saline (PBS). For hyaluronidase treatment, cell suspensions were incubated with 10 U/ml enzyme (EC 3.2.1.35; Sigma, Zwijndrecht-The Netherlands) for 10 min at 20 °C. Cells were then washed, resuspended in PBS and counted again.

Mice were anaesthetised by neuroleptanalgesia consisting of fluanisone, fentanyl and midazolam via subcutaneous injection.

Animals were fixed on the operation table and the heads were stabilized by a band placed between the teeth of the upper jaw. The neck was prepared for surgery by alcohol desinfection, and the skin was cut by a medial incision. After blunt dissection the pretracheal muscles were exposed. The muscles at the right side were longitudinally separated. The exposed right common carotid artery including the carotidal bifurcation was separated from the vagal and hypoglossal nerves. Internal carotid, external carotid and occipital artery were exposed. A ligature of 7-0 silk suture was placed around the origin of the common carotid artery. A second ligature was placed proximal to the carotidal bifurcation but was not closed immediately. The blood flow between both ligatures was temporarily stopped by lifting the second ligature, and in this part the artery was nicked with a pair of microscissors. A polyethylene tube connected to a syringe containing the cell suspension was filled with 20-40l physiological salt solution to prevent tumor cell contamination. The tube was inserted into the common carotid artery and the second ligature was tightened around it to prohibit leakage to the operation field. After tube insertion both the external carotid and occipital artery were temporarily compressed with a forceps and 100µl of the tumor cell suspension was slowly injected into the open left internal carotid artery. The external carotid and occipital artery were kept closed for 15 sec after injection. To prevent tumor cell reflux into the external carotid and occipital artery and subsequent local tumor cell spread, a small amount of blood was aspirated from the internal carotid artery into the tube after the 15s interval. Then, the

tube was removed and the second ligature was closed permanently. The operation wound was rinsed three times with physiological salt solution to wash out a possible tumor cell contamination and the skin was closed by sutures.

Transfection with integrin 3 subunit

Full length cDNA for the integrin 3 subunit [22], provided by Dr. Ruoslahti (La Jolla, CA), was cloned into the polylinker of the mammalian expression vector pBJ1neo [23], provided by Dr. R. de Waal-Malefijt (La Jolla, CA). Twenty g of this construct was used for stable transfection of BLM cells via the calcium phosphate precipitation method [24], using the Calcium Phosphate Transfection System (Life Technologies, Breda, The Netherlands). After 48h of recovery, stably transfected cells were selected by culture in the presence of 1 mg/ml G418 (Life Technologies) for two weeks. Single cell sorting was done on an Epics Elite flow cytometer using the anti- αvβ3 mAb LM609 (see also below). Cells were cultured in medium containing 200mg/ml G418 and regularly monitored for αvβ3 expression. Expression levels of αvβ3 were determined by FACS analysis using LM609 mAb and were similar for Mel57 and BLM-3 (data not shown). BLM transfected with the empty vector pBJ1neo (BLM Neo) was used as control.

Histology

Mice were sacrificed in case of severe cachexia, acutely developing neurological deficits, or visible tumor masses. Brain, meninges and skull were inspected macroscopically using an operation microscope.

Material for immunohistochemistry was snap-frozen in liquid nitrogen. Lung, heart, kidney, spleen and other tissues were fixed in buffered formalin, and embedded in paraffin. After euthanasia some heads were perfused via the left carotid artery with buffered formalin, fixed, decalcified and paraffin-embedded. Sections of 4 m underwent standard H&E staining.

Immunohistochemistry (IHC)

Mouse anti-human αvβ3 integrin monoclonal antibody LM609 (Merck, Darmstadt, Germany)(25) was diluted in PBS with 1% BSA. Frozen 4 m sections were fixed in acetone for 10 min, dried and incubated at room temperature with mAb for 1 h. After washing with PBS, bound Ab was detected with a horse anti-mouse Ig Ab (Vector Laboratories, Burlingame, CA) in a dilution of 1/200 in PBS with 1% BSA for 30 min. After washing, the bound Abs were visualized using the peroxidase-based Vectastain elite ABC kit (Vector Laboratories, Burlingame, CA) using 3-amino-9-ethylcarbazole as a chromogen. Sections were counterstained with hematoxylin.

Results

Different metastatic patterns of human melanoma cell lines to the CNS

In initial experiments mice received injections with varying amounts of cells to determine the threshold of reproducible tumorigenicity. Data are shown in Table I.

Table I. Metastasis Formation by Human Melanoma Cell Lines in Mice After Internal Carotid Artery Injection

Cell line (injected cell number)	Survival time (days) range (median)	Incidence of metastasis			
		CNS (primary site)		Visceral	
		Parenchyma	Meninges	Lung	Heart
Me157 (0.5×10^5)	22-35 (29.5)	4/4	0/4	0/4	0/4
Me157 (1×10^5)	29-36 (30)	3/3	0/3	0/3	0/3
Me157 (2.5×10^5)	26-27 (26.5)	4/4	1/4	1/4	0/4
Me157 (5×10^5)	21-27 (25.5)	4/4	0/4	0/4	0/4
Zkr (2.5×10^5)	35-61 (48)	4/4	1/4	0/4	0/4
MV3 (2.5×10^5)	34 and 54	0/2[1]	1/2	0/2	0/2
MV3 (5×10^5)	27-38 (33)	0/3[1]	3/3	0/3	0/3
BLM (1×10^5)	23-25 (23)	0/3[1]	3/3	3/3	0/3
BLM (2.5×10^5)	18-30 (22)	0/6[1]	6/6	3/6	0/6
BLM hyaluronidase (2.5×10^5)	20-28 (21)	0/5[1]	5/5	3/5	1/5
BLM-β_3 (1×10^5)	33-48 (41)	0/7[1]	6/7	1/7	0/7
BLM-Neo (1×10^5)	29-35 (33)	0/5[1]	5/5	2/5	0/5

[1] Indicated is the primary site of CNS involvement. Secondary parenchymal involvement was frequently observed.

Clinical signs of tumor growth differed between the cell lines. In mice receiving BLM or MV3 cells, macroscopically visible destruction of skull bone by tumor, disconnection of skull sutures by elevated intracranial pressure and loss of general activity and focal neurological deficits were observed. Cachexia was a minor symptom. In contrast, clinical signs of tumor growth in Mel57 and to a lesser extent in Zkr carrying mice were severe cachexia, and sometimes focal neurological deficits like slight hemipalsy or hemiataxia. In general, cachexia was the reason for euthanasia of mice with Mel57 and Zkr metastases.

Metastases formed by either MV3 or BLM involved the meninges (dura mater (fig.1a) and leptomeninges (fig.1b), frequently followed by secondary brain parenchyma involvement by tumor cell invasion along the vessels via the Virchow-Robin space (fig.1c). In cases with extensive parenchymal involvement, we could not exclude primary involvement, but based on the findings in animals bearing less tumor mass, occurrence of secondary involvement of the parenchyma was beyond doubt. Occasionally, lesions were found in the ventricles of the brain.

In contrast, all animals injected with Mel57 and Zkr cells showed primary metastatic involvement of brain parenchyma (fig.1d and 1g). Micrometastases and somewhat larger lesions presented with an infiltrative rather than solid growth pattern, whereas bulky lesions often had a central aspect of solid tumor formation, although an invasive front into the brain parenchyma was always present. Mice injected with a smaller number of tumor cells developed cachexia only slightly later. Nevertheless, larger individual metastases were found more often in animals injected with a small number of tumor cells. Leptomeningeal and dural Mel57 and Zkr metastases occurred rarely and were of microscopic size. Mel57 and Zkr metastases in the pituitary gland, pineal gland and ganglion gasseri were occasionally observed, which was not seen with BLM or MV3 cells. To detect integrin αvβ3 expression in situ by IHC, murine anti-human αvβ3 Ab LM609 was used to highlight membranous staining of single Mel 57 and Zkr (αvβ3 positive) tumor cells in the parenchyma (fig. 1e and 1g). Normally, antibodies raised in mice can not be used for staining purposes, as the secondary anti-mouse antiserum will bind with host (mouse) immunoglobulins (Ig) that are omnipresent in mouse tissues. However, host Ig only poorly pass the BBB. Therefore, mouse Ig levels in brain parenchyma are extremely low, which allows for the use of anti-mouse secondary antibodies in immunostaining of mouse brain tissue. Vessel lumina, containing plasma Ig, were visible as small red spots.

In contrast to Mel57, ZKr and MV3, BLM frequently produced pulmonary metastases after internal carotid artery injection (Table I). However, these were of a negligible size compared to the CNS lesions.

Hyaluronidase treatment does not affect the metastatic behavior of BLM melanoma cells

Cell suspensions obtained by trypsin treatment of BLM and MV3 cells often contained large amounts of multicellular aggregates that may be associated with high hyaluronic acid production[26]. Since hyaluronic acid production levels are correlated with spontaneous metastasis in melanoma xenograft models, embolism of larger sized meningeal vessels causing inhibition of further transport to smaller sized parenchymal capillaries might explain the predominant meningeal involvement. To test this possibility, BLM cell suspensions were treated with hyaluronidase after trypsin treatment, resulting in a single cell suspension. No differences in metastatic pattern were observed between BLM cells with or without hyaluronidase treatment. Again, a predominant meningeal involvement was observed, eventually followed by secondary parenchymal invasion.

BLM-3 and BLM-Neo melanoma lines show metastatic behavior identical to BLM

To investigate the involvement of integrin αvβ3 in metastasis formation in BLM cells, we transfected BLM cells with 3 cDNA, resulting in surface expression of αvβ3 protein. These cells, or cells transfected with empty vector only (BLM-Neo), were injected into mice, and metastatic patterns in the CNS were analysed.

Both transfected cell lines involved the meninges (fig. 1f), but general examination of the H&E stained slides suggested that the extent of invasion into the parenchyma of the transfected cells was less than that of untransfected cells. Expression of the αvβ3 transgen in the metastatic lesions in vivo was shown by immunohistochemical analysis (fig. 1f). BLM-Neo injected mice developed signs of tumor growth earlier than the BLM-3 injected ones (Table I). In vitro growth rates, determined by BrdU uptake, were similar for BLM, BLM-3 and BLM-Neo (data not shown).

Fig.1:
a) Meningeal (dura mater) metastasis of BLM human melanoma cell line. T=tumor, P=brain parenchyma, S=skull. Original magnification x40. H&E staining.
b) Meningeal metastasis of MV3 human melanoma cells in the leptomeninges of the cerebellum. SG=stratum granulosum, T=tumor. Original magnification x100. H&E staining.
c) Leptomeningeal metastasis: BLM human melanoma cells invading the brain along the Virchow-Robin space. E=nucleus of vessel cell, T=tumor cell. Original magnification x250. H&E staining.
d) Parenchymally infiltrating brain metastasis of Mel57 human melanoma cell line. Original magnification x100. H&E staining.
e) Parenchymal brain metastasis of Mel57 human melanoma cell line. Immunohistochemical staining of the $\alpha_v\beta_3$ integrin with mAb LM609 on the cell membrane. Counterstaining: hematoxylin. Original magnification x100.
f) Leptomeningeal metastasis of BLMβ_3 human melanoma cell line in the cerebellum. Immunohistochemical staining of the transfected $\alpha_v\beta_3$ integrin with mAb LM609 on the cell membrane. Counterstaining: hematoxylin. Original magnification x250.
g) Parenchymal brain metastasis of Zkr human melanoma cell line. Immunohistochemical staining of the $\alpha_v\beta_3$ integrin with mAb LM609 on the cell membrane. Counterstaining: hematoxylin. Original magnification x250. See also colour display page 149.

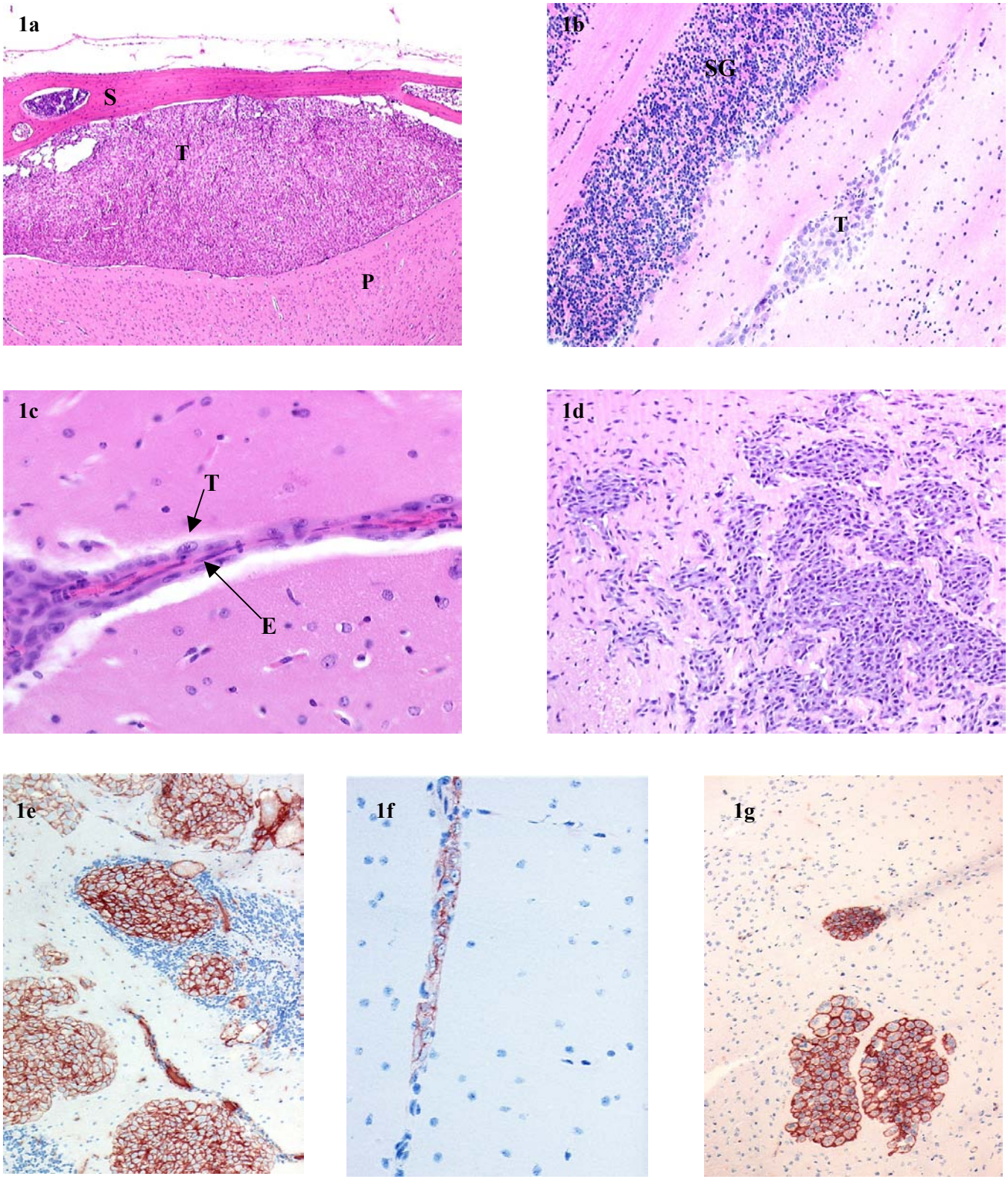

Figure 1

Discussion

Metastases of malignant melanoma to the CNS represent a complication of considerable relevance in clinical oncology. Reports on experimental data dealing with the pathobiological characteristics of this type of metastatic disease are scarce.

In this study we investigated the mechanisms involved in metastasis formation in the CNS in a human melanoma xenograft model. To parallel the patient situation, where melanoma metastasis formation to the CNS occurs exclusively via the hematogenous route, tumor cell application into the blood stream is a prerequisite. Internal carotid artery injection [17, 27-28] prevents the extensive visceral metastasis formation that is frequently observed in left cardiac ventricle injections [29]. In contrast to the human situation, the internal carotid artery (ACI) in rodents like mice and rats supplies the dura mater as well as brain parenchyma and leptomeninges [30-31]. This explains why in our model after ACI injection of tumor cells, metastases were found in all these compartments.

Interestingly, the different melanoma cell lines reproducibly metastasized to different compartments of the CNS. Similar results were described by Schackert et al. [32], who showed that human melanoma lines derived from non-CNS metastases predominantly produced meningeal involvement, whereas cell lines derived from brain metastases more frequently caused parenchymal metastases. The three cell lines used in the present study, Mel57, BLM and MV3, are all derived from non-CNS melanoma metastases. The reason for the observed differences in metastatic spread is not clear. Studies with radiolabeled tumor cells carried out by Schackert et al. showed that already the initial arrest of tumor cells was different among these cell lines. To exclude any effects of tumor cell embolism in large-sized leptomeningeal vessels by multicellular aggregates at the site of subsequent metastasis formation, we prepared single cell suspensions by hyaluronidase treatment. This treatment, however, had no effect on metastatic behavior, and, moreover, indicated that hyaluronic acid components on the cell surface are not directly involved in metastasis formation.

Several studies have described the role of cell adhesion molecules in melanoma progression [9, 33-35]. The acquirement of integrin αvβ3 expression is supposed to be an important step in melanoma progression, and has been described to be responsible for melanoma lymph node metastasis [12]. Integrin αvβ3 mediates adhesion of cells to various ECM molecules[5, 6, 25, 33, 36] via the RGD-amino acid sequence [5-6]. Although the function of integrin αvβ3 in cell-cell adhesion is not completely clear, it may be involved in tumor cell adhesion to endothelial cells and migration through vessel walls[8, 15].

Initially, it appeared that αvβ3 expression had a strong effect on the metastatic pattern in our model since the αvβ3 positive and αvβ3 negative cell lines metastasized towards completely different locations. Our transfection data, however, did not support a role for αvβ3 in this process, since induction of αvβ3 expression did not lead to a change in metastatic pattern. Possibly, Mel57 and Zkr on the one hand and BLM and MV3 on the other, express adhesion molecules other than integrin αvβ3 that interact with specific counterstructures present on parenchymal and meningeal vessels, respectively.

Both 3-transfected BLM cells as well as untransfected cells presented with meningeal involvement, but the results indicated a lower degree of tumorigenicity in comparison to the wild type BLM cells. The animals developed symptoms of tumor growth later, coinciding with a decreased intracranial tumor mass. Also, one out of 7 animals did not develop CNS metastasis at all, whereas the corresponding inoculum of wild type BLM cells was always tumorigenic, indicating a decrease in aggressiveness due to αvβ3 integrin expression. The in vitro growth was not affected by transfection. More likely, however, the lower tumorigenicity of the 3 -transfected line may be explained by disturbances of cellular functions by the transfected protein[35, 37-38] or the transfection procedure itself, since the empty vector-transfected BLM-Neo cell line was less aggressive as well.

Another experimental approach could have been masking of the αvβ3 integrin on Mel57 and Zkr cells, e.g. with help of an antibody like LM609, but this procedure may interfere with other cellular functions like induction of tumor cell apoptosis, and therefore, via other unrelated mechanisms, prevent metastasis to occur.

In summary, we postulate that selective receptors are present on brain capillary endothelium and/or tumor cells, which facilitate tumor cell adhesion and metastasis formation at restricted sites. Our results indicate that the metastatic pattern of human melanoma cells in our CNS metastasis model is not dependent on hyaluronic acid or integrin αvβ3 expression.

Acknowledgements

We thank A. van Kraats for expert technical assistance.

References

1. Mitchell MS. Relapse in the central nervous system in melanoma patients successfully treated with biomodulators. J clin Oncol 1989;7: 1701-9.
2. De-Clerck YA, Shimada H, Gonzalez GI, Raffel C. Tumoral invasion in the central nervous system. J Neurooncol 1993;18: 111-21.
3. Sobel RA. The extracellular matrix in multiple sclerosis lesions. J Neuropathol exp Neurol 1998;57: 205-17.
4. Weisenhorn DM, Roback J, Young AN, Wainer BH. Cellular aspects of trophic actions in the nervous system. Int Rev Cytol 1999;189: 177-265.
5. Ruoslahti E. Brain extracellular matrix. Glycobiology 1996;6: 489-92.
6. Ruoslahti E. RGD and other recognition sequences for integrins. Ann Rev cell Develop Biol 1996;12: 697-715.
7. Ruoslahti E. Integrin signaling and matrix assembly. Tumour Biol 1996;17: 117-24.
8. Tuszynski GP, Wang TN, Berger D. Adhesive proteins and the hematogenous spread of cancer. Acta Haematol 1997;97: 29-39.
9. Albelda SM, Mette SA, Elder DE, Stewart R, Damjanovich L, Herlyn M, et al. Integrin distribution in malignant melanoma: association of the beta 3 subunit with tumor progression. Cancer Res 1990;50: 6757-64.
10. Felding HB, Mueller BM, Romerdahl CA, Cheresh DA. 1992. Involvement of integrin alpha V gene expression in human melanoma tumorigenicity. J clin Invest 1992;89: 2018-22.
11. Gehlsen KR, Davis GE, Sriramarao P. Integrin expression in human melanoma cells with differing invasive and metastatic properties. Clin exp Metastasis 1992;10: 111-20.
12. Nip J, Shibata H, Loskutoff DJ, Cheresh DA, Brodt P. Human melanoma cells derived from lymphatic metastases use integrin alpha v beta 3 to adhere to lymph node vitronectin. J clin Invest 1992;90: 1406-13.
13. Nip J, Brodt P. The role of the integrin vitronectin receptor, alpha v beta 3 in melanoma metastasis. Cancer Metastasis Rev 1995;14: 241-52.
14. Petitclerc E, Stromblad S, Von-Schalscha TL, Mitjans F, Piulats J, Montgomery AM, et al. Integrin alpha(v)beta3 promotes M21 melanoma growth in human skin by regulating tumor cell survival. Cancer Res 1999;59: 2724-30.
15. Piali L, Hammel P, Uherek C, Bachmann F, Gisler RH, Dunon D, et al. CD31/PECAM-1 is a ligand for alpha v beta 3 integrin involved in adhesion of leukocytes to endothelium. J cell Biol 1995;130: 451-60.
16. Montgomery AM, Becker JC, Siu CH, Lemmon VP, Cheresh DA, Pancock JD, et al. Human neural cell adhesion molecule L1 and rat homologue NILE are ligands for integrin alpha v beta 3. J cell Biol 1996;132: 475-85.

17. Schackert G, Fidler IJ. Development of in vivo models for studies of brain metastasis. Int J Cancer 1988;41: 589-94.
18. Danen EH, Aota S, Van-Kraats AA, Yamada KM, Ruiter DJ, Van-Muijen GN. Requirement for the synergy site for cell adhesion to fibronectin depends on the activation state of integrin alpha 5 beta 1. J biol Chem 1995;270: 21612-8.
19. Danen EH, Jansen KF, Van-Kraats AA, Cornelissen IM, Ruiter DJ, Van-Muijen GN. Alpha v-integrins in human melanoma: gain of alpha v beta 3 and loss of alpha v beta 5 are related to tumor progression in situ but not to metastatic capacity of cell lines in nude mice (published erratum appears in Int J Cancer 1995 Jul 28;62(3):365). Int J Cancer 1995;61: 491-6.
20. Van-Muijen GN, Cornelissen LM, Jansen CF, Figdor CG, Johnson JP, Brocker EB, et al. Antigen expression of metastasizing and non-metastasizing human melanoma cells xenografted into nude mice. Clin exp Metastasis 1991;9: 259-72.
21. Van-Muijen GN, Jansen KF, Cornelissen IM, Smeets DF, Beck JL, Ruiter DJ. 1991. Establishment and characterization of a human melanoma cell line (MV3) which is highly metastatic in nude mice. Int J Cancer 1991;48: 85-91.
22. Van-Kuppevelt TH, Languino LR, Gailit JO, Suzuki S, Ruoslahti E. An alternative cytoplasmic domain of the integrin beta 3 subunit. Proc nat Acad Sci Wash 1989;86: 5415-8.
23. Lin AY, Devaux B, Green A, Sagerstrom C, Elliott JF, Davis MM. Expression of T cell antigen receptor heterodimers in a lipid-linked form. Science 1990;249: 677-9.
24. Wigler M, Silverstein S, Lee LS, Pellicer A, Cheng Y, Axel R. Transfer of purified herpes virus thymidine kinase gene to cultured mouse cells. Cell 1977;11: 223-32.
25. Cheresh DA, Spiro RC. Biosynthetic and functional properties of an Arg-Gly-Asp-directed receptor involved in human melanoma cell attachment to vitronectin, fibrinogen, and von Willebrand factor. J biol Chem 1987;262: 17703-11.
26. Van Muijen GN, Danen EH, Veerkamp JH, Ruiter DJ, Lesley J, Van Den Heuvel LP. Glycoconjugate profile and CD44 expression in human melanoma cell lines with different metastatic capacity. Int J Cancer 1995;61: 241-8.
27. Nicolson GL, Inoue T, Van-Pelt CS, Cavanaugh PG. Differential expression of a Mr approximately 90,000 cell surface transferrin receptor-related glycoprotein on murine B16 metastatic melanoma sublines selected for enhanced brain or ovary colonization. Cancer Res 1990;50: 515-20.
28. Schackert G, Fidler IJ. Site-specific metastasis of mouse melanomas and a fibrosarcoma in the brain or meninges of syngeneic animals. Cancer Res 1988;48: 3478-84.
29. Engebraaten O, Fodstad O. Site-specific experimental metastasis patterns of two human breast cancer cell lines in nude rats. Int J Cancer 1999;82: 219-25.
30. Paxinos G. The rat nervous system, 2nd edition. New York: Academic Press, 1995: 4-5.
31. Popesko P, Rajtova V, Horak J. A colour atlas of anatomy of small laboratory animals, volume 2: rat, mouse, hamster. London: Wolfe, 1992.

32. Schackert G, Price JE, Zhang RD, Bucana CD, Itoh K, Fidler IJ. Regional growth of different human melanomas as metastases in the brain of nude mice. Amer J Pathol 1990;136: 95-102.
33. Cheresh DA. Integrins in thrombosis, wound healing and cancer. Biochem Soc Trans 1991;19: 835-8.
34. Danen EH, Van-Muijen GN, Ten-Berge PJ, Ruiter DJ. Integrins and melanoma progression. Recent Results Cancer Res 1993;128: 119-32.
35. Danen EH, Van-Muijen GN, Ruiter DJ. Role of integrins as signal transducing cell adhesion molecules in human cutaneous melanoma. Cancer Surv 1995;24: 43-65.
36. Cheresh DA. Structure, function and biological properties of integrin alpha v beta 3 on human melanoma cells. Cancer Metastasis Rev 1991;10: 3-10.
37. Danen EH, Lafrenie RM, Miyamoto S, Yamada KM. Integrin signaling: cytoskeletal complexes, MAP kinase activation, and regulation of gene expression. Cell Adhes Commun 1998;6: 217-24.
38. Frisch SM, Vuori K, Ruoslahti E, Chan HP. Control of adhesion-dependent cell survival by focal adhesion kinase RGD and other recognition sequences for integrins, brain extracellular matrix, integrin signaling and matrix assembly. J cell Biol 1996;134: 793-9.

Chapter 3

Vascular Endothelial Growth Factor-A_{165} (VEGF-A_{165}) induces progression of melanoma brain metastases without induction of sprouting angiogenesis

Benno Küsters William PJ Leenders
(B.K. and W.P.J.L. contributed equally to this work; shared first authorship)
Pieter Wesseling
Debby Smits,
Kiek Verrijp
Dirk J Ruiter
Johannes PW Peters
Albert J van der Kogel
Robert MW de Waal

Cancer Res 2002, 62:341-345.

Abstract

We investigated the mechanisms of vascularization in a brain metastases model of malignant melanoma. Parenchymal metastases expressing little Vascular Endothelial Growth Factor-A (VEGF-A) co-opted the pre-existent brain vasculature, leading to an infiltrative phenotype. Metastases of the human melanoma cell line Mel57, engineered to express recombinant VEGF-A_{165} showed accelerated growth in a combined expansive and infiltrative pattern with marked central necrosis. This difference in growth profile was accompanied by dilatation of co-opted intra- and peritumoral vessels with concomitant induction of vascular permeability. Our data show that modulation of pre-existent vasculature can contribute to malignant progression without induction of sprouting angiogenesis.

Introduction

Brain metastases of malignant melanoma are a life-threatening complication of this disease. Primary and metastatic tumors of the central nervous system (CNS) are generally highly vascularized, therefore anti-angiogenic therapy has been considered promising [1]. However, the brain itself has a dense vascular bed and primary CNS tumors often show a highly infiltrative growth pattern. This raises the question whether the vessels in such tumors are formed by neo-angiogenesis or are pre-existent ones [2]. Indeed, employment of pre-existent vessels in early metastatic outgrowth in the brain, a process referred to as co-option, has been reported [3-5], which was followed by a switch to an angiogenic phenotype. Vessel co-option as a mean of tumor vascularization might have important consequences for diagnosis and therapy. For example, in contrast-enhanced magnetic resonance imaging (CE-MRI), tumor lesions are visualized by virtue of tumor-induced vascular changes like hyperpermeability, leading to extravasation of contrast agent. Although vascular hyperpermeability is considered to be a characteristic of tumor neovasculature, it is unclear whether co-opted vessels in CNS malignancies are modified in this respect. Secondly, vessel co-option obviously will have important consequences for application of tumor therapies using angiogenesis inhibitors. In this regard, it is important to realize that most studies with anti-angiogenic compounds have been carried out in animal models where tumors are grown subcutaneously (s.c.). Especially for CNS tumor biology, s.c. models have only limited clinical relevance because the subcutaneous space is essentially avascular. S.c. tumors will therefore be artificially selected to grow in an angiogenesis-dependent fashion while the microenvironmental conditions that exist in highly vascularized tissues like the brain are bypassed.

In previous work we showed that the human melanoma cell line Mel57 metastasizes to mouse brain parenchyma after injection into the internal carotid artery [6-8]. *In vitro*, Mel57 expresses very low amounts of Vascular Endothelial Growth Factor-A (VEGF-A)[9]. We report here on the mechanisms of tumor vascularisation in this model and on the effects of $VEGF_{165}$ expression on tumor growth and vascular parameters. We show that expression of $VEGF_{165}$ induced significant progression of tumor growth, which was not associated with classical (i.e. sprouting) angiogenesis but caused by architectural and functional changes of the co-opted pre-existent brain vasculature.

Materials and methods

Mice

Specific pathogen-free (SPF) male, 6 to 8 weeks old BALB/c nu/nu mice weighing 18-25g were purchased from the university central animal facility. Per cage 5 mice were housed under SPF conditions (temperature 20-24 °C; relative humidity 50-60%; 15 air changes per hour; light-dark periods 14 h/10 h). Water and food (RMH, Hope Farms, the Netherlands) were available to the animals ad libitum. Experiments were carried out in accordance with the national animal protection laws.

Cell lines, transfections and microsurgical injections

Human melanoma cell lines Mel57, M14 and 530 were cultured in Dulbecco's Modified Eagle's Medium (DMEM, Life Technologies, Breda, The Netherlands), supplemented with 10% fetal calf serum (FCS), streptomycin and penicillin at 37 °C. Mel57 cells were transfected using Fugene (Roche, Mannheim, Germany) with plasmid pVEGF-IRESneo or pEGFP-IRESneo (enhanced green fluorescent protein) as a control, according to the manufacturer's guidelines. pVEGF-IRESneo carries the cDNA for human $VEGF_{165}$ cloned in the EcoR1-BamH1 sites of vector pIRESneo (Clontech, Palo Alto, California) under control of the CMV promoter. Two days after transfection, selection of transfectants was started using 400 μg/ml G418. The use of an internal ribosome entry site (IRES) to generate neomycin resistance led in our hands to more than 95% positivity for the recombinant protein in G418-resistant cells. Therefore, after two weeks of selection, colonies of transfected cells were pooled, expanded and frozen. Levels of recombinant VEGF in conditioned media were determined using western blot analysis as described [9]. Metastasis was induced as described previously [6] by microsurgical injection of tumor cell suspensions into the right internal carotid artery of anaesthetised nude mice

Histological and immunohistochemical analysis

Mice were sacrificed after development of severe cachexia or acute neurological deficits. For immunohistochemistry, material was snap-frozen in liquid nitrogen or fixed in formaline and embedded in paraffin. Sections of 4 μm underwent conventional H&E staining. The brains of animals bearing lesions of the Mel57 cell lines, sacrificed 20-22 days after tumor cell injection were cut semi-serially and lesion sizes were determined using measurement oculars. Antibodies used were anti-murine CD31 (Mec 7.46; Hycult Biotechnology, Uden, The

Netherlands), anti-mouse tight junction protein ZO1 (mAB1520; Chemicon, California), rabbit anti-mouse Ki-67 (Dianova, Hamburg, Germany), mouse anti-human α-smooth muscle actin (α-Sm1, Sigma, Zwijndrecht, The Netherlands), anti-Glut-1 (Dako, Glostrup, Denmark), rabbit anti-KDR (Santa Cruz Biotechnology, Santa Cruz, California), rabbit anti-angiopoietin I (Santa Cruz Biotechnology, Santa Cruz, California) and rabbit anti-angiopoietin II (Santa Cruz Biotechnology, Santa Cruz, California). Frozen 4 μm sections were fixed in acetone for 10 min, dried and incubated with Ab for 1 h at room temperature in phosphate-buffered saline containing 1% bovine serum albumin (PBS/BSA). After washing with PBS, bound Abs were detected with a peroxidase-conjugated secondary Ab (Vector, Burlingame, California) using the Vectastain elite ABC kit (Vector, Burlingame, California). Sections were counterstained with hematoxylin. Integrity of the blood-brain barrier (BBB) was investigated by staining for extravasated mouse immunoglobulins as described previously [10]. In all stainings a negative control was included in which primary antibodies were omitted. These controls were always negative.

Tumor cell proliferation assays

The S-phase marker bromodeoxyuridine (BrdU) (Sigma, Zwijndrecht, The Netherlands) was administered intraperitoneally at a dose of 100 mg/kg in 0.5 ml 0.9% NaCl 15 min. prior to sacrifice. The proliferation index of individual Mel57-lesions (*n*=3) and Mel57-VEGF-lesions (*n*=6) in different mice was determined in frozen brain sections by quantification of incorporated BrdU as described previously [11]. Tumor cell proliferation *in vitro* was determined as follows: $5x10^3$ cells were seeded in six-well culture plates and cultured in serum-free medium. After 2, 3 and 4 days cells were trypsinized and counted using a Coulter counter. All experiments were performed in triplicate.

Results

Growth of Mel57 lesions in brain parenchyma

Three to five weeks after injection of Mel57 cells in the right internal carotid artery, animals started to suffer from cachexia. Morphological analysis showed that numerous parenchymal lesions with diameters up to 3 mm were present in each brain with preferential localization in the right side of the brain (cerebrum, cerebellum and brain stem). These tumors exhibited an

infiltrative growth pattern in the parenchyma (Fig. 1*A*). Tumor cells exploited the pre-existent brain vessels by growing in the space of Virchow-Robin (forming lesions containing remnants of pre-existent brain parenchyma (Fig. 1*A*, inset)). Tumor growth in the space of Virchow-Robin was also seen in metastases derived from the human melanoma cell lines M14 and 530 (Fig.1*E* and *F*). The cell line Mel57 was chosen for further studies. We did not detect differences between the vasculature within the lesions and that in the surrounding normal brain tissue with regard to vessel diameter (Fig. 1*C*), activation status of the endothelium (assessed by KDR/Flk-1, Fig. 2*G* and CD105 expression, not shown) and maturation status (assessed by pericyte coverage, Fig. 2*I*). Also, intratumoral vessels still had all characteristics of an intact blood brain barrier (BBB) as demonstrated by unaltered morphology (Fig. 1*C*), lack of mouse IgG extravasation (Fig. 2*A*) and the presence of endothelial glucose transporter 1 (Glut-1) (Fig. 2*C*) and zonula occludens ZO-1 (Fig. 2*E*) at levels similar to those found in normal brain parenchyma. Vessel density within the lesions was slightly lower than in the surrounding normal brain parenchyma (Fig. 1*C*) indicating that there was no angiogenic compensation for the tissue volume increase at the lesion site. This lack of angiogenesis was in line with the overall absence of vascular changes. Despite the absence of neo-vascularization, necrosis was scarce in these lesions, implying that the blood supply from the pre-existent vascular bed sufficed to provide the tumor cells with oxygen and nutrients. Although injection of higher numbers of cells led to a proportionally higher number of lesions, the morphology of the individual lesions was not affected (not shown). All together, the infiltrative character, the low intratumoral vessel density and the intact BBB strongly suggested that these lesions grew by mere vessel co-option without induction of an angiogenic switch.

There were neither qualitative nor quantitative differences in tumor growth patterns between parental Mel57 and control Green Fluorescent Protein (EGFP) transfectants (data not shown).

Fig. 1 – Growth patterns of Mel57 (*A,C*), Mel57-VEGF$_{165}$ (*B*,*D*), M14 (*E*) and 530 (*F*) melanoma brain metastases. H&E staining (*A,B*) and CD31 staining (*C,D*) of brains containing Mel57 lesions (*A,C*) and Mel57-VEGF$_{165}$ lesions (*B,D*). The insets in *A* and *B* show that tumor cells invade the brain parenchyma along the brain vessels in the space of Virchow-Robin. The inset in D shows a decrease of vessel dilatation with distance to a small sized lesion. Note the vessel dilatation in Mel57-VEGF$_{165}$ lesions and the presence of central necrosis in Mel57-VEGF$_{165}$ lesions (*B*) but not in Mel57 lesions (*A*). The cell lines M14 and 530, producing low amounts of VEGF *in vitro*, also display an infiltrative growth pattern by vascular co-option in brain metastases. Note the Glut-1 blood-brain barrier marker on co-opted vessels in (*E*). T=tumor, N=necrosis, V=vessel. See also colour display page 150.

Figure 1

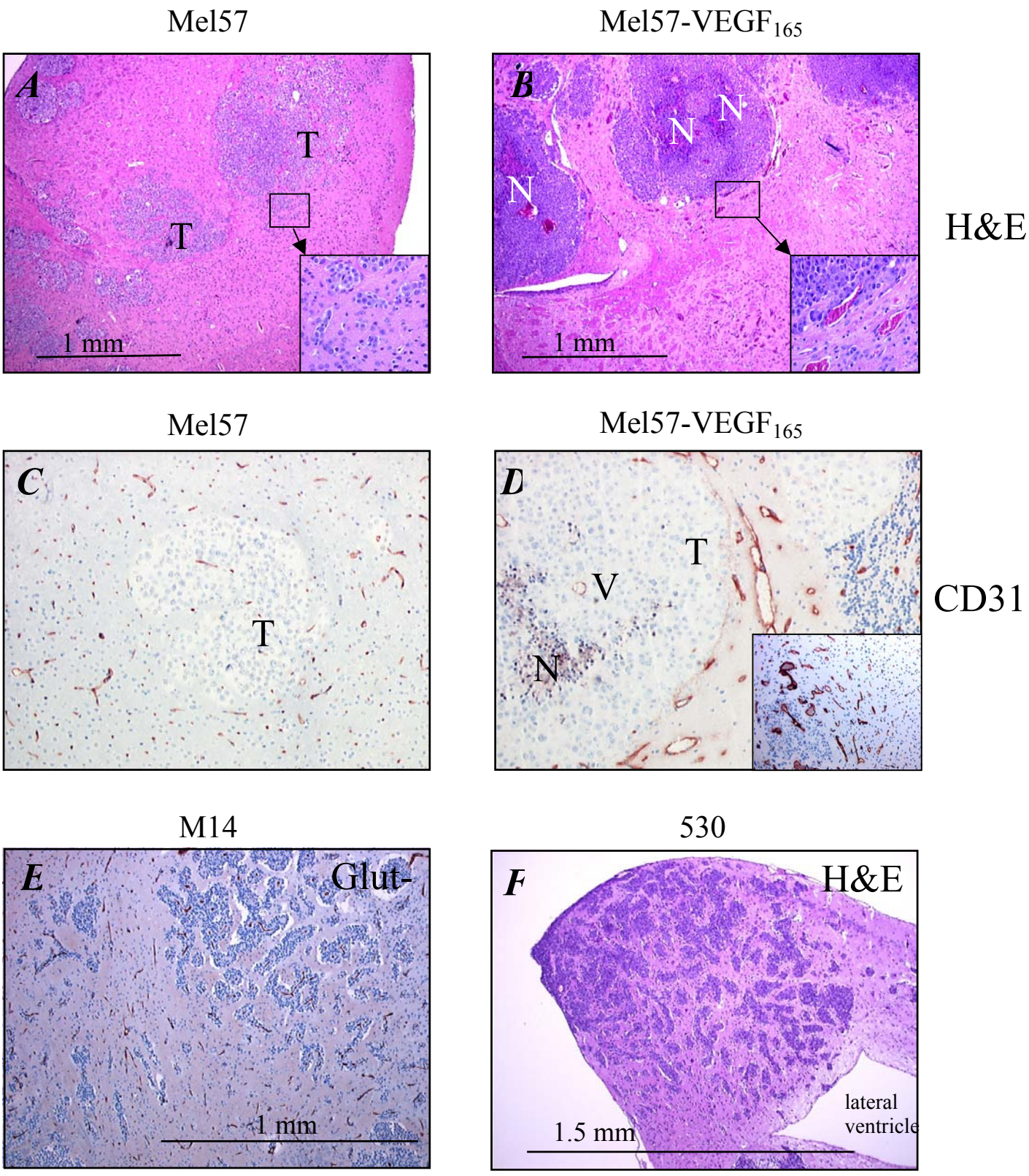
Mel57
Mel57-VEGF165
A
T
T
1 mm
B
N
N
N
1 mm
H&E
Mel57
Mel57-VEGF165
C
T
D
T
V
N
CD31
M14
530
E
Glut-
1 mm
F
H&E
lateral
ventricle
1.5 mm

Effects of $VEGF_{165}$ on growth of Mel57 lesions

Since Mel57 produces low levels of VEGF *in vitro* (approximately 30 pg/10^6 cells/24 hrs, data not shown), and sprouting angiogenesis was absent in Mel57 CNS-lesions, we were interested in the effects of expression of this potent angiogenic factor in this model. To this end, we created stable transfectants of Mel57 which produced high levels of $VEGF_{165}$ (approximately 30 ng/10^6 cells/24 hr) and analysed the growth profile. Mel57-$VEGF_{165}$ developed a growth pattern that was completely different from parental tumor cells. These lesions had a more solid and expansive rather than infiltrative growth pattern (Fig. 1*B*) although at the tumor rim infiltration into the parenchyma, again along pre-existing vessels, was still present (Fig. 1*B*, inset). Like in Mel57 lesions, the intratumoral vessel density was lower than in the surrounding brain parenchyma (Fig. 1*D*). However, now there were marked differences between intra/peri-tumoral vessels and extratumoral vessels. (Peri-)tumoral vessels were irregularly dilated (Fig. 1*D*) and showed upregulation of KDR (Fig. 2*H*) and CD105 expression (not shown), indicating that VEGF had induced an activated state of the endothelium. Vessel dilatation gradually decreased with increasing distance from the lesion (see Fig. 1*D*, inset) pointing at tumor-derived VEGF as the causative factor. Staining for mouse immunoglobulins indicated high permeability of blood vessels in the tumor and at the tumor periphery (compare Fig. 2*B* to 2*A*). The dilated vessels still stained positive for the BBB markers Glut-1 and ZO-1 (Fig. 2*D*, *F*), indicating that these vessels are truely pre-existent and not neo-angiogenic. Interestingly, Glut-1 expression on the endothelium in intratumoral vessels was markedly decreased as compared to that in normal brain vessels (compare Fig. 2*D* to 2*C* and note the Glut-1 negative vessel indicated by the arrow in Fig. 2*D*).

Staining for alpha-smooth muscle actin revealed a high grade of pericyte coverage of tumor vessels (Fig. 2*J*), indicating the presence of a mature phenotype. Despite the lack of sprouting angiogenesis, both endothelial cells and pericytes responded to VEGF by proliferation, as these cells frequently stained positive for (murine) nuclear antigene Ki-67 (MIB-1, Fig. 2*L*). This was clearly a VEGF effect since vascular cells in Mel57 parental lesions were quiescent (Fig. 2*K*). Despite all the vascular changes observed, we did not see induction of angiogenesis in terms of sprouting and branching of new capillaries in Mel57-$VEGF_{165}$ lesions. Average diameters of Mel57-$VEGF_{165}$ lesions were increased approximately 2-fold as compared to parental Mel57 lesions (Fig. 3*A*), while the proliferation index of the Mel57-$VEGF_{165}$ lesions was more than 4-fold higher than that of control tumors (Fig. 3*B*). Proliferation was boosted by factors from the tumor environment since there was no

difference in growth rate between the Mel57 transfectants and the parental line *in vitro* (results not shown). The high proliferation rate, in combination with the lack of sprouting angiogenesis in the Mel57-$VEGF_{165}$ lesions led to evident hypoxia as shown by upregulation of Glut-1 in tumor cells themselves (Fig. 2*D* and (12)) and subsequently to necrosis, even in small lesions (Fig. 1*B*). In immunohistochemistry we detected no differences in expression of both angiopoietins I and II between tumors from Mel57 and Mel57-$VEGF_{165}$ cells, both angiopoietins were expressed (not shown).

Discussion

Tumors are considered to start as avascular masses that become vascularized by sprouting angiogenesis, a process that is induced by tumor-derived factors such as VEGF. However, several groups have reported that tumors can also utilize the pre-existent vasculature in the host tissue. Holash et al. [3] described initial growth of a brain tumor by vessel co-option, which was followed by vessel regression and induction of classical angiogenesis via upregulation of VEGF and angiopoietin-2 [3, 4]. Li et al. described a subcutaneous model of early tumor outgrowth where vasodilatation was followed by sprouting angiogenesis in lesions as small as a few thousand cells [5].

Here we show in a brain microenvironment that tumors consisting of several hundreds of thousands of cells can grow without induction of sprouting angiogenesis, even in the presence of high levels of VEGF. Obviously, the capillary network of the brain parenchyma is one of the densiest in the mammalian body. Thus, in such an environment tumors can thrive in an angiogenesis-independent manner and produce lesions that in the murine brain can reach diameters of up to 3 mm (approximately 14 mm^3), far beyond Folkman's angiogenic switch threshold of 2 mm^3 [13].

Figure 2

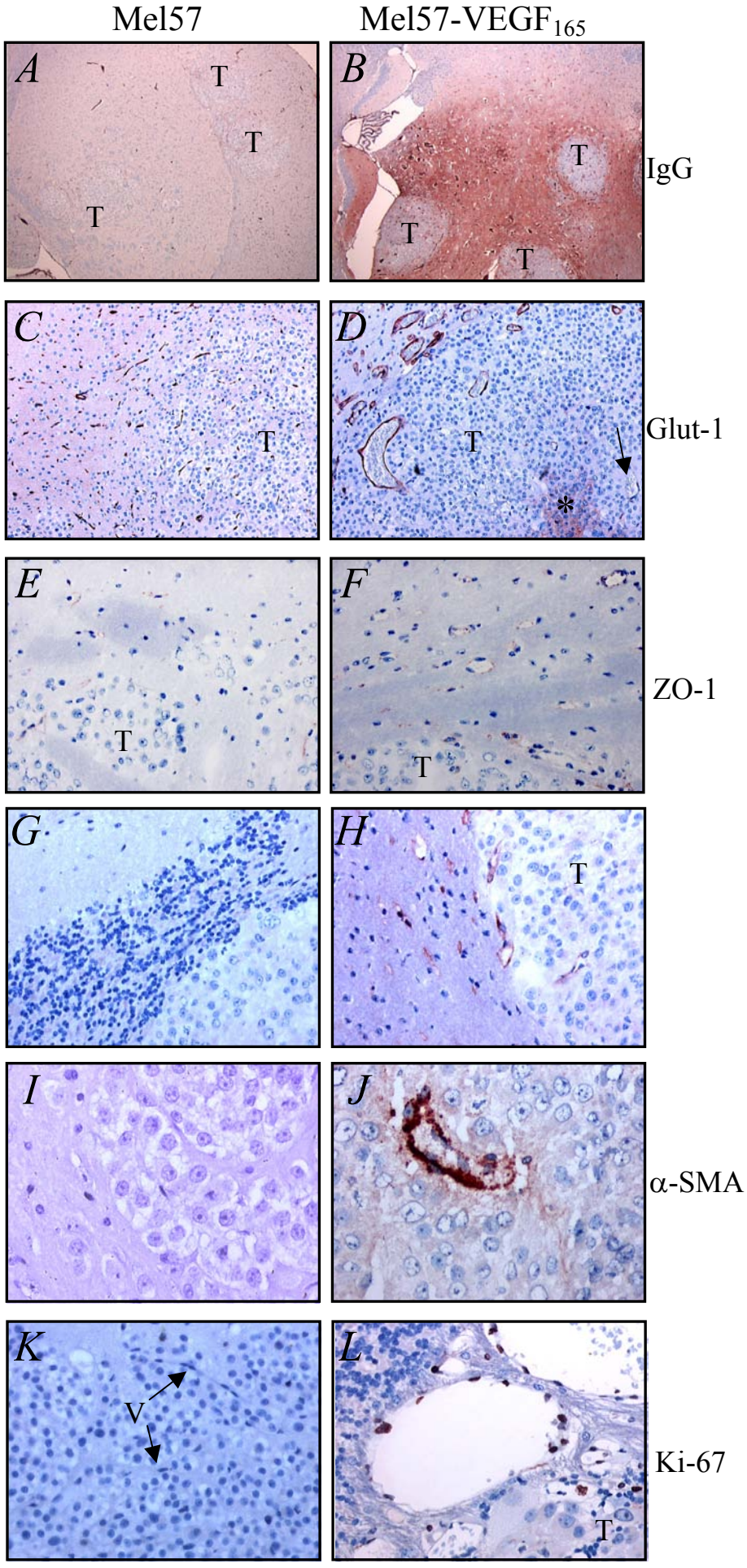
Mel57
Mel57-VEGF165
A
T
T
T
B
T
T
T
IgG
C
T
D
T
*
Glut-1
E
T
F
T
ZO-1
G
H
T
I
J
α-SMA
K
V
L
T
Ki-67

Fig. 2 – Effect of $VEGF_{165}$ on blood-brain barrier function. Brains containing Mel57 lesions (*A,C,E*) or Mel57-$VEGF_{165}$ lesions (*B,D,F*) were stained for mouse IgG (*A,B*), Glut-1 (*C,D*) or ZO-1 (*E,F*) as described in the text. Only vessels in and around Mel57-$VEGF_{165}$ lesions are leaky as demonstrated by the presence of extravasated IgG (*B*). Dilated vessels in Mel57-$VEGF_{165}$ lesions express the BBB markers ZO-1 (B) and Glut-1 (*D*) although expression on vessels within the lesions is clearly downregulated. The arrow in (*D*) points at a Glut-1 negative vessel. Glut-1 is expressed in tumor cells adjacent to necrosis, indicating hypoxia (*D*,*). Activation of vascular endothelium by $VEGF_{165}$. Immunostaining of Mel57 (*G,I,K*) and Mel57-$VEGF_{165}$ (*H,J,L*) lesions for VEGFR-2/Flk-1 (*G,H*), α-smooth muscle actin (α-SMA) (*I,J*) and Ki-67 (*K,L*). VEGFR-2/Flk-1 is upregulated on vessels in and around the Mel57-$VEGF_{165}$ lesions, indicating an activated state of the endothelium. These vessels display a mature phenotype as indicated by the high pericyte coverage (*J*) compared to vessels in lesions from the parental cell line (I). Although VEGF-A_{165} in these tumors induces proliferation of endothelial cells, as demonstrated by Ki-67 staining (*L*), this is not accompanied by vascular sprouting. V=vessel, T=tumor. See also colour display page 151.

Figure 3

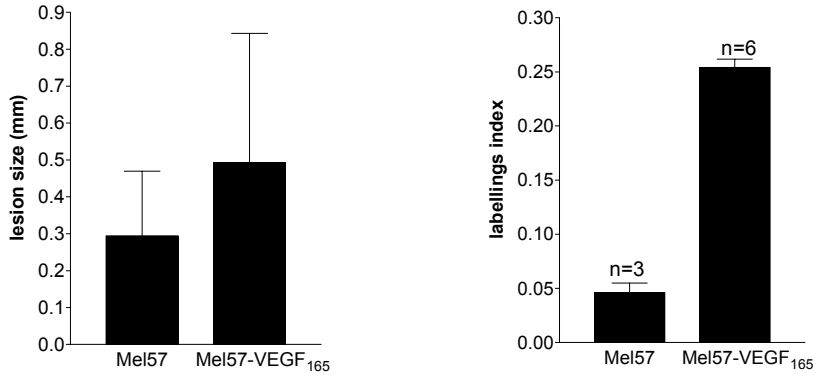

A *B*

Fig. 3 – Effects of $VEGF_{165}$ expression on lesion size and proliferation. *A*) Size of Mel57 and Mel57-$VEGF_{165}$ lesions, expressed as diameter (mm). Lesions in 5 mice brains were used in this analysis. Mice were sacrificed 21±1 days after intracarotid injection of tumor cells. Lesions were measured as described in the text. Sizes differed significantly between the groups ($P<0.001$, Students T-test). *B*) Tumor cell proliferation index *in vivo* as determined by BrdU incorporation (see text). Data are expressed as fraction of labelled tumor cell nuclei ($P<0.001$, Students T-test). Error bars represent standard deviations.

In vitro, Mel57 produces minimal amounts of angiogenic factors like VEGF, bFGF, IL-8 and PDGF [9]. The absence of vascular changes in Mel57 and Mel57-EGFP lesions demonstrates that VEGF was not upregulated *in vivo* as well. In a previous paper we reported low expression levels of VEGF in melanoma lines M14 and 530 as well [9]. Brain metastases derived from these cell lines behaved comparably to those derived from Mel57, showing that the phenomenon of vascular co-option is not restricted to one cell line.

Based on several criteria, we conclude that there were neither morphological nor functional differences between intratumoral and distant vessels in Mel57 or Mel57-EGFP lesions. The blood brain barrier was intact, as demonstrated by the absence of extravasated immunoglobulins and by the presence of Glut-1 and ZO-1. From these results we conclude that VEGF production was not essential for the formation of brain metastases. Clearly, the capacity to metastasize to the brain in the absence of VEGF may be tumor type-dependent, since Yano et al. showed that anti-sense VEGF cDNA transfection of human carcinoma cell lines decreased the metastatic capacity to the brain of these cells [14].

In contrast to the prevailing idea that $VEGF_{165}$ induces sprouting angiogenesis, brain metastases of stable $VEGF_{165}$ -transfectants of Mel57 did not have a classical angiogenic phenotype: despite a high proliferation rate of endothelial cells and pericytes, there was no branching or sprouting of the otherwise extensively dilated capillaries in these tumors. This is in accordance with recent reports on VEGF effects in non-tumorous settings [10, 15]. Another remarkable observation was that VEGF severely deteriorated BBB function leading to vascular hyperpermeability, which is in line with previous reports [16-18].

Despite the lack of classical (i.e. sprouting) angiogenesis, $VEGF_{165}$ expression did lead to tumor progression, which was reflected by increased tumor cell proliferation rates and larger lesion sizes. This resulted in a more solid, expansive growth of the lesions with lack of blood supply in the center of the lesions, often causing central necrosis, even in relatively small lesions.

Since the growth rates of the different tumor cell lines *in vitro* were equal, the overall increased tumor growth of the Mel57-$VEGF_{165}$ tumors must have been caused by modulation of the pre-existent vascular bed. The dilatation of the blood vessels may have led to elevated perfusion thereby providing the lesions with a better blood supply. This, however, occurred predominantly in the peritumoral zone. The inability to induce sprouting angiogenesis caused a lack of neovasculature within the tumor lesions and subsequent local necrosis. Our data therefore suggest that tumor-derived factors, other than $VEGF_{165}$, are required for sprouting angiogenesis to occur. Angiopoietins have been reported to play an important role in

angiogenesis too [3, 4, 19]. IHC staining for angiopoietins I and II demonstrated that these factors were produced by both parental Mel57 and Mel57-$VEGF_{165}$ cells, implying that the angiopoietin/Tie2 system probably is not of significance in this model. It has also been reported that expression of the larger VEGF-isoforms by tumors correlates with poor prognosis [20]. We are currently investigating the effects of expression of these isoforms in our model.

Most data on tumor growth, angiogenesis and angiogenesis inhibition are derived from experimental settings in which tumors are grown in the largely avascular subcutaneous space and therefore are selected for angiogenic capacity. In our model we closely mimick the human situation of hematogenous CNS metastasis formation [8]. We show that mere vessel co-option can account for providing tumor blood supply in highly vascularized organs. Constitutive VEGF expression *per se* does not lead to classical angiogenesis but may promote tumor growth by functional modulation of the co-opted vessels. Thus, the irregularly shaped and dilated vessels that are often found in human CNS malignancies may not always represent newly formed vessels, but morphologically and functionally altered pre-existent ones.

Our results might have clinical relevance with regard to diagnosis and therapy. As in CE-MRI tumors are detected on the basis of vascular changes (e.g. hyperpermeability), the absence thereof, such as we observed in the Mel57 lesions, will hamper tumor detection. With regard to therapy, our results show that anti-angiogenic treatment of brain tumors like glioblastoma multiforme, high-grade astrocytomas and metastases with vascular changes may give a benefit in that tumor progression might be slowed down. However, an important unwanted side effect might be that blockade of VEGF leads to a non-permeable tumor vasculature, potentially with a concomitant resistance to chemotherapeutic treatment. These issues are currently under investigation in our lab.

References

1. Plate, K. H. and Risau, W. Angiogenesis in malignant gliomas. Glia, *15*: 339-347, 1995.

2. Wesseling, P., Ruiter, D. J., and Burger, P. C. Angiogenesis in brain tumors; pathobiological and clinical aspects. J. Neurooncol., *32*: 253-265, 1997.

3. Holash, J., Maisonpierre, P. C., Compton, D., Boland, P., Alexander, C. R., Zagzag, D., Yancopoulos, G. D., and Wiegand, S. J. Vessel cooption, regression, and growth in tumors mediated by angiopoietins and VEGF. Science, *284*: 1994-1998, 1999.

4. Holash, J., Wiegand, S. J., and Yancopoulos, G. D. New model of tumor angiogenesis: dynamic balance between vessel regression and growth mediated by angiopoietins and VEGF. Oncogene, *18*: 5356-5362, 1999.

5. Li, C. Y., Shan, S., Huang, Q., Braun, R. D., Lanzen, J., Hu, K., Lin, P., and Dewhirst, M. W. Initial stages of tumor cell-induced angiogenesis: evaluation via skin window chambers in rodent models. J. Natl. Cancer Inst., *92*: 143-147, 2000.

6. Küsters, B., Westphal, J. R., Smits, D., Ruiter, D. J., Wesseling, P., Keilholz, U., and De Waal, R. M. W. The pattern of metastasis of human melanoma to the central nervous system is not influenced by integrin alpha(v)beta(3) expression. Int. J. Cancer, *92*: 176-180, 2001.

7. Schackert, G. and Fidler, I. J. Development of in vivo models for studies of brain metastasis. Int. J. Cancer, *41*: 589-594, 1988.

8. Fidler, I. J., Schackert, G., Zhang, R. D., Radinsky, R., and Fujimaki, T. The biology of melanoma brain metastasis. Cancer Metastasis Rev., *18*: 387-400, 1999.

9. Westphal, J. R., Van't Hullenaar, R., Peek, R., Willems, R. W., Crickard, K., Crickard, U., Askaa, J., Clemmensen, I., Ruiter, D. J., and de Waal, R. M. Angiogenic balance in human melanoma: expression of VEGF, bFGF, IL-8, PDGF and angiostatin in relation to vascular density of xenografts in vivo. Int. J. Cancer, *86*: 768-776, 2000.

10. Proescholdt, M. A., Heiss, J. D., Walbridge, S., Muhlhauser, J., Capogrossi, M. C., Oldfield, E. H., and Merrill, M. J. Vascular endothelial growth factor (VEGF) modulates vascular permeability and inflammation in rat brain. J. Neuropathol. Exp. Neurol., *58*: 613-627, 1999.

11. Bussink, J., Kaanders, J. H., Rijken, P. F., Martindale, C. A., and van der Kogel, A. J. Multiparameter analysis of vasculature, perfusion and proliferation in human tumour xenografts. Br. J. Cancer, *77*: 57-64, 1998.

12. Clavo, A. C., Brown, R. S., and Wahl, R. L. Fluorodeoxyglucose uptake in human cancer cell lines is increased by hypoxia . J. Nucl. Med., *36*: 1625-1632, 1995.

13. Folkman, J. What is the evidence that tumors are angiogenesis dependent? [editorial]. J. Natl. Cancer Inst., *82*: 4-6, 1990.

14. Yano, S., Shinohara, H., Herbst, R. S., Kuniyasu, H., Bucana, C. D., Ellis, L. M., Davis, D. W., McConkey, D. J., and Fidler, I. J. Expression of vascular endothelial growth factor is necessary but not sufficient for production and growth of brain metastasis. Cancer Res., *60*: 4959-4967, 2000.

15. Rosenstein, J. M., Mani, N., Silverman, W. F., and Krum, J. M. Patterns of brain angiogenesis after vascular endothelial growth factor administration in vitro and in vivo. Proc. Natl. Acad. Sci. U.S.A., *95*: 7086-7091, 1998.
16. Dvorak, H. F., Brown, L. F., Detmar, M., and Dvorak, A. M. Vascular permeability factor/vascular endothelial growth factor, microvascular hyperpermeability, and angiogenesis. Am. J. Pathol., *146*: 1029-1039, 1995.
17. Berkman, R. A., Merrill, M. J., Reinhold, W. C., Monacci, W. T., Saxena, A., Clark, W. C., Robertson, J. T., Ali, I. U., and Oldfield, E. H. Expression of the vascular permeability factor/vascular endothelial growth factor gene in central nervous system neoplasms. J. Clin. Invest., *91*: 153-159, 1993.
18. Strugar, J. G., Criscuolo, G. R., Rothbart, D., and Harrington, W. N. Vascular endothelial growth/permeability factor expression in human glioma specimens: correlation with vasogenic brain edema and tumor-associated cysts. J. Neurosurg., *83*: 682-689, 1995.
19. Jones, N., Iljin, K., Dumont, D.J., Alitalo, K. Tie receptors: new modulators of angiogenic and lymphangiogenic responses. Nat. Rev. Mol. Cell Biol., 2: 257-267, 2001.
20. Cheng, S. Y., Nagane, M., Huang, H. S., and Cavenee, W. K. Intracerebral tumor-associated hemorrhage caused by overexpression of the vascular endothelial growth factor isoforms VEGF121 and VEGF165 but not VEGF189. Proc. Natl. Acad. Sci. U.S.A., *94*: 12081-12087, 1997.

Chapter 4

Vascular endothelial growth factor-A determines detectability of experimental melanoma brain metastasis in Gd-DTPA-enhanced MRI

William PJ Leenders Benno Küsters
(W.P.J.L and B.K. contributed equally to this work; shared first authorship)
Jeroen Pikkemaat
Pieter Wesseling
Dirk Ruiter
Arend Heerschap
Jelle Barentsz
Robert MW de Waal

Int J Cancer, 2003; 105: 437-44

Abstract

We have previously shown that the dense vascular network in mouse brain allows for growth of human melanoma xenografts (Mel57) by co-option of pre-existent vessels. Overexpression of recombinant VEGF-A by such xenografts induced functional and morphological alterations of pre-existent vessels. We now describe the effects of VEGF-A expression on visualization of these brain tumors in mice by magnetic resonance imaging (MRI), using gadolinium diethylenetriaminepenta-acetic acid (Gd-DTPA) and ultra small paramagnetic iron oxide particles (USPIO) as contrast agents.

Brain lesions derived from (mock-transfected) Mel57 cells were undetectable in MRI after Gd-DTPA injection. However, the majority of such lesions became visible after injection of USPIO, due to the lower vascular density in the lesions as compared to the surrounding parenchyma. In contrast, VEGF-A-expressing lesions were visualized using Gd-DTPA-enhanced MRI by a rapid circumferential enhancement, due to leaky peritumoral vasculature. USPIO-enhanced MRI on these tumors corroborated the immunohistochemical finding that peritumorally located, highly irregular and dilated vessels were present while intratumoral vessel density was low.

This study shows that VEGF-A is a key factor in imaging of brain neoplasms. Our data also demonstrate that, at least in brain, blood-pool agent-enhanced MRI may be a valuable diagnostic tool to detect malignancies that are not visible on Gd-DTPA enhanced MRI. Furthermore, the involvement of VEGF-A in MRI visibility suggests that care must be taken with MRI-based evaluation of anti-angiogenic therapy, as anti-VEGF treatment might revert a tumor to a co-opting phenotype, resulting in loss of contrast enhancement in MRI.

Introduction

Primary brain tumors and brain metastases of various origins are important clinical problems[1]. In patients with advanced malignant melanoma the cause of death is frequently related to brain metastasis and accompanying neurological complications [2]. For diagnosis as well as planning and evaluation of therapy, imaging techniques like computer-assisted tomography (CT) and (contrast-enhanced) magnetic resonance imaging (CE-MRI) are invaluable tools. In CE-MRI, contrast enhancement of tumor tissue is usually accomplished by extravasation and subsequent accumulation in the interstitium of small contrast agents like gadolinium diethylenetriaminepenta-acetic acid (Gd-DTPA). Tumor vessels generally are more leaky than normal vessels and will thus permit faster extravasation. Hence, dynamic CE-MRI measurements allow identification of suspected malignancies by highlighting regions with increased rates of wash-in and wash-out of contrast agents [3]. The difference between tumor and normal vessels is especially pronounced in brain, since the blood-brain barrier function of normal brain vessels precludes extravasation of these agents [4].

Unfortunately, not all patients with brain tumors are recognized as such in contrast-enhanced MRI. Examples are infiltratively growing brain tumors like low grade diffuse astrocytomas (WHO grade II) and gliomatosis cerebri, which generally do not enhance in MRI after Gd-DTPA adminstration because they grow without increasing vessel permeability [5, 6]. On the other hand, the most malignant astrocytic tumor, i.e. glioblastoma multiforme (WHO grade IV) is readily detectable in MRI because in these tumors the blood vessels are tortuous and leaky. Nevertheless, Gd-DTPA often fails to identify the exact tumor boundary since enhancement may also occur at some distance from the tumor. In addition, in such tumors, which generally have a very heterogeneous morphology, regions can be found that are characterized by infiltrative growth and lack of Gd-DTPA-enhancement in MRI.

One of the candidate factors responsible for detectability in Gd-DTPA-enhanced MRI is Vascular Endothelial Growth Factor-A (VEGF-A) which is also well known for its potency to induce vessel permeability [7]. VEGF-A is regarded as the most potent angiogenic factor and in preclinical tumor models, inhibition of VEGF-A-signaling leads to inhibition of tumor angiogenesis and tumor growth [8-10]. A number of compounds that target VEGF-A or its cognate receptors have made it to phase III clinical trials (see internet page http://www.cancer.gov/clinical_trials/). However, results so far are disappointing and some compounds (e.g. SU5416, a potent inhibitor of VEGF receptor-2) have been withdrawn from trial because of lack of response. One possible explanation for the discrepancy between clinical and preclinical results might be that the clinical targets, i.e. metastatic tumors that

typically grow in organs with high vascular densities such as liver, lung and brain, are less dependent on angiogenesis than tumors grown in preclinical mouse models where tumor cells are injected in the, largely avascular, subcutaneous space. Indeed, there is increasing evidence that some (metastatic) human tumors can grow without inducing an angiogenic switch [11-14]. Therefore, it is important to develop a clinical tool that is able to predict which tumors are angiogenesis-dependent and thus susceptible to anti-angiogenic therapy and which tumors are not. CE-MRI could qualify as such because it is a non-invasive technique that allows detection of the vascular functional abnormalities associated with angiogenesis. CE-MRI modifications detecting angiogenesis-independent tumors still need to be identified, however. We recently showed that some human melanoma cell lines, like Mel57, express very low levels of VEGF-A and have low angiogenic potential in a mouse model of hematogenous brain metastasis [15]. For blood supply and growth, these tumors co-opted the dense vascular bed in the brain parenchyma, allowing tumor growth in the absence of angiogenesis [16]. Interestingly, vessel density and vascular volume within these lesions were lower than in the surrounding brain tissue, due to the increase of tumor volume in between pre-existent vessels without accompanying compensating angiogenesis. Remarkably, these tumors had a phenotype, at least partially resembling that of diffuse infiltrative, low grade gliomas: highly infiltrative tumor growth and no influence on blood-brain barrier function [15]. However, when Mel57 tumors were grown that were engineered to express VEGF-A, a phenotype frequently seen in glioblastoma multiforme developed, i.e. combined expansive and infiltrative growth with highly dilated, irregularly shaped and leaky vessels.

The differences in vascular phenotypes between Mel57 and Mel57-VEGF tumors led us to investigate whether these were reflected in patterns of contrast enhancement in MRI. Our data implicate VEGF-A as a crucial factor for the detection of brain tumors in MRI. They also suggest that USPIO-enhanced MRI might provide additional diagnostic information in patients in whom Gd-DTPA CE-MRI was inconclusive.

Materials & Methods

Cell lines and transfections

Mel57 cells were cultured at 37°C in Dulbecco's modified Eagle's Medium (DMEM, Life Technologies, Breda, The Netherlands), supplemented with 10% fetal calf serum (FCS), streptomycin and penicillin. Plasmid pEGFP-IRESneo was from Clontech (Palo Alto, CA, USA). Human VEGF-A_{121} cDNA was cloned in plasmid pIRESneo. Transfections were

performed using Fugene reagent (Roche, Mannheim, Germany) according to the manufacturer's guidelines. Transfected cells were selected in medium containing 400 µg/ml G418 (Roche, Mannheim, Germany) and maintained in medium containing 200 µg/ml G418. Cell clones were expanded, pooled and frozen. Cells were not individually cloned since the use of the IRES for G418-resistance warrants that close to 100% of the cells are positive for the transgene. Levels of recombinant VEGF-A in conditioned media were determined by western blot analysis as described [17].

Animal experiments

Specific pathogen-free (SPF) male, 6 to 8 weeks old BALB/c nu/nu mice were purchased from the university central animal facility. Five mice per cage were housed under SPF conditions (temperature 20-24 °C; relative humidity 50-60%; 15 air changes per hour; light-dark periods 14 h/10 h). Water and food (RMH, Hope Farms, the Netherlands) were available to the animals ad libitum. Experiments were carried out in accordance with the national animal protection laws and approval was obtained from the Animal Experimental Committee. Brain metastases were induced as described previously [18]. Briefly, cells were trypsinized, washed twice with phosphate-buffered saline (PBS) and counted using a Coulter Counter. For each cell line, a volume of 100 µl containing $1x10^5$ cells was microsurgically injected into the right internal carotid artery of anesthetized nude mice. After development of cachexia (typically after 22-25 days for control tumors and 18-20 days for VEGF-expressing tumors) CE-MRI was performed according to the protocol described below. Groups of 5 mice were used in this study for each cell line.

Contrast-enhanced magnetic resonance imaging

Mice were anaesthetized (1.3% isoflurane; 1:1 (v/v) N_2O/O_2 mixture), catheterized in the tail vein, and placed in an MR spectrometer (S.M.I.S. console equipped with a Magnex Scientific 7T/200mm horizontal bore magnet and a 150mT/m gradient set). Body temperature was maintained by placing the mice on a 37^{o}C circulating warm water bed. A 12 mm diameter radiofrequency surface coil was positioned over the skull. After initial monitoring of the brain with fast gradient-echo scout images, 20 contiguous high-resolution coronal MR images were acquired with T_2-weighted multislice spin-echo imaging (echo time = 50 ms; repetition time = 3000 ms; number of averages = 1; field of view = 40x40 mm; matrix size = 512x512; slice thickness = 1 mm). This imaging protocol was repeated 2 minutes after intravenous injection of USPIO (Sinerem®, Guerbet, France) [19] at a dose of 12.5 mg/kg. Due to a shortening of T_2-

relaxation, injection of Sinerem leads to a signal decrease in this spin-echo sequence. In case of Gd-DTPA contrast enhancement, 16 contiguous images were acquired with a T_1-weighted multislice gradient-echo sequence (T_E= 8 ms; T_R = 100 ms; flip angle = 90º; number of averages = 1; field of view = 25x25 mm; matrix size = 256x256; slice thickness = 1 mm) before and 1, 2, 10 and 20 minutes after injection of Gd-DTPA (Magnevist®, Schering, Germany) at a dose of 0.2 mmol/kg. Each animal received a single intravenous bolus injection of either Sinerem® or Magnevist®. For each contrast agent and tumor cell line, 5 mice were imaged. For quantification of data, voxels were selected that encompassed a complete lesion and intensity within a voxel was measured pre-contrast and at different time points post contrast, using the S.M.I.S. software package. In this way, signal intensities of 9 lesions in 5 mice were measured

Histological and immunohistochemical analysis

After MRI, mice were sacrificed and brains removed and formalin-fixed. Brains were cut in coronal slices and embedded in paraffin. Sections of 4 μm were subjected to conventional H&E staining or immunostained for the endothelial marker CD34. MRI images were matched to histology as closely as possible, although a perfect match was impossible because of the difference between thicknesses of MRI and histology slices (1 mm vs. 4μm).

Results

Parental and mock-transfected Mel57 cells

We have previously shown that metastatic Mel57 lesions grow in mouse brain parenchyma by co-option of pre-existing brain vessels. The presence of tumor did not affect the integrity of the brain vascular bed as illustrated by intactness of the blood-brain barrier [15]. In precontrast T1-weighted images these tumors could not be recognized, even after having reached considerable size (compare the image in Figure 1A to the matched H&E staining in Figure 1C). In line with intact blood-brain barrier function, these lesions were not highlighted in Gd-DTPA-enhanced MRI experiments as well (Figure 1B and figure 3). Note in this figure that large meningeal and/or skull blood vessels were contrast-enhanced, showing that Gd-DTPA had entered the circulation. This same result was obtained in all ten mice carrying parental and mock-transfected Mel57 tumors.

In T_2-weighted spin-echo images, parental Mel57 lesions were also not visible (compare the image in Figure 1D with the matched H&E-stained section in Figure 1F). However, after intravenous injection of the USPIO Sinerem, most of the lesions became visible as

hyperintense regions, compared to healthy brain parenchyma (compare Figure 1E to Figure 1F, the arrows point at lesions). Comparison of post- to pre-contrast images revealed that this effect was due to a signal decrease in the highly vascularized normal brain parenchyma while inside the lesions MR signal intensity was less affected. Identical results were obtained using both contrast agents with EGFP-transfected control tumors (data not shown). In all mice carrying parental- or mock-transfected tumors we did not detect any tumor in CE-MRI although we were able to prove histologically that tumors were abundantly present in every mouse.

VEGF-A expressing Mel57 tumors

In brains containing VEGF-A-expressing Mel57 tumors a completely different pattern of contrast enhancement was observed, both with T_1-weighted Gd-DTPA and T_2-weighted USPIO MRI. Although small lesions were not detected in precontrast T_1-weighted images, large lesions became faintly visible as hyperintense regions (compare the image in Figure 2A to its matched histological counterpart in Figure 2C). Intravenous administration of Gd-DTPA resulted in a marked, predominantly circumferential contrast enhancement of all lesions (Figure 2B). Acquisition of MR images at different time points post injection revealed that wash-out of the contrast agent occurred rapidly. MR signals in the tumor tarted to decline as soon as 2 minutes post injection (figure 3). Twenty minutes post injection, tumors could not be distinguished anymore on MR images (not shown). At that time, extravasated Gd-DTPA had redistributed through the entire brain, including tumor, leading to overall higher MR signal intensities than pre-contrast (see also figure 3). Again, this result was very reproducible as all five Mel57-VEGF carrying mice showed circumferential enhancement after Gd-DTPA injection.

Figure 1

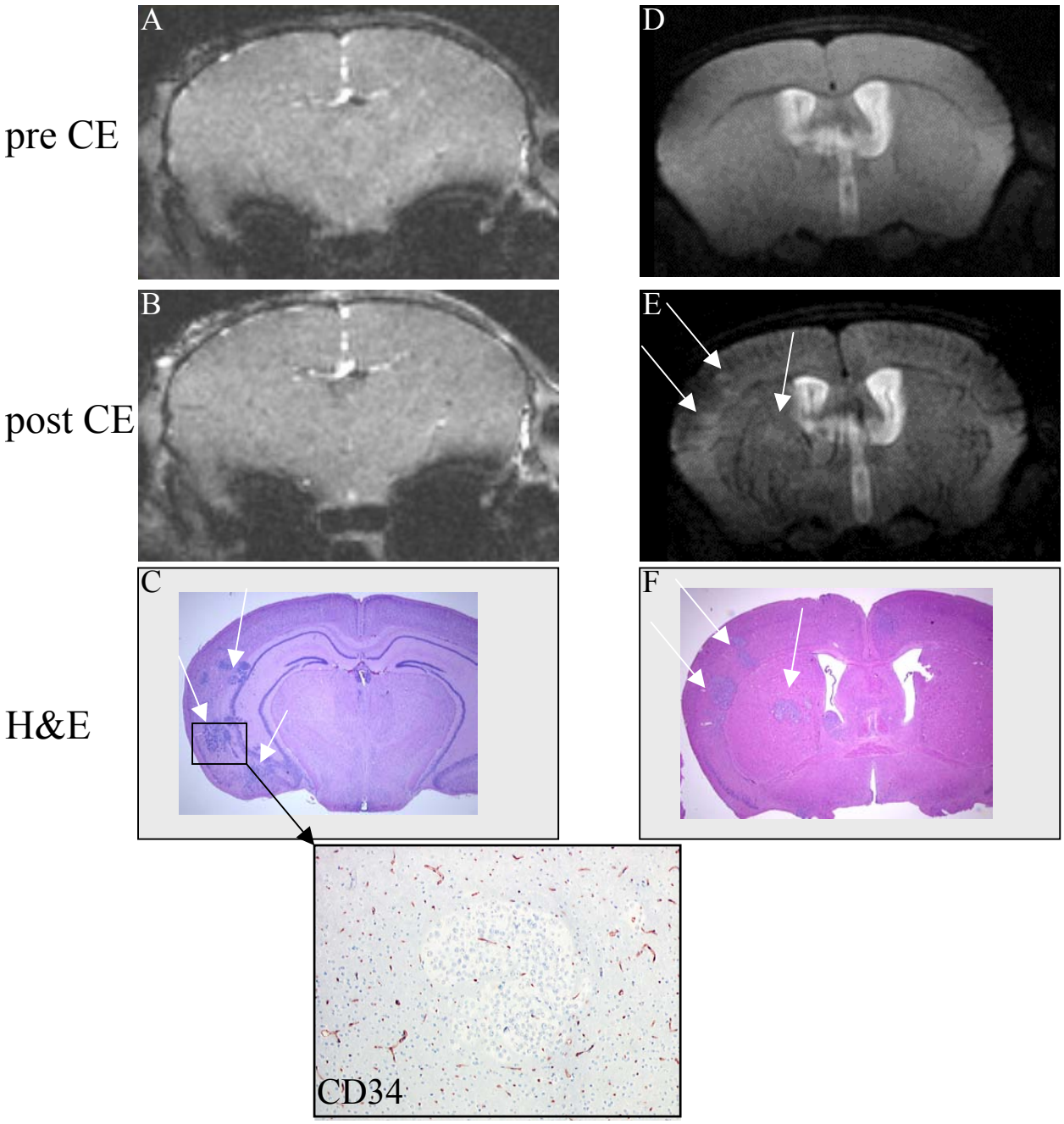

Fig 1. CE-MRI of mouse brain metastases of parental Mel57 human melanoma cells. T1-weighted gradient-echo images were acquired before (A) or directly after (B) injection of the contrast agent Gd-DTPA. Note that the contrast agent reached the brain as is evidenced by signal increase in the skull. C) Histology (H&E staining) of the slice corresponding to that in (A) and (B). Note that the lesions that are evident in C) are not recognized on the MR images, both pre- and post-contrast. In a different mouse, T2-weighted spin-echo MR images of brain, containing parental Mel57 tumors were acquired before (D) and after (E) injection of USPIO. The histology of the corresponding section is displayed in (F). Note that before contrast injection no lesions are visible, whereas after USPIO injection most lesions are visible as hyperintense regions (arrows in figure 1E and 1F). The inset shows a CD34 staining of the boxed tumor in C). Note also that the images, acquired in the MRI represent 1 mm slices while for H&E staining 4 µm slices are used. Perfect matching is therefore hardly possible. See also colour display page 152.

Figure 2

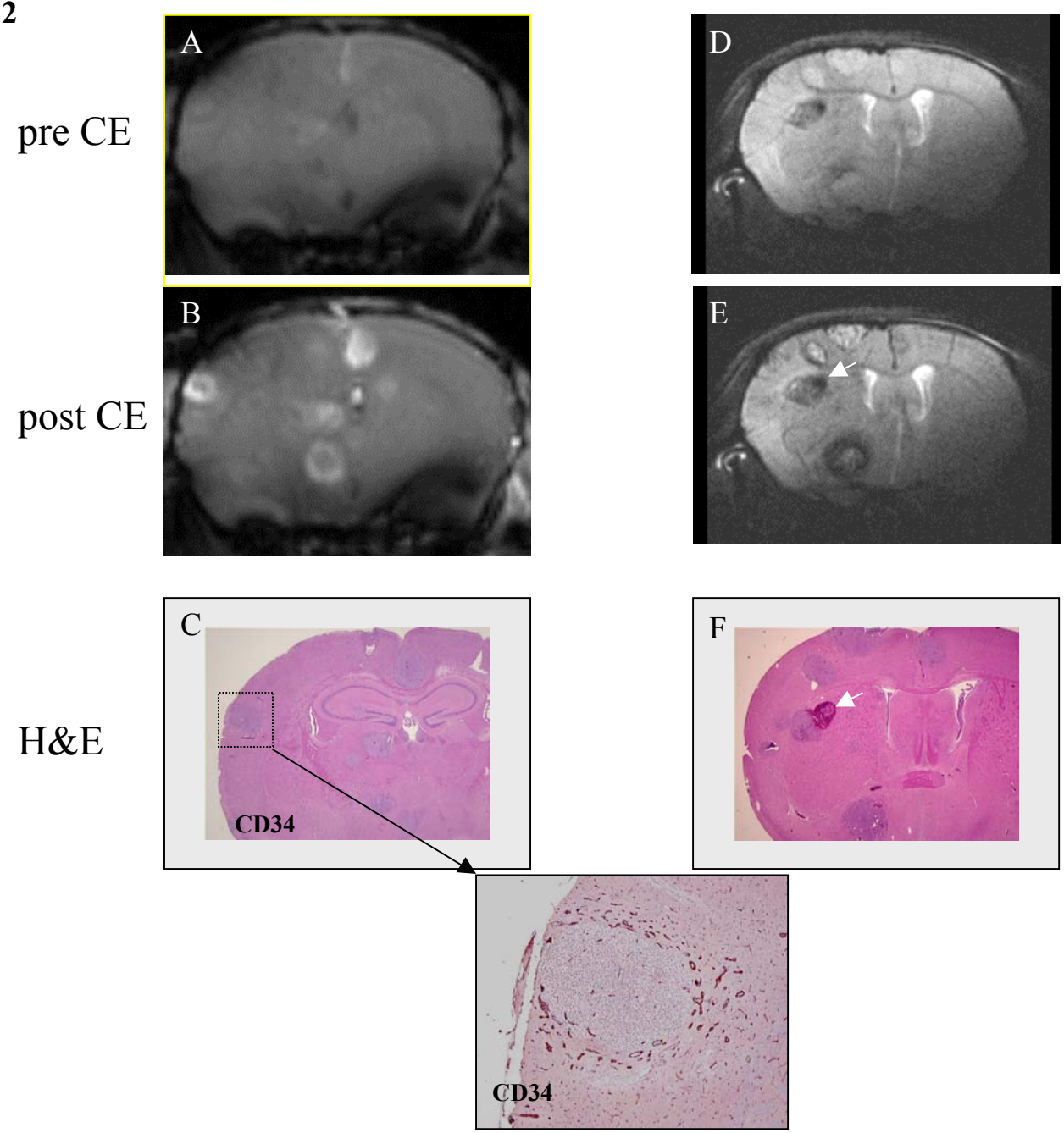

Fig 2. CE-MRI of Mel57 brain metastases, expressing VEGF-A. T1-weighted gradient-echo images were acquired before (A) or directly after (B) injection of the contrast agent Gd-DTPA. C) Histology (H&E staining) of the slices corresponding to that in (A) and (B). A CD34-immunostaining of the boxed tumor in (C) is shown to highlight the vasculature. Note that in (B) a strong peritumoral contrast enhancement is present, corresponding to dilated peritumoral, leaky vessels (inset in C). In a different mouse, T2-weighted spin-echo MR images of mouse brain Mel57-VEGF-A tumors were acquired before (D) and 2 minutes after (E) injection of USPIO. Histology of the corresponding section is displayed in (F). The arrowhead points at an intracerebral hemorrhage. Before injection of USPIO, lesions are detectable as hyperintense lesions while after injection lesions are strongly demarcated by peritumoral signal decrease. Intratumoral signal decrease is weaker than in the surrounding brain tissue, reflecting lower vessel density (F). See also colour display page 153.

Regions with contrast enhancement corresponded mainly to dilated vessels which were located at the tumor rim and in the peritumoral zone, adjacent to the main tumor mass. This conclusion is based on our histological finding that high numbers of irregular and highly dilated vessels were present in this peritumoral zone (Figure 2C, inset). We have previously demonstrated that these vessels were leaky by staining tissue sections for extravasated mouse immunoglobulins [15] and confirmed the permeability of these dilated vessels in all the VEGF-tumors investigated here (not shown). Therefore, these vessels must be the ones from which Gd-DTPA extravasates. The observation that contrast enhancement was mainly confined to the tumor rim/peritumoral zone and did occur only limited in the central parts of the lesions was in line with our previous finding that intralesional vessel density in these tumors was low [15]. Individual intratumoral, dilated and leaky vessels could also be recognized after Gd-DTPA injection as hyperintense spots.

In pre-contrast T_2-weighted spin echo images, Mel57-VEGF lesions were visible as hyper-intense areas (Figure 2D). Also, some lesions appeared as hypo-intense, presumably because of large haemoglobin concentrations and/or hemorrhages (arrow in figure 2D,F). After USPIO injection, the signal intensity of the peritumoral regions markedly decreased (Figure 2E), corroborating our previous histological finding that these regions contained highly dilated blood vessels [15]. Occasionally, within the lesions dot-shaped signal decreases were observed that corresponded to dilated individual intratumoral vessels (not shown).

Like in Gd-DTPA imaging, in USPIO-enhanced MRI the signal intensity change in Mel57-VEGF-A tumor-containing brains was confined to the peritumoral areas. Comparable to parental Mel57 tumors, the post-contrast signal intensity of the tumor mass was higher than that of the surrounding brain parenchyma, due to a lower intravascular volume inside the tumor (Figure 2C,F and inset).

Figure 3

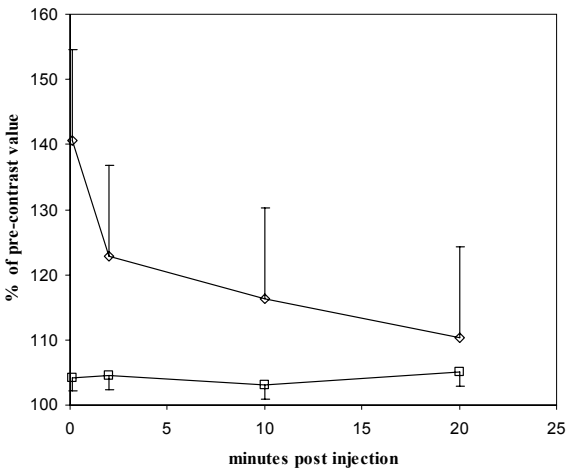

Fig 3. Semi-quantification of signal intensities after Gd-DTPA injection and wash out from mock-transfected or parental control tumors (□) or tumors expressing VEGF-A (◊).
Voxels containing tumor were selected and signal intensities measured over time. Values are depicted as mean of 9 lesions (in 5 different mice) +/- the standard deviation with the intensity of the pre-contrast voxels set at 100%. Note that, within this time frame, post contrast intensities do not return to pre-contrast levels, probably due to diffusion of Gd-DTPA through the brain. Differences in signal intensities between Mel57-VEGF and parental Mel57 tumors after Gd-DTPA injection were highly significant ($p<0.001$ for all time points examined).

Discussion

In a previous study we analyzed patterns of vascularization in a mouse model of hematogenous brain metastasis, utilizing the human melanoma cell line Mel57 [15]. Upon intracarotid injection, this cell line which produces minimal amounts of VEGF-A, grew in brain parenchyma solely by vascular co-option, i.e. without induction of an angiogenic switch. In Mel57 brain metastases that expressed high levels of the angiogenic factor VEGF-A we found that co-opted vessels, situated predominantly at the tumor periphery, were altered functionally and morphologically as they were irregularly dilated and permeable for large plasma proteins like immunoglobulins.

Here we have used two contrast agents with different properties to investigate the consequences of the different tumor vessel characteristics on radiological behavior in CE-MRI experiments. Gd-DTPA is a small, paramagnetic molecule which extravasates from leaky vessels into the surrounding interstitium. The rate and extent at which this occurs depend on several parameters, such as blood flow, vascular surface area, vessel permeability, interstitial pressure and extravascular space [3, 20]. In clinical practice, Gd-DTPA is used to detect vascular abnormalities that frequently occur in malignancies. The other contrast agent is an USPIO consisting of superparamagnetic iron oxide particles, coupled to polydextrane (Sinerem). Due to its relatively large size, USPIOs are regarded as blood pool agents [19, 21], especially immediately after i.v. injection [22]. The ironoxide causes T2 and T2* relaxation effects [23], of which the latter can be measured using gradient-echo MR sequences. Since at 7 T, spin-echo images were of better quality in our hands, we chose to acquire T2-weighted spin-echo images for Sinerem measurements.

When mice carrying parental Mel57 brain lesions were subjected to T_1-weighted MRI, lesions were not visible, even after injection of Gd-DTPA. This is consistent with our previous observation that vessels in these tumors are pre-existent brain capillaries in which the blood-

brain barrier is not affected [15]. On spin echo images after i.v. injection of USPIO, Mel57 lesions were visible as hyperintense regions due to lower vessel density than in the surrounding brain parenchyma.

There is clear clinical relevance to this finding. Low grade diffuse glial tumors also infiltrate brain parenchyma without inducing significant vascular changes [24]. Consequently, radiological diagnosis of these malignancies is often difficult, due to a lack of contrast enhancement by Gd-DTPA [5, 6]. Otherwise, tumors like glioblastoma multiforme often have a heterogeneous phenotype with areas lacking the vascular changes, considered typical for such tumors. The presence of such regions often leads to radiological underestimation of tumor size [25]. Our observations suggest that differences between vessel densities of tumor tissue and surrounding brain parenchyma, which often exist, are readily detectable using USPIO-enhanced MRI. This may therefore be a valuable additional tool for diagnosis of vessel co-opting brain tumors that do have altered vascular densities but lack functional vascular changes and thus are not detected using standard Gd-DTPA enhanced MRI.

In contrast to parental Mel57 brain lesions, large VEGF-A- producing lesions were frequently detected in both T_1-weighted gradient echo images and T_2-weighted spin echo images, probably due to hyperpermeability-induced edema in or around the tumor or to higher water contents in the tumor (e.g. due to larger interstitial space). Also, the increased concentration of haemoglobin, a result of vessel dilatation associated with Mel57-VEGF-A tumors, might have contributed to the appearance of these tumors in pre-contrast images (see also the appearance of the hemorrhage in figure 2D and F (arrow)). After Gd-DTPA injection, strong circumferential contrast enhancement readily demarcated these lesions. This contrast enhancement was transient, as within 10 minutes most of the contrast agent had spread through the brain tissue. The ring-shaped contrast enhancement was in line with our histological observation that dilated, hyperpermeable vessels were abundantly present immediately adjacent to the tumor lesions, in the tumor rim/peritumoral zones[15].

Clinical studies have already shown a correlation between VEGF-A production by tumors and Gd-DTPA contrast enhancement in MRI in primary and metastatic brain neoplasms [26, 27], but direct evidence for such a correlation has been lacking so far. Our data provide solid proof that VEGF-A, also known as Vascular Permeability Factor (VPF) [7], is a key factor that determines whether a tumor is visible in Gd-DTPA-enhanced MRI.

Interestingly, the pathology (growth pattern, central necrosis) and radiological behavior (ring-shaped contrast enhancement) of Mel57-VEGF-A lesions partly resembled that typical for high grade gliomas like glioblastoma multiforme (GBM), tumors that are infamous for high

VEGF-A expression levels. Our findings with Mel57-VEGF-A brain xenografts might also provide an explanation for the fact that in GBM, Gd-DTPA-enhancement frequently occurs at some distance from the tumor mass: VEGF-A, secreted by the tumor might diffuse over small distances from the tumor through the brain and cause permeability of vessels at the tumor rim and adjacent peritumoral vessels. In this respect it is important to realize that in our study we have used VEGF-A_{121}, the isoform of VEGF that can diffuse freely since it lacks affinity for extracellular matrix components like heparan sulfate proteoglycans (HSPGs) [28]. We are currently investigating whether expression of the larger VEGF isoforms, that are at least partially retained by the extracellular matrix, leads to different patterns of contrast enhancement.

The low intratumoral vessel density in Mel57-VEGF-A metastases was also evident from USPIO-enhanced MRI. The lesions did not show the signal decrease that was observed in distant brain tissue. In line with the high vascular volume at the tumor periphery, due to highly dilated vessels, the peritumoral zone displayed a very strong signal decrease. This demonstrated that these peritumoral vessels were perfused, supporting our hypothesis that enhanced tumor growth of Mel57-VEGF-A, as compared to parental Mel57 lesions, was due to a higher blood supply via dilated peritumoral vessels [15].

Interestingly, macromolecular contrast agents like USPIO have been used to improve MRI visualization of gliomas in a protocol where imaging was performed 12 hours post injection of contrast agent [29]. Whether at this stage the agent still can be considered blood-pool restricted is not clear since USPIOs may be phagocytosed by tumor cells or macrophages [30]. Performing MRI scans at an earlier time point may yield additional information.

Our observations have a number of important consequences:

1) In patients, suffering from vessel-co-opting brain tumors, in whom radiological diagnosis proves difficult due to low or absent Gd-DTPA enhancement, USPIO-enhanced MRI might yield valuable additional diagnostic information based on lower vessel densities within the tumor. Evenmore, it would also be worthwhile to subject patients, already diagnosed with GBM, to USPIO-enhanced MRI since vessel-co-opting regions within the tumor which do not enhance using Gd-DTPA may be identified as such.

2) Prudence is in order in CE-MRI follow-up of anti-angiogenic therapy, aimed at inactivation of VEGF-A. Tumors may initially become (partially) invisible in Gd-DTPA enhanced MR images, not because the lesion was irradicated, but because it was converted to a co-opting phenotype. We have recently demonstrated that this indeed occurs (manuscript in preparation). Otherwise, an anti-angiogenic treatment might be considered effective because

during MRI follow-up the tumor did not seem to have progressed, while it actually may have done so via vessel co-option. Recently, such adaptation of a tumor in response to anti-VEGF treatment has indeed been described [10, 31]. Also in these cases USPIO-enhanced MRI follow-up might be informative. We are currently testing this hypothesis by investigating the effects of anti-angiogenic therapies in our model.

3) From combined Gd-DTPA and USPIO– enhanced MRI images one might be able to predict whether anti-angiogenic treatment of tumors will be succesfull. Our data suggest that non-Gd-DTPA enhancing tumors will not be susceptible to anti-VEGF therapy.

Acknowledgements

B. Küsters is recipient of a research fellowship grant (920-03-149) from the Nederlandse Organisatie voor Wetenschappelijk Onderzoek (NWO, Dutch Organization for Scientific Research). This study was supported by the Dutch Cancer Society (grants KUN 2000-2302 and KUN 2001-2399). We are grateful to Debby Smits and Ilona v.d. Brink for technical assistance with the carotid artery injections and to Guerbet (Cedex, France) for providing Sinerem.

References

1. DeAngelis LM. Brain tumors. *N Engl J Med* 2001;344(2):114-23.

2. Middleton MR, Grob JJ, Aaronson N, Fierlbeck G, Tilgen W, Seiter S, et al. Randomized phase III study of temozolomide versus dacarbazine in the treatment of patients with advanced metastatic malignant melanoma. *J Clin Oncol* 2000;18(1):158-66.

3. Evelhoch JL. Key factors in the acquisition of contrast kinetic data for oncology. *J Magn Reson Imaging* 1999;10(3):254-9.

4. Earnest Ft, Kelly PJ, Scheithauer BW, Kall BA, Cascino TL, Ehman RL, et al. Cerebral astrocytomas: histopathologic correlation of MR and CT contrast enhancement with stereotactic biopsy. *Radiology* 1988;166(3):823-7.

5. Bendszus M, Warmuth-Metz M, Klein R, Burger R, Schichor C, Tonn JC, et al. MR spectroscopy in gliomatosis cerebri. *AJNR Am J Neuroradiol* 2000;21(2):375-80.

6. Ponce P, Alvarez-Santullano MV, Otermin E, Santana MA, Garcia Ludena MV. Gliomatosis cerebri: findings with computed tomography and magnetic resonance imaging. *Eur J Radiol* 1998;28(3):226-9.

7. Dvorak HF, Brown LF, Detmar M, Dvorak AM. Vascular permeability factor/vascular endothelial growth factor, microvascular hyperpermeability, and angiogenesis. *Am J Pathol* 1995;146(5):1029-39.
8. Bergers G, Javaherian K, Lo KM, Folkman J, Hanahan D. Effects of angiogenesis inhibitors on multistage carcinogenesis in mice. *Science* 1999;284(5415):808-12.
9. Borgstrom P, Bourdon MA, Hillan KJ, Sriramarao P, Ferrara N. Neutralizing anti-vascular endothelial growth factor antibody completely inhibits angiogenesis and growth of human prostate carcinoma micro tumors in vivo. *Prostate* 1998;35(1):1-10.
10. Kunkel P, Ulbricht U, Bohlen P, Brockmann MA, Fillbrandt R, Stavrou D, et al. Inhibition of Glioma Angiogenesis and Growth in Vivo by Systemic Treatment with a Monoclonal Antibody against Vascular Endothelial Growth Factor Receptor-2. *Cancer Res* 2001;61(18):6624-8.
11. Vermeulen PB, Colpaert C, Salgado R, Royers R, Hellemans H, Van Den Heuvel E, et al. Liver metastases from colorectal adenocarcinomas grow in three patterns with different angiogenesis and desmoplasia. *J Pathol* 2001;195(3):336-42.
12. Pezzella F, Pastorino U, Tagliabue E, Andreola S, Sozzi G, Gasparini G, et al. Non-small-cell lung carcinoma tumor growth without morphological evidence of neo-angiogenesis. *Am J Pathol* 1997;151(5):1417-23.
13. Passalidou E, Trivella M, Singh N, Ferguson M, Hu J, Cesario A, et al. Vascular phenotype in angiogenic and non-angiogenic lung non-small cell carcinomas. *Br J Cancer* 2002;86(2):244-9.
14. Neves S, Mazal PR, Wanschitz J, Rudnay AC, Drlicek M, Czech T, et al. Pseudogliomatous growth pattern of anaplastic small cell carcinomas metastatic to the brain. *Clin Neuropathol* 2001;20(1):38-42.
15. Kusters B, Leenders WP, Wesseling P, Smits D, Verrijp K, Ruiter DJ, et al. Vascular endothelial growth factor-A(165) induces progression of melanoma brain metastases without induction of sprouting angiogenesis. *Cancer Res* 2002;62(2):341-5.
16. Leenders W, Kusters B, De Waal R. Vessel co-option: How tumors obtain blood supply in the absence of sprouting angiogenesis. *Endothelium* 2002;9:83-87.
17. Leenders W, van Altena M, Lubsen N, Ruiter D, De Waal R. In vivo activities of mutants of vascular endothelial growth factor (VEGF) with differential in vitro activities. *Int J Cancer* 2001;91(3):327-33.
18. Kusters B, Westphal JR, Smits D, Ruiter DJ, Wesseling P, Keilholz U, et al. The pattern of metastasis of human melanoma to the central nervous system is not influenced by integrin alpha(v)beta(3) expression. *Int J Cancer* 2001;92(2):176-80.
19. Berry I, Benderbous S, Ranjeva JP, Gracia-Meavilla D, Manelfe C, Le Bihan D. Contribution of Sinerem used as blood-pool contrast agent: detection of cerebral blood volume changes during apnea in the rabbit. *Magn Reson Med* 1996;36(3):415-9.

20. van der Sanden BP, Rozijn TH, Rijken PF, Peters HP, Heerschap A, van der Kogel AJ, et al. Noninvasive assessment of the functional neovasculature in 9L-glioma growing in rat brain by dynamic 1H magnetic resonance imaging of gadolinium uptake. *J Cereb Blood Flow Metab* 2000;20(5):861-70.
21. Tropres I, Grimault S, Vaeth A, Grillon E, Julien C, Payen JF, et al. Vessel size imaging. *Magn Reson Med* 2001;45(3):397-408.
22. Sayegh Y, Pochon S, Vallee JP, Becker M, Lazeyras F, Tournier H, et al. Detection of experimental hepatic tumors using long circulating superparamagnetic particles. *Invest Radiol* 2001;36(1):15-21.
23. Yablonskiy DA, Haacke EM. Theory of NMR signal behavior in magnetically inhomogeneous tissues: the static dephasing regime. *Magn Reson Med* 1994;32(6):749-63.
24. Burger PC, Scheithauer BW. Tumors of the central nervous system, vol. 10. Washington: Armed Forces Institute of Pathology, 1994.
25. Nagashima G, Suzuki R, Hokaku H, Takahashi M, Miyo T, Asai J, et al. Graphic analysis of microscopic tumor cell infiltration, proliferative potential, and vascular endothelial growth factor expression in an autopsy brain with glioblastoma. *Surg Neurol* 1999;51(3):292-9.
26. Strugar J, Rothbart D, Harrington W, Criscuolo GR. Vascular permeability factor in brain metastases: correlation with vasogenic brain edema and tumor angiogenesis. *J Neurosurg* 1994;81(4):560-6.
27. Strugar JG, Criscuolo GR, Rothbart D, Harrington WN. Vascular endothelial growth/permeability factor expression in human glioma specimens: correlation with vasogenic brain edema and tumor-associated cysts. *J Neurosurg* 1995;83(4):682-9.
28. Park JE, Keller GA, Ferrara N. The vascular endothelial growth factor (VEGF) isoforms: differential deposition into the subepithelial extracellular matrix and bioactivity of extracellular matrix-bound VEGF. *Mol Biol Cell* 1993;4(12):1317-26.
29. Enochs WS, Harsh G, Hochberg F, Weissleder R. Improved delineation of human brain tumors on MR images using a long-circulating, superparamagnetic iron oxide agent. *J Magn Reson Imaging* 1999;9(2):228-32.
30. Dousset V, Gomez C, Petry KG, Delalande C, Caille JM. Dose and scanning delay using USPIO for central nervous system macrophage imaging. *Magma* 1999;8(3):185-9.
31. Rubenstein JL, Kim J, Ozawa T, Zhang M, Westphal M, Deen DF, et al. Anti-VEGF antibody treatment of glioblastoma prolongs survival but results in increased vascular cooption. *Neoplasia* 2000;2(4):306-14.

Chapter 5

Differential effect of VEGF-A isoforms in a mouse brain metastasis model of human melanoma

Benno Küsters
Robert M.W. de Waal
Pieter Wesseling
Kiek Verrijp
Cathy Maass
Arend Heerschap
Jelle O. Barentsz
Fred Sweep
Dirk J. Ruiter
William P.J. Leenders

Cancer Res, 2003; 63: 5408-5413

Abstract

We previously described that VEGF-A expression by Mel57 human melanoma cells leads to tumor progression in a murine brain metastasis model in an angiogenesis-independent fashion by dilation of co-opted pre-existent vessels and concomitant enhanced blood supply[1]. Here, we compare the activities of the 121, 165 and 189 VEGF-A isoforms in this model by transfecting Mel57 cells with the respective cDNAs and injecting the resulting stably transfected cell lines in the internal carotid artery of nude mice (n=10 for each isoform). Although the three isoforms had similar potency to induce endothelial cell proliferation, $VEGF_{121}$ expression did not result in sprouting angiogenesis, but rather led to extensive vasodilation and increased permeability of pre-existent, predominantly peritumoral vessels. Sometimes, proliferating endothelial cells accumulated in vessel lumina, giving these a microvascular glomeruloid-proliferation-like appearance. Expression of $VEGF_{165}$ or $VEGF_{189}$ was associated with induction of an intratumoral neovascular bed. In $VEGF_{165}$-expressing tumors, daughter endothelial cells were distributed among newly formed vessels which were heavily dilated. This also occurred in $VEGF_{189}$-tumors but there, vasodilation was less pronounced. Using contrast-enhanced magnetic resonance imaging (CE-MRI), the different vascular phenotypes were reflected by characteristic radiological images. $VEGF_{165}$ expression was the most unfavorable of the three: mice carrying $VEGF_{165}$ tumors became moribund earlier than those carrying $VEGF_{121}$ expressing tumors (16+/- 4 days vs. 22 +/- 3 days). Our data demonstrate that VEGF-A-isoforms differ in angiogenic properties which can be visualized by CE-MRI.

Introduction

Angiogenesis, the formation of new blood vessels from pre-existing ones, is a complex process that is regulated by a vast array of stimulators and inhibitors. Of these, Vascular Endothelial Growth Factor-A (VEGF-A) is regarded as the most potent pro-angiogenic factor. Via binding and activation of the tyrosine kinase receptors VEGFR1 and VEGFR2 (also named Flt-1 and KDR/Flk-1, respectively), endothelial cell proliferation, migration, and expression of Tissue Factor and proteases are induced[2,3]. These concerted actions lead to blood vessel permeability, followed by extravascular deposition of a fibrin network which serves as a provisional matrix for newly formed daughter endothelial cells [4].

VEGF-A is member of a family of growth factors also comprising VEGF-B,C,D,E, Placental Growth Factor (PlGF) and the platelet derived growth factors (PDGF-A and B) [2]. Alternative splicing of VEGF-A pre-mRNA leads to secretion of six variants of this homodimeric molecule consisting of 121, 145, 165, 183, 189 and 206 amino acid residues, respectively [5,6]. In mice these isoforms have one amino acid residue less. With the exception of $VEGF_{121}$, these proteins have affinity for heparin and heparan sulphate proteoglycans (HSPGs) that increases with length due to the presence of positively charged domains, encoded by exon 7 in $VEGF_{165}$ and exons 6 and 7 in $VEGF_{189}$ and $VEGF_{206}$ [7,8]. The exon 7-encoded sequence also confers affinity upon $VEGF_{165}$ for the co-receptors neuropilin 1 and 2. In cell culture $VEGF_{189}$, and to a lesser extent $VEGF_{165}$, are sequestered by HSPGs on the cell surface. It is assumed that in this way the extracellular matrix functions as a reservoir of biologically inactive VEGF-A which, when needed, can be released quickly as aminoterminal bio-active fragments by the action of proteases [9-11].

Although $VEGF_{121}$ itself does not bind to heparin or HSPGs, the latter are required for efficient receptor activation [7]. Both VEGFR1 and VEGFR2 have heparin binding domains, suggesting that receptor-bound HSPGs stabilize the ligand-receptor complex [12-14]. *In vitro*, $VEGF_{121}$ binds to VEGFR1 with 20-fold lower affinity than $VEGF_{165}$ [15] and it is also less potent in activating VEGFR2 [11]. Remarkably, $VEGF_{121}$ and $VEGF_{165}$ have been reported to have similar angiogenic activities *in vivo* [16,17]. The presence of ligand-receptor complex-stabilizing HSPGs *in vivo* that are absent *in vitro* may account for the apparent difference in $VEGF_{121}$ potencies in both settings.

In vitro studies have unraveled in detail the molecular biology and cell biology of VEGF/VEGFR signaling. However, it is only since recently that attention is paid to *in vivo* activities of individual VEGF-A isoforms. Data obtained by the group of Carmeliet using knock-in mice that selectively express individual VEGF-A isoforms in cardiac muscle showed

that $VEGF_{164}$ is sufficient for normal embryonic vascular development. In hearts where only $VEGF_{188}$ was expressed, arterial development was significantly affected, while venous development appeared normal. Exclusive $VEGF_{120}$ expression led to lethal disturbances in vascular development [18,19].

Contradictory reports exist towards the functional importance of $VEGF_{121}$ in tumor biology. When overexpressed in a colon tumor xenograft model, $VEGF_{121}$ increased vascularity and enhanced tumor growth [20] while in recent reports expression of $VEGF_{165}$ and $VEGF_{189}$, but not $VEGF_{121}$, correlated with increased vascular density and poor prognosis [21-23].

Interestingly, Guo et al. described that the ability of $VEGF_{121}$ to induce angiogenesis depended on the site of tumor growth: $VEGF_{121}$ minimally enhanced angiogenesis in and growth of subcutaneous gliomas, whereas in brain the same $VEGF_{121}$-expressing tumor generated an angiogenic response [24]. Some reports described that $VEGF_{121}$ and $VEGF_{165}$ expression in brain tumor models led to cerebral hemorrhage and $VEGF_{189}$ caused sprouting angiogenesis, while other reports stated that $VEGF_{189}$ lacks any angiogenic activity [25,26].

We previously described that the human melanoma cell line Mel57 has low background production of angiogenic factors and grew in murine brain parenchyma by co-option of pre-existent brain vessels, i.e. without inducing an angiogenic response and without notably affecting pre-existing vessels [1]. In these tumors, even after having reached considerable size, hardly any hypoxia developed. This makes this system particularly convenient to study angiogenic activities of different factors, since results are not biased by upregulation of endogenous VEGF-A, an event known to occur in response to hypoxia. Using this model, we previously described that recombinant VEGF-A was not able to induce an angiogenic response but instead modulated pre-existent vessels by dilation, induction of hyperpermeability, loss of blood-brain barrier markers and upregulation of a number of molecules, characteristic for activated endothelial cells [1] . In contrast-enhanced magnetic resonance imaging (CE-MRI) scans, VEGF-A-expressing tumors were easily recognized, while parental Mel57 tumors were undetectable [27].

Here we report on the vascular phenotypes and MRI behaviour of Mel57 brain tumors expressing either of the three VEGF-A isoforms.

Materials and Methods

Cell lines and transfections. Mel57 human melanoma cells were maintained in Dulbecco's Modified Eagles Medium (DMEM, Life Technologies, Breda, The Netherlands) supplemented with 10% fetal calf serum (FCS) and penicillin/streptomycin. cDNAs encoding

the 121, 165 and 189 aa VEGF isoforms (human origin) were cloned in vector pIRESneo (Clontech) to generate plasmids pIRESneoVEGF$_{121}$, pIRESneoVEGF$_{165}$ and pIRESneoVEGF$_{189}$. All sequences were verified by DNA sequencing (AbiPrism, Applied Biosystems). Plasmid pIRESneoVEGF$_{165}$ was different from the VEGF$_{165}$ construct published before [1] as the cDNA in that plasmid had a slightly modified 3' end. Plasmids were stably transfected into Mel57 cells as described [1]. Presence of recombinant proteins in conditioned media was confirmed by SDS-PAGE and western blotting experiments using antibody VEGF-A20 (Santa Cruz). In case of VEGF$_{189}$, 5 IU/ml heparin (Leo systems, Breda, The Netherlands) was included in the culture medium prior to analysis. VEGF concentrations were also determined using an in-house developed ELISA[28].

Animal experiments. All experiments were approved by the Animal Experiment Committee of the Nijmegen University. The hematogenous brain metastasis protocol has been described previously [29]. In short, 10^5 Mel57 (transfectant) cells were microsurgically injected into the right internal carotid artery of BALB/C nude mice (n= at least 10 for each cell line). After 14-21 days, depending on which isoform was expressed, animals became moribund, due to cachexia or development of neurological defects. At this stage, CE-MRI was performed (see below) after which animals were killed by intravenous injection of an overdose barbiturates. Brains were removed and either fixed in formalin or snap-frozen in liquid nitrogen.

3D-reconstruction of tumor vessels by ink perfusion. Moribund tumor-bearing mice (three from each group) were anaesthesized and microsurgically injected into the supra-aortic branches with 5 ml of indian ink, containing 5,000 U/ml heparin. After this procedure, brains were removed, fixed in buffered formalin for 24 hrs and 0.5 mm sections were cut and examined under a transmission microscope with bright light. By focussing through different layers of the section a good impression of the 3D vascular structure was obtained.

Immunohistochemistry. Immunostainings were performed using antibodies directed against murine Ki67 as a proliferation marker (Dianova, Hamburg, Germany), the endothelial markers CD31 and CD34 (Hycult, Uden, The Netherlands), VEGFR2 (Santa Cruz, CA, USA) and the blood brain barrier marker Glut-1 (DAKO, Glostrup, Denmark). Antibodies against the pericyte marker α-smooth muscle actin were obtained from Sigma (Zwijndrecht, The Netherlands). Extravascular mouse immunoglobulins were detected with a biotin-labeled anti-

mouse IgG. Secondary biotin-labeled antibodies were visualized by ABC staining according to standard protocols (VECTOR, Burlingame, CA, USA).

Magnetic resonance imaging. Mice were anaesthetized (1.3% isoflurane; 1:1 (v/v) N_2O/O_2 mixture), catheterized in the tail vein, and placed in an MR spectrometer (S.M.I.S. console equipped with a Magnex Scientific 7T/200mm horizontal bore magnet and a 150mT/m gradient set). Body temperature was maintained at 37^{o}C with a circulating warm water bed. After initial monitoring of the mouse brain with fast gradient-echo scout images using a 12 mm surface coil, twenty contiguous high-resolution coronal MR images were acquired with T_2-weighted multislice spin-echo imaging (T_E = 50 ms; T_R = 3000 ms; FOV= 40x40 mm; matrix size = 512x512; slice thickness = 1 mm) before and 2 minutes after intravenous injection of 0.2 ml of USPIO (ultrasmall superparamagnetic iron oxide-coated dextran, Sinerem®, Guerbet, France) (12.5 mg/kg). In case of Gd-DTPA (gadolinium diethylenetriaminepenta-acetic acid) contrast enhancement, 16 contiguous images were acquired with a T_1-weighted multislice gradient-echo sequence (T_E= 8 ms; T_R = 100 ms; field of view = 25x25 mm; matrix size = 256x256; slice thickness = 1 mm) before and at several time points (0, 2, 10 and 20 minutes) after bolus injection (0.2 ml; 0.2 mmol/kg) of Magnevist® (Schering, Germany).

Results

Effects of VEGF-A isoforms on growth of Mel57 brain lesions. To examine the effects of the 121, 165 and 189 isoforms of VEGF-A on tumor growth in mouse brain, we generated stable transfectants of the human melanoma cell line Mel57, expressing either isoform *in vitro* at levels of 30-100 ng/ml/10^6 cells/48 hrs (as determined by ELISA, not shown). Recombinant proteins were of the correct molecular weights as determined by western blotting (not shown). Before transfection, this cell line expresses very low endogenous levels of angiogenic factors, especially VEGF-A [30,31]. After intracarotid injection of parental Mel57 cells, metastatic lesions formed in the parenchyma that grew infiltratively by vascular co-option without notable vascular changes [1,27]. In tumors expressing either VEGF-A isoform we found upregulation of the endothelial markers CD31, CD34, VEGFR2 and the activated pericyte marker α-smooth muscle actin (figure 1A-C and not shown). There was no significant effect of VEGF-A isoform expression on the number of lesions that developed (not shown). All isoforms induced proliferation of endothelial cells, as demonstrated by mouse-specific immunostaining for the proliferation marker Ki67 (figure 1J-L). Furthermore, staining for

murine IgGs, that normally do not pass the blood brain barrier, revealed that all isoforms caused extravasation of macromolecules indicating vessel hyperpermeability (figure 1G-I). Besides these common VEGF-A effects, striking differences were found between vascular morphologies as described below. *In situ* hybridization with an antisense VEGF-A RNA probe revealed that also *in vivo,* expression levels of the three isoforms were comparable (not shown), indicating that the differences were qualitative.

VEGF$_{121}$

After injection of Mel57-VEGF$_{121}$ cells, tumors developed with a combined infiltrative and expansive phenotype. Animals were moribund due to cachexia or neurological defects reproducibly three to four weeks after injection of tumor cells. Immunostaining for the endothelial marker CD34 revealed that in the peritumoral zone irregularly dilated vessels were present (figure 1A). Tumor cells could often be observed along these vessels indicating migration in the perivascular space (arrow in figure 1A, inset). Vessel densities within tumor nests were relatively low as was demonstrated by CD34 immunohistochemistry (figure 1A) and by 3D visualization established by ink perfusion (figure 2B). The low intratumoral vessel density and the morphology of peritumoral vessels indicated a lack of sprouting angiogenesis. In some tumors, the low intratumoral vessel density resulted in central hypoxia and necrosis (figure 1D, note that Glut-1, besides being a marker for the blood brain barrier (see below), also is upregulated on hypoxic cells). Although VEGF$_{121}$ clearly lacked the capacity to induce sprouting angiogenesis, it was yet a strong inducer of endothelial proliferation (see the murine Ki67 staining in figure 1J). Focally, glomeruloid-like microvascular proliferations consisting of endothelial cells and pericytes were present (arrow in figure 1J), resembling a phenotype that is often encountered in high grade glial brain tumors like glioblastoma multiforme [32]. Glucose transporter-1 (Glut-1) is a membrane protein that is specifically expressed on endothelial cells of brain vessels and is regarded as a blood-brain barrier marker [33]. The dilated vessels in and around VEGF$_{121}$ lesions had a mosaic Glut-1 phenotype, some endothelial cells being positive and others negative (figure 1D), consistent with a loss of blood-brain barrier function.

VEGF$_{121}$-induced peritumoral vascular effects were reflected in CE-MRI. Intravenous injection of the paramagnetic, low molecular weight compound Gd-DTPA in mice carrying VEGF$_{121}$-expressing lesions led to predominantly circumferential signal increase immediately after injection, whereas centrally in tumor nests no notable enhancement was observed (figure

3A). Peritumoral enhancement was entirely due to expression of $VEGF_{121}$, since it was absent in mice carrying parental Mel57 lesions [27]. A similar pattern of enhancement was obtained after intravenous injection of USPIOs that, due to large size, are assumed to remain intravascularly [34]. Again predominantly circumferential enhancement occurred (figure 3B), although individual, dilated, intratumoral vessels were also highlighted (note that the nature of MR sequence used, causes a drop of signal intensity). This enhancement pattern lasted for up to 4 hours post injection, while Gd-DTPA enhancement was much more transient, having disappeared within 20 minutes post injection (not shown).

$VEGF_{165}$ and $VEGF_{189}$

When $VEGF_{165}$ or $VEGF_{189}$ was expressed by Mel57 brain tumors, mice developed terminal cachexia and neurological defects approximately two and three weeks post injection, respectively. The tumor vasculature that had formed was very different from that induced by $VEGF_{121}$. Now, extensive neo-angiogenesis had occurred (see CD34 staining in figure 1B,C and 3D visualization in figures 2C,D) while peritumoral vascular effects were hardly observed, in contrast to the $VEGF_{121}$ situation (figure 2B). $VEGF_{165}$-expressing lesions displayed prominent vessel dilation and permeability with numerous proliferating endothelial cells (figure 1B,E,K). Consistent with the high vascular volume in these tumors, necrosis was never observed. In the border regions of these tumors, vessels were partly Glut-1 negative (figure 1E, thin arrowhead) while this protein was completely absent in vessels in the tumor centre (bold arrowhead). In the $VEGF_{189}$-expressing metastases, a dense network of microcapillaries had formed that were leaky and had diminished Glut-1 expression, whereas vessel dilation was minimal. Consistent with the high intratumoral vascular volumes, $VEGF_{165}$- or $VEGF_{189}$-expressing tumor nests were entirely contrast-enhanced in Gd-DTPA and USPIO-enhanced MR images (figure 3C-F). The wash-out rates of Gd-DTPA were not notably different from that of the $VEGF_{121}$-expressing tumors, since 10-20 minutes post injection signals had returned to basal levels (not shown). Due to the earlier time point at which mice carrying $VEGF_{165}$ -lesions became moribund, these lesions were generally smaller than $VEGF_{121}$ lesions.

Figure 1

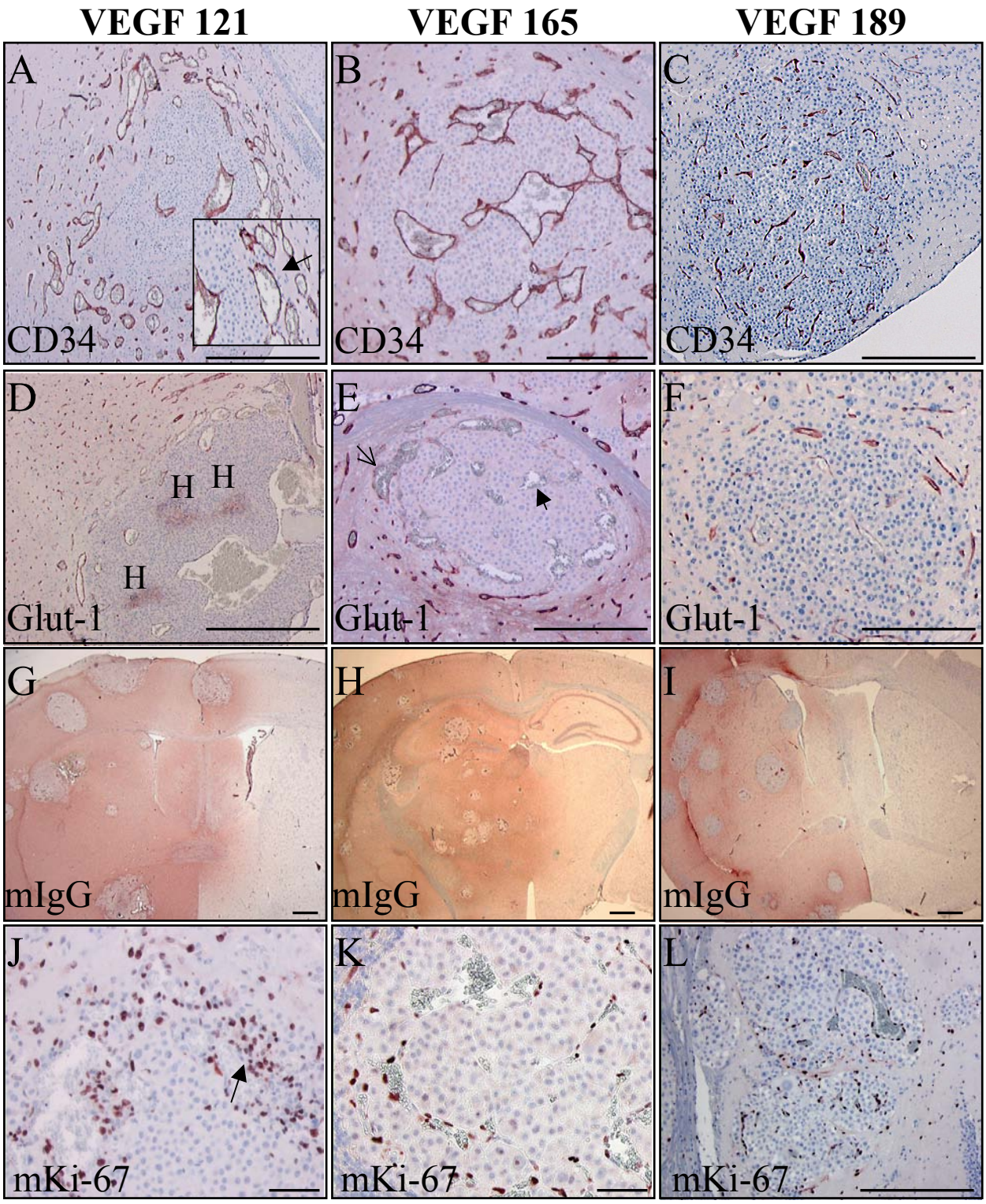

Fig 1 – Immunohistochemical analysis of mouse brain Mel57 lesions, expressing VEGF isoforms as indicated. A-C: CD34 endothelial staining, D-F: staining for Glut-1, a blood-brain barrier specific protein, G-I: staining for murine IgG, showing cumulative leakage of immunoglobulins from permeable vessels, J-L: staining for the murine proliferation marker Ki67. The arrow in J) points at a glomeruloid-like vascular proliferation, while in K) and L) daughter endothelial cells are redistributed over newly formed vessels. Note the predominantly peritumoral effects on the vasculature by $VEGF_{121}$ (A) while expression of the two other isoforms lead to predominantly intratumoral vascular effects (B,C). The arrows in E) point at Glut-1 negative (arrow) and mosaic vessels (small arrowhead). H=hypoxia, which manifests as Glut-1 positivity . The bars represent 0.5 mm. See also colour display page 154.

Figure 2

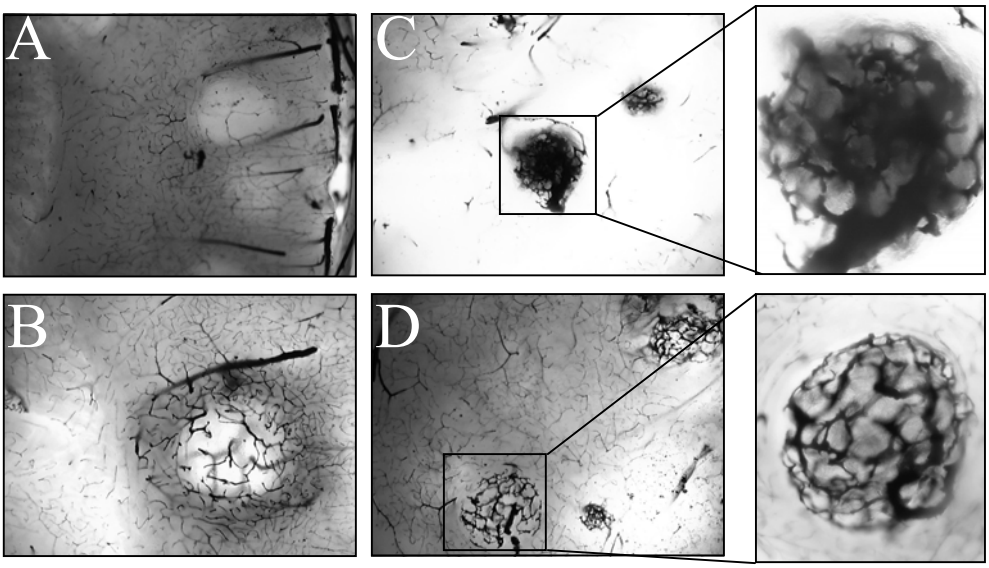

Fig 2 –3D visualization of brain tumor vasculature. Mice carrying parental Mel57 (A), Mel57-VEGF121 (B), Mel57-VEGF165 (C) and Mel57-VEGF189 (D) tumors were perfused with indian ink as described in Materials and Methods. Brains were cut into 0.5 mm sections and examined under a transmission light microscope. Lesions were easily identified on basis of different optical breaking indices compared to normal brain tissue. White areas in A and B represent the (poorly vascularized) lesions. Microscope magnifications were 50x and 200x (insets). Since mice carrying $VEGF_{165}$-lesions became moribund 14 days post injection of the tumor cells, i.e. one week earlier than the other mice (see text), $VEGF_{165}$ lesions were relatively small. Due to the amount of light needed to visualize these relatively small, very dark lesions, the surrounding brain tissue is hardly visible in C.

Figure 3

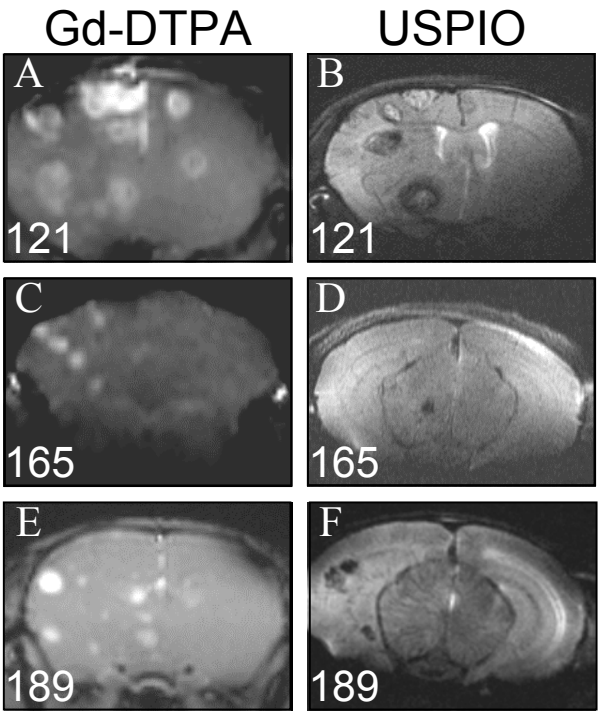

Fig 3 – Contrast-enhanced MRI of murine brains carrying Mel57 lesions expressing the different VEGF-isoforms. T1-gradient echo (A,C,E) or T2-spin echo sequences (B,D,F) were used to detect Gd-DTPA and USPIOs respectively. The images shown are acquired 2 minutes after intravenous bolus injection of both contrast agents.

Discussion

We report here that, in striking contrast to $VEGF_{165}$ and $VEGF_{189}$, $VEGF_{121}$ is not able to induce angiogenic sprouting in metastatic melanoma in mouse brain. Rather, the small isoform caused extensive dilation and permeability of pre-existent blood vessels, a phenotype which is very similar to what we described previously for $VEGF_{165}$ [1]. However, in that study we used a $VEGF_{165}$ molecule that carried a mutation of the carboxyl terminus. At that time we considered this a wild type protein as the carboxyl terminus had not been recognized in the literature as functionally important. Furthermore, this protein was indistinguishable from commercially obtained $wtVEGF_{165}$ in a number of *in vitro* functional and receptor binding assays. To our surprise we have now found that when the carboxyl terminus was unmodified, a different vascular phenotype developed than we previously described, indicating that the carboxyl terminus is critical for full VEGF activity. These findings imply that different biological activities of $VEGF_{165}$ can be dissected using these mutants (manuscript in preparation).

Interestingly, in a recent report Bates et al. described the identification of $VEGF_{165b}$, a splice variant which lacks the carboxyterminal exon 8 sequence [35]. Despite intact binding domains for VEGFR1, VEGFR2 and neuropilins, this protein behaved as a VEGF receptor antagonist, thus confirming the importance of the carboxyl terminus for VEGF activity. How exactly exon 8-encoded sequences contribute to VEGF-A activity is still enigmatic.

In contrast to $VEGF_{121}$, $VEGF_{165}$ and $VEGF_{189}$ induced extensive sprouting angiogenesis in our model. The phenotypes of tumors expressing these larger isoforms could also be distinguished since $VEGF_{165}$ induced profound vasodilation, whereas $VEGF_{189}$ failed to do so. Interestingly, expression of $VEGF_{165}$ appeared to correlate with worse clinical outcome since we consistently found that mice carrying $VEGF_{165}$-expressing brain tumors became symptomatic already after approximately two weeks, one week earlier than those expressing $VEGF_{121}$ or $VEGF_{189}$. The reason for this difference is not clear: it is not likely to be a result of enhanced growth of the $VEGF_{165}$-expressing tumors. In a time-matched experiment, we found no significant differences between the sizes of the various brain lesions, although within individual animals tumor sizes showed a high degree of heterogeneity (not shown). Possibly the combination of extensive vasodilation and hyperpermeability induced by $VEGF_{165}$ led to more severe edema in the surrounding brain tissue than that induced by the other isoforms. We have not examined this in detail.

In all VEGF-expressing tumors, irrespective of the isoform, the blood brain barrier marker Glut-1 was absent or only partially expressed on vessels. Whether VEGF-A actively

downregulates Glut-1 expression on pre-existing brain vessels, or newly formed endothelium simply does not express this brain endothelium-specific protein, is not completely clear. The fact that in $VEGF_{165}$-lesions intratumoral vessels were completely negative for Glut-1 while at the tumor rim mosaic vessels were found, is in favor of the second option: at the tumor rim, pre-existent vessels become gradually influenced by tumor-derived VEGF-A leading to a mixture of mother endothelial cells (Glut-1 positive) and daughter cells (Glut-1 negative). As endothelial cell proliferation continues, Glut-1-negative endothelial cells will become more and more abundant until in the intratumoral vessels, they prevail.

Depending on which VEGF-isoform was expressed, tumors had distinct patterns of contrast-enhancement in MRI experiments. Tumors that expressed $VEGF_{121}$ characteristically showed a circumferential enhancement, due to a peritumorally located, dilated and leaky vasculature, combined with low intratumoral vessel density. The larger isoform-expressing tumors showed a more homogeneous, bulky enhancement. These MR images were in good agreement with our morphological findings. Peritumoral Gd-DTPA enhancement in the $VEGF_{121}$-expressing tumors indicated the presence of leaky vessels outside the main tumor mass from which the contrast agent could extravasate and accumulate in the surrounding tissue, while the strong signal drop after USPIO injection was in accordance with the high density of dilated vessels, causing a high local vascular volume. The relatively low intratumoral vessel density accordingly led to low levels of enhancement of the lesion itself, both with Gd-DTPA and USPIOs. The bulky enhancement seen in $VEGF_{165}$ and $VEGF_{189}$ lesions was also in accordance with the high vascular volume of these tumors. Whether CE-MR images of human tumors can be correlated to VEGF isoform expression is not known. If so, it may be of help for prognosis and possibly for selection of patients that are candidates for anti-VEGF therapy. In a preliminary study we found that the heterogeneity in expression levels of the different VEGF-isoforms in human tumors makes this question difficult to answer.

Differential effects of the various VEGF-A isoforms have only recently received attention in the literature. Via targeted disruption of specific VEGF exons, Carmeliet et al. have generated mice that selectively express $VEGF_{120}$. $VEGF_{120}$ could not substitute for the larger isoforms as during development these mice developed severe angiogenesis-related abnormalities [36,37]. These defects might in fact be related to vasculogenesis rather than angiogenesis, since $VEGF_{121}$ and $VEGF_{165}$ are equally effective in inducing angiogenesis in the chick chorioallantoic membrane angiogenesis assay and collateral formation in ischemic rabbit hindlegs [17]. In a recent report, $VEGF_{120}$ was described to be relatively incapable of inducing branching of blood vessels in various organs during development [38].

In tumors, controversial observations have been reported regarding VEGF isoform activities. VEGF-null fibroblasts have been generated and used to establish fibrosarcomas expressing each individual VEGF isoform [39]. Analysis of subcutaneous tumors grown from these cell lines revealed that only $VEGF_{164}$ could compensate for the lack of the endogenous VEGF gene while $VEGF_{120}$ had a negligible angiogenic effect. In this model $VEGF_{188}$ expression led to highly vascularized, yet small, tumors. From these data the hypothesis emerged that $VEGF_{120}$ diffuses away from the tumor and recruits vasculature from surrounding tissue, while the ECM-binding isoform $VEGF_{188}$ induces local branching and sprouting angiogenesis. In this model, the $VEGF_{164}$ isoform has intermediate activity. This model is consistent with our current findings: whereas $VEGF_{121}$ failed to induce an intratumoral neovascular bed, $VEGF_{189}$ expression in our brain model led to highly vascularized and relatively large tumors. This largely confirms results from other groups [24,25] and might be explained by the fact that in the vessel-dense brain there is no need for extra recruitment of blood vessels from the surroundings [1].

The difference between $VEGF_{121}$ and $VEGF_{165}$ is the presence of the exon 7-encoded domain in $VEGF_{165}$, which is responsible for neuropilin and HSPG binding. Neuropilin 1 potentiates the activity of the VEGF-A/VEGFR2 complex [40] and HSPGs can act as chaperone for $VEGF_{165}$ [41] or even transmit $VEGF_{165}$ signals [42]. In this light it was a remarkable observation that $VEGF_{121}$ induced extensive endothelial cell proliferation, a VEGFR2-mediated response, in pre-existent vessels to an extent that at least equaled that induced by the larger VEGF isoforms. This suggests that neuropilin 1- enhanced VEGFR2 binding can not account for the difference between the *in vivo* activities of the 121 and 165 -isoforms. A second argument against a role for neuropilin and HSPGs in the $VEGF_{165}$-induced tumor phenotype can now be found in our previous study, in which we used a $VEGF_{165}$ mutant (see above) [1]. This mutant did contain the intact exon 7 sequence and therefore had intact neuropilin and HSPG affinity. Nevertheless, it did not induce sprouting angiogenesis but led to a $VEGF_{121}$-like vascular phenotype.

An interesting observation was that $VEGF_{121}$ was an efficient inducer of endothelial cell proliferation in the absence of sprouting angiogenesis. This shows that activation of VEGFR2, the receptor that is responsible for proliferation, occurred but was not sufficient for angiogenesis in this model, contrary to what is generally believed. Obviously, endothelial proliferation via VEGFR2 activation is a critical step in the initial stages of angiogenesis, but is not sufficient for completion of this process: migration, adhesion and protease activities obviously are necessary as well. Remarkably, in a recent report it was shown that $VEGF_{121}$, in

contrast to the larger VEGF-A isoforms, was unable to mediate endothelial migration in vitro [43], possibly because extracellular matrix-bound VEGF-A is needed for migration. Whether this concept also explains our *in vivo* results remains to be established. Alternatively, certain signals, induced by $VEGF_{165}$ and $VEGF_{189}$ may fail to occur in the $VEGF_{121}$-induced signal transduction cascade, thereby rendering $VEGF_{121}$ unable to induce sprouting angiogenesis. It would be interesting to know the nature of these signals and the receptors from which they emerge, since apparently the differences between $VEGF_{121}$ and $VEGF_{165}$ activities can not be solely attributed to differential binding to neuropilins, VEGFR2 and HSPGs.
These issues are currently under investigation in our lab.

Acknowledgements – We are grateful to Debby Smits, Geert Poelen and Ilona van der Brink for technical assistance with the carotid artery injections and to Guerbet (Cedex, France) for providing Sinerem.

References

1. Kusters, B., Leenders, W. P., Wesseling, P., Smits, D., Verrijp, K., Ruiter, D. J., Peters, J. P., van Der Kogel, A. J., and de Waal, R. M. Vascular endothelial growth factor-A(165) induces progression of melanoma brain metastases without induction of sprouting angiogenesis. Cancer Res., *62:* 341-345, 2002.

2. Neufeld, G., Cohen, T., Gengrinovitch, S., and Poltorak, Z. Vascular endothelial growth factor (VEGF) and its receptors. Faseb J., *13:* 9-22, 1999.

3. Clauss, M. Molecular biology of the VEGF and the VEGF receptor family.[In Process Citation]. Semin. Thromb. Hemost., *26:* 561-569, 2000.

4. Nagy, J. A., Meyers, M. S., Masse, E. M., Herzberg, K. T., and Dvorak, H. F. Pathogenesis of ascites tumor growth: fibrinogen influx and fibrin accumulation in tissues lining the peritoneal cavity. Cancer Res., *55:* 369-375, 1995.

5. Poltorak, Z., Cohen, T., and Neufeld, G. The VEGF splice variants: properties, receptors, and usage for the treatment of ischemic diseases. Herz, *25:* 126-129, 2000.

6. Poltorak, Z., Cohen, T., Sivan, R., Kandelis, Y., Spira, G., Vlodavsky, I., Keshet, E., and Neufeld, G. VEGF145, a secreted vascular endothelial growth factor isoform that binds to extracellular matrix. J. Biol. Chem., *272:* 7151-7158, 1997.

7. Cohen, T., Gitay-Goren, H., Sharon, R., Shibuya, M., Halaban, R., Levi, B. Z., and Neufeld, G. VEGF121, a vascular endothelial growth factor (VEGF) isoform lacking heparin binding ability, requires cell-surface heparan sulfates for efficient binding to the VEGF receptors of human melanoma cells. J. Biol. Chem., *270:* 11322-11326, 1995.
8. Grutzkau, A., Kruger-Krasagakes, S., Baumeister, H., Schwarz, C., Kogel, H., Welker, P., Lippert, U., Henz, B. M., and Moller, A. Synthesis, storage, and release of vascular endothelial growth factor/vascular permeability factor (VEGF/VPF) by human mast cells: implications for the biological significance of VEGF206. Mol. Biol. Cell, *9:* 875-884, 1998.
9. Park, J. E., Keller, G. A., and Ferrara, N. The vascular endothelial growth factor (VEGF) isoforms: differential deposition into the subepithelial extracellular matrix and bioactivity of extracellular matrix-bound VEGF. Mol. Biol. Cell, *4:* 1317-1326, 1993.
10. Houck, K. A., Leung, D. W., Rowland, A. M., Winer, J., and Ferrara, N. Dual regulation of vascular endothelial growth factor bioavailability by genetic and proteolytic mechanisms. J. Biol. Chem., *267:* 26031-26037, 1992.
11. Keyt, B. A., Berleau, L. T., Nguyen, H. V., Chen, H., Heinsohn, H., Vandlen, R., and Ferrara, N. The carboxyl-terminal domain (111-165) of vascular endothelial growth factor is critical for its mitogenic potency. J. Biol. Chem., *271:* 7788-7795, 1996.
12. Tessler, S., Rockwell, P., Hicklin, D., Cohen, T., Levi, B. Z., Witte, L., Lemischka, I. R., and Neufeld, G. Heparin modulates the interaction of VEGF165 with soluble and cell associated flk-1 receptors. J. Biol. Chem., *269:* 12456-12461, 1994.
13. Park, M. and Lee, S. T. The fourth immunoglobulin-like loop in the extracellular domain of FLT-1, a VEGF receptor, includes a major heparin-binding site. Biochem. Biophys. Res. Commun., *264:* 730-734, 1999.
14. Dougher, A. M., Wasserstrom, H., Torley, L., Shridaran, L., Westdock, P., Hileman, R. E., Fromm, J. R., Anderberg, R., Lyman, S., Linhardt, R. J., Kaplan, J., and Terman, B. I. Identification of a heparin binding peptide on the extracellular domain of the KDR VEGF receptor. Growth Factors, *14:* 257-268, 1997.
15. Gitay-Goren, H., Cohen, T., Tessler, S., Soker, S., Gengrinovitch, S., Rockwell, P., Klagsbrun, M., Levi, B. Z., and Neufeld, G. Selective binding of VEGF121 to one of the three vascular endothelial growth factor receptors of vascular endothelial cells. J. Biol. Chem., *271:* 5519-5523, 1996.
16. Wilting, J., Birkenhager, R., Eichmann, A., Kurz, H., Martiny-Baron, G., Marme, D., McCarthy, J. E., Christ, B., and Weich, H. A. VEGF121 induces proliferation of vascular endothelial cells and expression of flk-1 without affecting lymphatic vessels of chorioallantoic membrane. Dev. Biol., *176:* 76-85, 1996.
17. Cherng, J. M., Lin, C. M., Lin, C. L., Huang, S. M., Chang, H. L., Lee, C. C., Chiang, L. C., and Chang, P. Y. Effects of VEGF121 and/or VEGF165 gene transfection on collateral circulation development. J. Formos Med. Assoc., *99:* 603-611, 2000.

18. Mattot, V., Moons, L., Lupu, F., Chernavvsky, D., Gomez, R. A., Collen, D., and Carmeliet, P. Loss of the VEGF(164) and VEGF(188) Isoforms Impairs Postnatal Glomerular Angiogenesis and Renal Arteriogenesis in Mice. J. Am. Soc. Nephrol., *13:* 1548-1560, 2002.
19. Stalmans, I., Ng, Y. S., Rohan, R., Fruttiger, M., Bouche, A., Yuce, A., Fujisawa, H., Hermans, B., Shani, M., Jansen, S., Hicklin, D., Anderson, D. J., Gardiner, T., Hammes, H. P., Moons, L., Dewerchin, M., Collen, D., Carmeliet, P., and D'Amore, P. A. Arteriolar and venular patterning in retinas of mice selectively expressing VEGF isoforms. J. Clin. Invest., *109:* 327-336, 2002.
20. Kondo, Y., Arii, S., Mori, A., Furutani, M., Chiba, T., and Imamura, M. Enhancement of angiogenesis, tumor growth, and metastasis by transfection of vascular endothelial growth factor into LoVo human colon cancer cell line. Clin. Cancer Res., *6:* 622-630, 2000.
21. Lee, Y. H., Tokunaga, T., Oshika, Y., Suto, R., Yanagisawa, K., Tomisawa, M., Fukuda, H., Nakano, H., Abe, S., Tateishi, A., Kijima, H., Yamazaki, H., Tamaoki, N., Ueyama, Y., and Nakamura, M. Cell-retained isoforms of vascular endothelial growth factor (VEGF) are correlated with poor prognosis in osteosarcoma. Eur. J. Cancer, *35:* 1089-1093, 1999.
22. Oshika, Y., Nakamura, M., Tokunaga, T., Ozeki, Y., Fukushima, Y., Hatanaka, H., Abe, Y., Yamazaki, H., Kijima, H., Tamaoki, N., and Ueyama, Y. Expression of cell-associated isoform of vascular endothelial growth factor 189 and its prognostic relevance in non-small cell lung cancer. Int. J. Oncol., *12:* 541-544, 1998.
23. Tokunaga, T., Oshika, Y., Abe, Y., Ozeki, Y., Sadahiro, S., Kijima, H., Tsuchida, T., Yamazaki, H., Ueyama, Y., Tamaoki, N., and Nakamura, M. Vascular endothelial growth factor (VEGF) mRNA isoform expression pattern is correlated with liver metastasis and poor prognosis in colon cancer. Br. J. Cancer, *77:* 998-1002, 1998.
24. Guo, P., Xu, L., Pan, S., Brekken, R. A., Yang, S. T., Whitaker, G. B., Nagane, M., Thorpe, P. E., Rosenbaum, J. S., Su Huang, H. J., Cavenee, W. K., and Cheng, S. Y. Vascular endothelial growth factor isoforms display distinct activities in promoting tumor angiogenesis at different anatomic sites. Cancer Res., *61:* 8569-8577, 2001.
25. Cheng, S. Y., Nagane, M., Huang, H. S., and Cavenee, W. K. Intracerebral tumor-associated hemorrhage caused by overexpression of the vascular endothelial growth factor isoforms VEGF121 and VEGF165 but not VEGF189. Proc. Natl. Acad. Sci. U.S.A., *94:* 12081-12087, 1997.
26. Yu, J. L., Rak, J. W., Klement, G., and Kerbel, R. S. Vascular endothelial growth factor isoform expression as a determinant of blood vessel patterning in human melanoma xenografts. Cancer Res., *62:* 1838-1846, 2002.
27. Leenders, W., Küsters, B., Pikkemaat, J., Wesseling, P., Ruiter, D., Heerschap, A., Barentsz, J., and de Waal, R. M. W. Vascular endothelial growth factor-A determines detectability of experimental melanoma brain metastasis in Gd-DTPA-enhanced MRI. Int. J. Cancer, *105:* 437-443, 2003.

28. Span, P. N., Grebenchtchikov, N., Geurts-Moespot, J., Westphal, J. R., Lucassen, A. M., and Sweep, C. G. EORTC Receptor and Biomarker Study Group Report: a sandwich enzyme-linked immunosorbent assay for vascular endothelial growth factor in blood and tumor tissue extracts. Int. J. Biol. Markers, *15:* 184-191, 2000.
29. Kusters, B., Westphal, J. R., Smits, D., Ruiter, D. J., Wesseling, P., Keilholz, U., and de Waal, R. M. The pattern of metastasis of human melanoma to the central nervous system is not influenced by integrin alpha(v)beta(3) expression. Int. J. Cancer, *92:* 176-180, 2001.
30. Westphal, J. R., Van't Hullenaar, R., Peek, R., Willems, R. W., Crickard, K., Crickard, U., Askaa, J., Clemmensen, I., Ruiter, D. J., and De Waal, R. M. Angiogenic balance in human melanoma: expression of VEGF, bFGF, IL-8, PDGF and angiostatin in relation to vascular density of xenografts in vivo. Int. J. Cancer, *86:* 768-776, 2000.
31. Westphal, J. R., van't Hullenaar, R. G., van der Laak, J. A., Cornelissen, I. M., Schalkwijk, L. J., van Muijen, G. N., Wesseling, P., de Wilde, P. C., Ruiter, D. J., and de Waal, R. M. Vascular density in melanoma xenografts correlates with vascular permeability factor expression but not with metastatic potential. Br. J. Cancer, *76:* 561-570, 1997.
32. Wesseling, P., Schlingemann, R. O., Rietveld, F. J., Link, M., Burger, P. C., and Ruiter, D. J. Early and extensive contribution of pericytes/vascular smooth muscle cells to microvascular proliferation in glioblastoma multiforme: an immuno-light and immuno-electron microscopic study. J. Neuropathol. Exp. Neurol., *54:* 304-310, 1995.
33. Rosenstein, J. M., Mani, N., Silverman, W. F., and Krum, J. M. Patterns of brain angiogenesis after vascular endothelial growth factor administration in vitro and in vivo. Proc. Natl. Acad. Sci. U.S.A., *95:* 7086-7091, 1998.
34. Berry, I., Benderbous, S., Ranjeva, J. P., Gracia-Meavilla, D., Manelfe, C., and Le Bihan, D. Contribution of Sinerem used as blood-pool contrast agent: detection of cerebral blood volume changes during apnea in the rabbit. Magn. Reson. Med., *36:* 415-419, 1996.
35. Bates, D. O., Cui, T. G., Doughty, J. M., Winkler, M., Sugiono, M., Shields, J. D., Peat, D., Gillatt, D., and Harper, S. J. VEGF165b, an inhibitory splice variant of vascular endothelial growth factor, is down-regulated in renal cell carcinoma. Cancer Res., *62:* 4123-4131, 2002.
36. Maes, C., Carmeliet, P., Moermans, K., Stockmans, I., Smets, N., Collen, D., Bouillon, R., and Carmeliet, G. Impaired angiogenesis and endochondral bone formation in mice lacking the vascular endothelial growth factor isoforms VEGF(164) and VEGF(188). Mech. Dev., *111:* 61-73, 2002.
37. Zelzer, E., McLean, W., Ng, Y. S., Fukai, N., Reginato, A. M., Lovejoy, S., D'Amore, P. A., and Olsen, B. R. Skeletal defects in VEGF(120/120) mice reveal multiple roles for VEGF in skeletogenesis. Development, *129:* 1893-1904, 2002.
38. Ruhrberg, C., Gerhardt, H., Golding, M., Watson, R., Ioannidou, S., Fujisawa, H., Betsholtz, C., and Shima, D. T. Spatially restricted patterning cues provided by heparin-binding VEGF-A control blood vessel branching morphogenesis. Genes Dev., *16:* 2684-2698, 2002.

39. Grunstein, J., Masbad, J. J., Hickey, R., Giordano, F., and Johnson, R. S. Isoforms of vascular endothelial growth factor act in a coordinate fashion To recruit and expand tumor vasculature. Mol. Cell. Biol., *20:* 7282-7291, 2000.
40. Soker, S., Miao, H. Q., Nomi, M., Takashima, S., and Klagsbrun, M. VEGF(165) mediates formation of complexes containing VEGFR-2 and neuropilin-1 that enhance VEGF(165)-receptor binding. J. Cell.Biochem., *85:* 357-368, 2002.
41. Gengrinovitch, S., Berman, B., David, G., Witte, L., Neufeld, G., and Ron, D. Glypican-1 is a VEGF165 binding proteoglycan that acts as an extracellular chaperone for VEGF165. J. Biol. Chem., *274:* 10816-10822, 1999.
42. Simons, M. and Horowitz, A. Syndecan-4-mediated signalling. Cell Signal., *13:* 855-862, 2001.
43. Hutchings, H., Ortega, N., and Plouet, J. Extracellular matrix-bound vascular endothelial growth factor promotes endothelial cell adhesion, migration, and survival through integrin ligation. Faseb J., in press, 2003.

Chapter 6

Anti-agiogenic therapy of cerebral melanoma metastasis results in sustained tumor progression via vessel co-option

William PJ Leenders Benno Küsters
(W.P.J.L and B.K. contributed equally to this work; shared first authorship)
Kiek Verrijp
Cathy Maass
Pieter Wesseling
Arend Heerschap
Dirk Ruiter
Andy Ryan
Robert de Waal

Clin Cancer Res 2004 Sep 15;10(18 Pt 1):6222-30.

Abstract

Purpose - In brain, tumors may grow without inducing angiogenesis, via co-option of the dense pre-existent capillary bed. The purpose of this study was to investigate how this phenomenon influences the outcome of anti-angiogenic therapy.

Experimental design - Mice carrying brain metastases of the human, highly angiogenic melanoma cell line Mel57-VEGF-A were either or not treated with different dosages of ZD6474, a VEGFR2 tyrosine kinase inhibitor with additional activity against EGFR. Effect of treatment was evaluated using contrast-enhanced MRI and (immuno)morphological analysis.

Results – Placebo-treated Mel57-VEGF-A brain metastases evoked an angiogenic response and were highlighted in contrast-enhanced (CE)- MRI. Following treatment with ZD6474 (100 mg/kg), CE-MRI failed to detect tumors, either in prevention or therapeutic treatment regimens. However, (immuno)histological analysis revealed the presence of numerous small, non-angiogenic lesions. Treatment with 25 mg/kg ZD6474 resulted also in efficient blockade of vessel formation, but did not fully inhibit vascular leakage, thereby still allowing visualization in CE-MRI scans.

Conclusions - Our data show that, although angiogenesis can be effectively blocked by ZD6474, in vessel-dense organs this may result in sustained tumor progression via co-option, rather than in tumor dormancy. Importantly, blocking VEGF-A may result in undetectability of tumors in CE-MRI scans, leading to erroneous conclusions about therapeutic efficacy during MRI follow-up. The maintenance of VEGF-A-induced vessel leakage in the absence of neovascularization at lower ZD6474 doses may be exploited to improve delivery of chemotherapeutic agents in combined treatment regimens of anti-angiogenic and chemotherapeutic compounds.

Introduction

The continuously increasing demand for oxygen and nutrients of growing solid tumors can be met by induction of a neovascular bed. This is accomplished by an hypoxia-driven mechanism, which results in expression of a number of effector molecules among which is Vascular Endothelial Growth Factor-A (VEGF-A), the most potent angiogenic factor known to date [1]. The notion that abrogation of the blood supply to a tumor will prevent further outgrowth and induce dormancy, has led to the development of numerous compounds that target one of the events in the multi-step process of angiogenesis. These include: naturally occurring angiogenesis inhibitors such as tumstatin, endostatin and angiostatin (proteolytic fragments of collagen IV, XVIII and plasminogen respectively) [2-9]; protease inhibitors that prevent degradation of the basal lamina of blood vessels [10]; and compounds that interfere with adherence of endothelial cells to matrix proteins (eg via blockade of $\alpha_v\beta_3$ integrin) [11,12]. However, since VEGF-A by itself has the potency to initiate most, if not all, necessary steps in the angiogenic process, most research has focused on targeting VEGF-A or its receptors VEGFR-1 (Flt-1) and VEGFR-2 (KDR/Flk-1). This has resulted in the development of VEGF antagonists [13,14], humanized antibodies against VEGF-A [15,16] or VEGFR-2 [17,18], and soluble chimeric VEGF receptor ectodomains [19], compounds with tumor growth inhibitory activities in a number of animal models [19,20]. One novel class of compounds targeting VEGF comprises small molecule agents that can be administered orally against the tyrosine kinase moieties of VEGF receptors [21-23]. Included in this class is ZD6474, which selectively inhibits VEGFR-2 kinase activity and has additional inhibitory activity against epidermal growth factor receptor (EGFR) tyrosine kinase. It has previously been shown that this compound has potent antitumor activity against a broad spectrum of histologically diverse subcutaneous tumor xenografts in mice [21].

These promising preclinical data have led to high expectations for anti-angiogenic approaches in the clinic. However, it seems unlikely that inhibition of VEGF-dependent angiogenesis will demonstrate the same pan-tumor activity in the clinic that has been seen in preclinical models. There are several reasons to expect discrepancies in results between preclinical models and clinical trials in man. First, slowly growing, large human tumors may differ in their sensitivity towards angiogenesis inhibitors from the rapidly growing tumors that are often used in mouse models of cancer, and human tumors may have regions with relatively mature and stable tumor vessels that are less susceptible to anti-VEGF therapy. Indeed, in Rip-Tag mice (a transgenic mouse model of spontaneous pancreatic islet carcinoma formation) it was shown that targeting VEGFRs resulted in inhibition of tumor angiogenesis and growth only in early

stages of tumor development. Affecting vessel integrity, by targeting platelet-derived growth factor receptors (PDGFRs) leading to pericyte loss, resulted in regression of vessels in more established tumors. In this model simultaneous targeting of VEGFRs and PDGFRs was more efficient than targeting of either receptor alone [24]. Secondly, candidate patients for Phase I trials with anti-angiogenic therapy are predominantly patients with disseminated cancer, in which other therapeutic options are no longer available, and one may ask the question whether disseminated tumors have the same angiogenesis-dependency as the originating tumor: since tumor metastasis occurs through lymph and blood vessels, outgrowth of metastases mostly will occur in vessel dense organs like lung, liver and brain. In these organs tumors (both primary and metastatic) may grow independently of angiogenesis via a process of co-option of pre-existent vessels [25-28]. This implies that, whereas compounds may be efficient inhibitors of angiogenesis and tumor growth in angiogenesis-dependent tumors (such as subcutaneous tumor xenografts), their effects may be limited in tumors, growing in tissues with an intrinsic vascular density that allows for co-option by infiltrative tumors.

Here we investigated this hypothesis by treating mice, carrying brain tumors of the human melanoma cell line Mel57, with the anti-angiogenic agent ZD6474. While parental Mel57 xenografts grow in brain parenchyma of immunocompromized mice exclusively via co-option of brain capillaries, Mel57 tumors stably expressing VEGF-A_{165} evoke a fulminant angiogenic response [29]. In contrast to parental tumors, those expressing VEGF-A are readily detected in CE-MRI due to VEGF-induced vascular leakage 30. Here we show that ZD6474 is a potent inhibitor of angiogenesis in this tumor model. However, this inhibition does not lead to tumor regression, or increased survival. Tumor growth is able to continue via co-option of pre-existent vessels, a growth pattern that is not detected by Gd-DTPA-enhanced MRI. Intermediate doses of ZD6474 inhibited new vessel formation but not VEGF-A-induced vessel leakage, still allowing MRI detection of treated tumors.

These data indicate that in clinical settings where switching to vessel co-option is possible, the interpretation of CE-MRI data to monitor antitumor effects should be used with caution. Decreases in CE-MRI signal can effectively determine if an agent reduces tumor vessel permeability, but may be a poor indicator of antitumor response, particularly if the tumor can adopt a vessel co-option phenotype.

Materials and Methods

Cell lines and transfections

Culture of the Mel57 human melanoma cell line and generation of stably transfected Mel57 cell lines, expressing enhanced green fluorescent protein (EGFP) or VEGF-A_{165} has previously been described [27,29]. EGFP and VEGF-A_{165} cDNAs were under control of the CMV promoter, and expression of the proteins of interest was linked to that of the neomycin-resistance gene product via an internal ribosome entry site, enabling effective selection for EGFP or VEGF-A- expressing cells.

Animal experiments

Specific pathogen-free (SPF) male BALB/c nu/nu mice were purchased from the university central animal facility breeding program. Experiments were carried out in accordance with the national animal protection laws and approval was obtained from the Animal Experimental Committee. To establish brain metastases, 7 week-old mice were anaesthesized (1.3 % isoflurane/O_2/N_2O) and tumor cells ($1x10^5$ Mel57-EGFP or Mel57-VEGF-A_{165} cells in 100 µl phosphate buffered saline [PBS]) were injected in the right internal carotid artery as previously described [31]. Three sets of experiments were performed. In one experiment, mice carrying Mel57-VEGF-A_{165} brain lesions were treated with 100 mg/kg ZD6474 (n=9) or placebo (n=10) starting at day 2 or 10 post tumor cell injection. In a second experiment, tumor-bearing mice (n=10) were treated with 50 mg/kg ZD6474, starting at day 1, 5, 9, 13 or 17 post injection (n=2 for each time point). Finally, an experiment was performed in which a 1:1 mixture of Mel57-VEGF-A_{165} and Mel57-EGFP cells was injected to compare the effects of ZD6474 on angiogenic and co-opting lesions within one animal (n=10). In this case, mice were treated with 25 mg/kg starting at day 2 post-injection. ZD6474 (as a suspension in 1% polysorbate-80) or placebo (1% polysorbate-80) was administered p.o. once daily in a volume of 100 µl. After 16-20 days when clinical symptoms due to tumor growth were apparent (weight loss, neurological defects), CE-MRI was performed according to the protocol described below.

Contrast-enhanced magnetic resonance imaging

CE-MRI was performed as previously described [30]. Briefly, mice were anaesthesized (1.3% isoflurane; 1:1 (v/v) N_2O/O_2 mixture), catheterized in the tail vein, and placed in an MR spectrometer (S.M.I.S. console equipped with a Magnex Scientific 7T/200mm horizontal bore

magnet and a 150mT/m gradient set). Body temperature was maintained by placing the mice on a 37°C circulating warm water bed. A 12 mm diameter surface coil was positioned over the skull. After initial monitoring of the brain with fast gradient-echo scout images, 16 contiguous images were acquired with a T_1-weighted multislice gradient-echo sequence (T_E= 8 ms; T_R = 100 ms; flip angle = 90º; number of averages = 1; field of view = 25x25 mm; matrix size = 256x256; slice thickness = 1 mm) before and 1, 2, 10 and 20 minutes after bolus injection of Gd-DTPA (Magnevist®, Schering, Germany) at a dose of 0.2 mmol/kg.

Histological and immunohistochemical analysis

After MRI, mice were sacrificed by injecting an overdose of barbiturate and brains removed and fixed in buffered formalin. Brains were cut coronal slices and embedded in paraffin. Sections of 4 μm were processed for conventional H&E staining or immunostaining for mouse IgG (to examine the presence of extravasated proteins), the endothelial marker CD34 (Hycult, Uden, The Netherlands), GLUT-1 (as a blood-brain barrier marker and a hypoxia marker, DAKO, Glostrup, Denmark), MIB-1 (anti-human Ki67, DAKO, Glostrup, Denmark) and anti-mouse Ki67 (Dianova, Hamburg, Germany). MRI images were matched to histology as closely as possible. To confirm stable VEGF-A expression, tumors were also subjected to VEGF in situ hybridization (ISH) using a digoxigenin-labeled VEGF-A antisense RNA probe. The corresponding sense probe was used as a control.

Results

We have recently described that Mel57 tumors grow in mouse brain via co-option of pre-existent vessels without inducing an angiogenic switch, whereas the same tumors, engineered to express $VEGF_{165}$, evoked a fulminant angiogenic response [25,29]. Parental Mel57 lesions were invisible in Gd-DTPA-enhanced MRI scans, whereas VEGF-A_{165}-induced vessel leakage led to clear MRI visibility [30]. To investigate the effects of the anti-VEGF therapy on MRI representation and tumor phenotype, we treated mice carrying highly angiogenic Mel57-VEGF-A_{165} brain tumors with ZD6474. Treatment with 100 mg/kg, starting early during tumor development (2 days post-injection of tumor cells), led to complete inhibition of VEGF-A effects. In treated animals, tumors grew via co-option of pre-existent vessels as was evident from a number of observations. First, vessel dilatation as observed in placebo-treated controls was absent in the treated tumors (Figure 1A and F). Secondly, the upregulation of a number of endothelial markers such as CD34, which was evident in placebo-treated Mel57-VEGF-A_{165} tumors (Figure 1B), was absent in ZD6474- treated tumors (Figure 1G).

Furthermore, in contrast to tumor vessels in placebo-treated animals, tumor vessels in treated animals expressed GLUT-1, a characteristic property of the highly specialized blood-brain barrier, suggesting that these vessels were pre-existent rather than newly formed (compare Figures 1C and H). Vessels were not leaky, as evidenced by absence of extravasated mouse immunoglobulins (not shown). Also, VEGF-A-induced proliferation of mouse endothelial cells, which occurred abundantly in the control animals, failed to appear in the treated animals (see mouse-specific Ki67 stainings in Figures 1D and I). Importantly, in both the control and the ZD6474-treated animals, tumor cells had a high proliferation index (see MIB-1 immunostaining in Figures 1E and J) indicating that blood supply from co-opted pre-existent brain capillaries was sufficient for tumor progression. This was also evident from the fact that hypoxia and necrosis were never observed in these tumors. Importantly, using the intracarotid injection technique, multiple lesions develop in brain parenchyma. Typically, 20-50 lesions are found in each brain. All lesions responded to therapy in a similar manner.

Mel57 cells express VEGFR-2 but do not respond to VEGF-A by increased proliferation (unpublished results). The high proliferation index in ZD6474-treated tumors (figure 1J) confirms that the effects of ZD6474 are indeed the result of inhibition of VEGFR-2 on endothelial cells rather than a direct effect on the tumor cells.

The absence of vessel leakage in ZD6474-treated tumors was reflected in MRI: treated tumors were not visible (Figure 2B) whereas lesions in control-treated animals were clearly enhanced after injection of Gd-DTPA (Figure 2A). To exclude the possibility that the co-opting phenotype of ZD6474-treated tumors was due to incidental loss of VEGF-A expression, we performed ISH with an antisense VEGF-A probe which demonstrated that the co-opting phenotype was caused by ZD6474 treatment and not by incidental loss of VEGF-A exppression (Figure 1K).

In this tumor model, 12 days after tumor cell injection small lesions were present that already exerted marked effects on the vasculature such as vasodilatation and vessel leakage, as demonstrated by IgG leakage around the lesions (not shown), and which were detectable by Gd-DTPA in MRI as small hyperintense spots (Figure 2D, arrows). To investigate the effects of ZD6474 on tumors in which VEGF-A effects are already distinct, mice were injected with Mel57-VEGF-A cells and treatment with 100 mg/kg ZD6474 was initiated 10 days later. After another five days, mice were subjected to Gd-DTPA-enhanced brain MRI and sacrificed. Again, tumor lesions grew by vascular co-option, with some lesions showing remnants of dilated vasculature (not shown). Vessels were, however, not leaky as illustrated

by an absence of Gd-DTPA extravasation (Figure 2C). This was confirmed once more by the presence of only very little extravasated mouse immunoglobulin (not shown).
At a dose of 100 mg/kg, ZD6474 very efficiently prohibited the development of an angiogenic tumor phenotype, forcing tumor cells to grow by co-option of pre-existent vessels, much like parental Mel57 tumors. In order to understand the switch to a vessel co-option phenotype better we tested the effects of lower doses of ZD6474 (25 and 50 mg/kg) in this model.
Mice that were treated with 50 mg/kg ZD6474 starting at day 2 after tumor cell injection showed a strikingly different tumor phenotype compared with the 100 mg/kg treatment group. Now, tumors had an expansive appearance and were poorly vascularized. In approximately 50-70% of the lesions, central hypoxia (evidenced by GLUT-1 staining of tumor cells, arrow in Figure 3C) and necrosis (Figure 3A) were observed. At the tumor rims, cells co-opted pre-existent, GLUT-1 positive, vessels (Figure 3C). Surprisingly, a similar tumor phenotype was observed when 50 mg/kg treatment was initiated 1, 5, 9 and 13 days post tumor cell injection (Figure 4 and data not shown). Only when treatment was given for 2 days, starting at day 17 post-tumor cell injection, was a tortuous, dilated and leaky tumor vasculature without apparent signs of hypoxia or necrosis observed (Figure 3E-G and Figure 4D). While in these tumors, cells proliferated abundantly, as demonstrated by anti-pan Ki67 stainings, proliferating mouse endothelial cells in the dilated vasculature were only sparsely detected (data not shown). This suggests that ZD6474 treatment for as little as 2 days led to marked inhibition of endothelial cell proliferation.

Fig 1 – Effects of 100 mg/kg ZD6474 on Mel57-VEGF-A_{165} brain tumor morphology.
Mice were injected in the internal carotid artery with Mel57-VEGF-A_{165} cells and oral treatment with placebo (A-E) or 100 mg/kg ZD6474 (F-J) was intiated 2 days post injection. Sixteen days post injection of tumor cells mice were sacrificed and brains removed and fixed in formalin. Four-µm sections were stained with conventional H&E (A,F), and with antibodies against the anti-endothelial marker CD34 (B,G), the brain-endothelium marker GLUT-1 (C,H), Ki67 (proliferation antigen, mouse specific, D,I) and with MIB-1 (anti-pan Ki67 E,J). In treated tumors, GLUT-1 was expressed on tumor vessels (arrow in H), whereas it was absent on placebo-treated tumors (arrow in C points at a tumor vessel). Note the absence of proliferating mouse endothelial cells in the ZD6474-treated tumors (I), while numerous proliferating (endothelial) cells are present in placebo-treated tumors. By contrast, tumor cell proliferation was not inhibited by ZD6474 (compare MIB staining in E and J), and ZD6474-treated tumors progressed by vascular co-option. Treated tumors were highly invasive but still expressed VEGF-A as demonstrated by ISH using an anti-sense VEGF probe (K). ISH using a sense control probe was negative (not shown). See also colour display page 155.

Figure 1

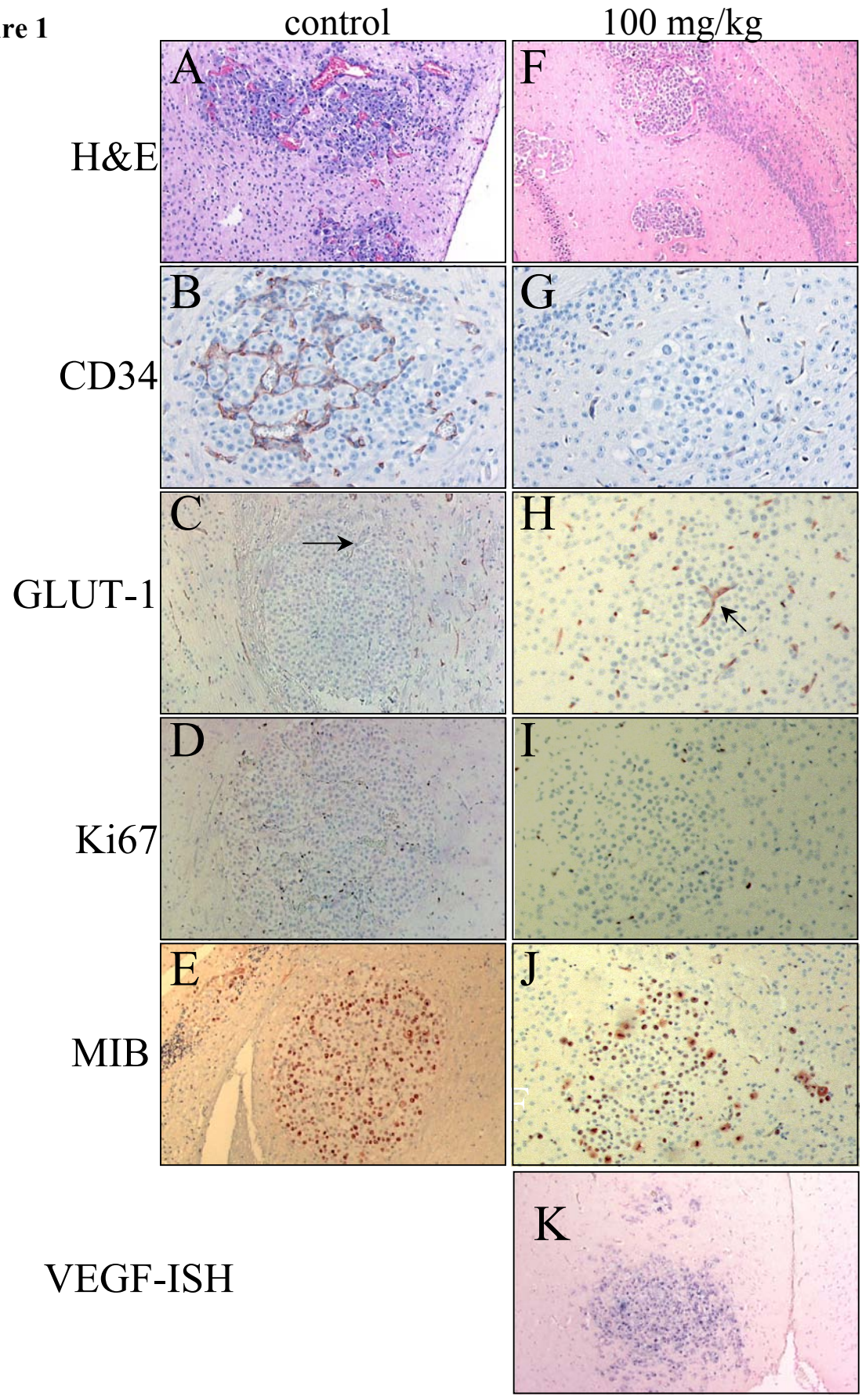
control
100 mg/kg
A
F
H&E
B
G
CD34
C
H
GLUT-1
D
I
Ki67
E
J
MIB
K
VEGF-ISH

Although at 50 mg/kg ZD6474 effectively inhibited angiogenesis, it did not completely prevent vascular leakage as evidenced by the presence of extravasated mouse immunoglobulins around the lesions (Figure 3D) and the fact that tumors were readily detected in Gd-DTPA-enhanced MRI as ring-enhancing lesions (Figure 4). The ring-enhancement observed in Figures 4A-C corrobated the histological finding that within these tumor lesions the vessel density was low, leading to central (non-enhancing) necrosis. The bulky enhancement of the lesions in Figure 4D (arrows) is in agreement with the absence of necrosis and the high vessel density in these tumors (Figure 3E-G).

Lowering the dose even further to 25 mg/kg yielded similar results: vessel leakiness was not inhibited in contrast to angiogenesis, again resulting in central necrosis in approximately 50% of the lesions (not shown).

In our brain tumor model, lesions arise by clonal expansion (manuscript submitted for publication). This enabled us to compare the effects of ZD6474 on angiogenic Mel57-$VEGF_{165}$ tumors and co-opting Mel57-EGFP tumors within one animal, by making use of EGFP-expression to discrimate between the different Mel57 transfectants. Similar experiments have been recently published in which clonality of metastases was determined using this approach [32]. In a time-matched experiment, a 1:1 mixture of Mel57-EGFP and Mel57-$VEGF_{165}$ was injected in carotid arteries and treatment with 25 mg/kg ZD6474 or placebo was initiated 2 days later (n=5 for each group). Again, tumors were analysed at day 20 post injection.

EGFP staining of brain tissue revealed that necrosis only occurred in Mel57-VEGF-A tumors, and never in Mel57-EGFP tumors (arrow in Figure 4E), indicating that co-opting Mel57-EGFP lesions were not notably affected by ZD6474 treatment. As in the 50 mg/kg experiment, ZD6474 treatment led to a ring-shaped appearance of tumors in Gd-DTPA enhanced MRI, presumably because of the presence of central, non-enhancing necrosis (not shown).

Figure 2

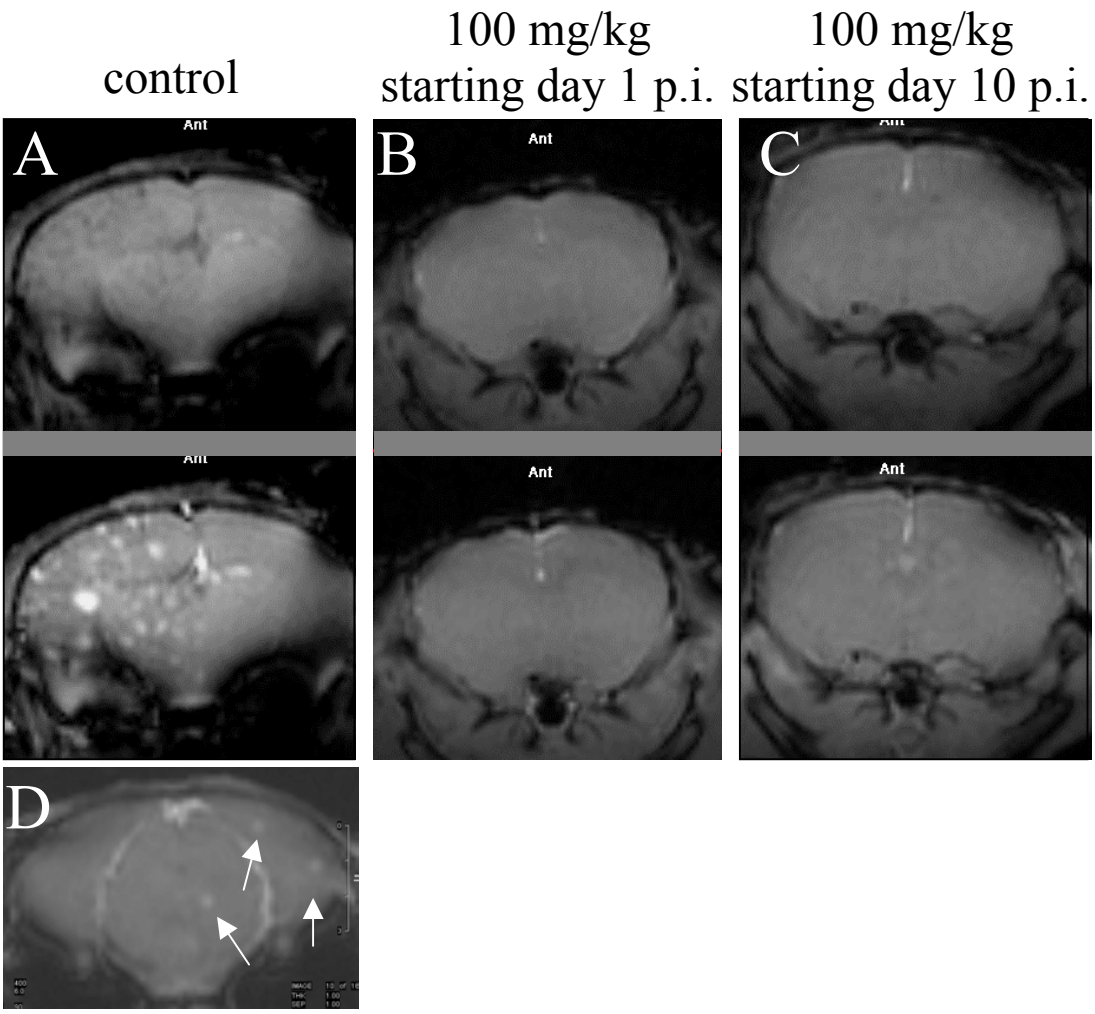

Fig 2 – Effects of ZD6474 treatment of Gd-DTPA-enhanced MRI.
Before sacrifice, control-treated (A) and ZD6474-treated (B,C) mice were subjected to CE-MRI as described in the text. Treatment was initiated at day 2 (B) or day 10 (C) post-injection. The images shown were acquired before (upper panels) and 2 minutes after injection of Gd-DTPA in the tail vein. Note the enhancement in meningeal vessels in B and C, indicating that Gd-DTPA did enter the circulation in these mice. (D) MRI image of mouse brain containing Mel57-VEGF-A lesions, recorded 12 days post-injection of tumor cells. Image was taken immediately after injection of Gd-DTPA. Arrows indicate small lesions.

Figure 3

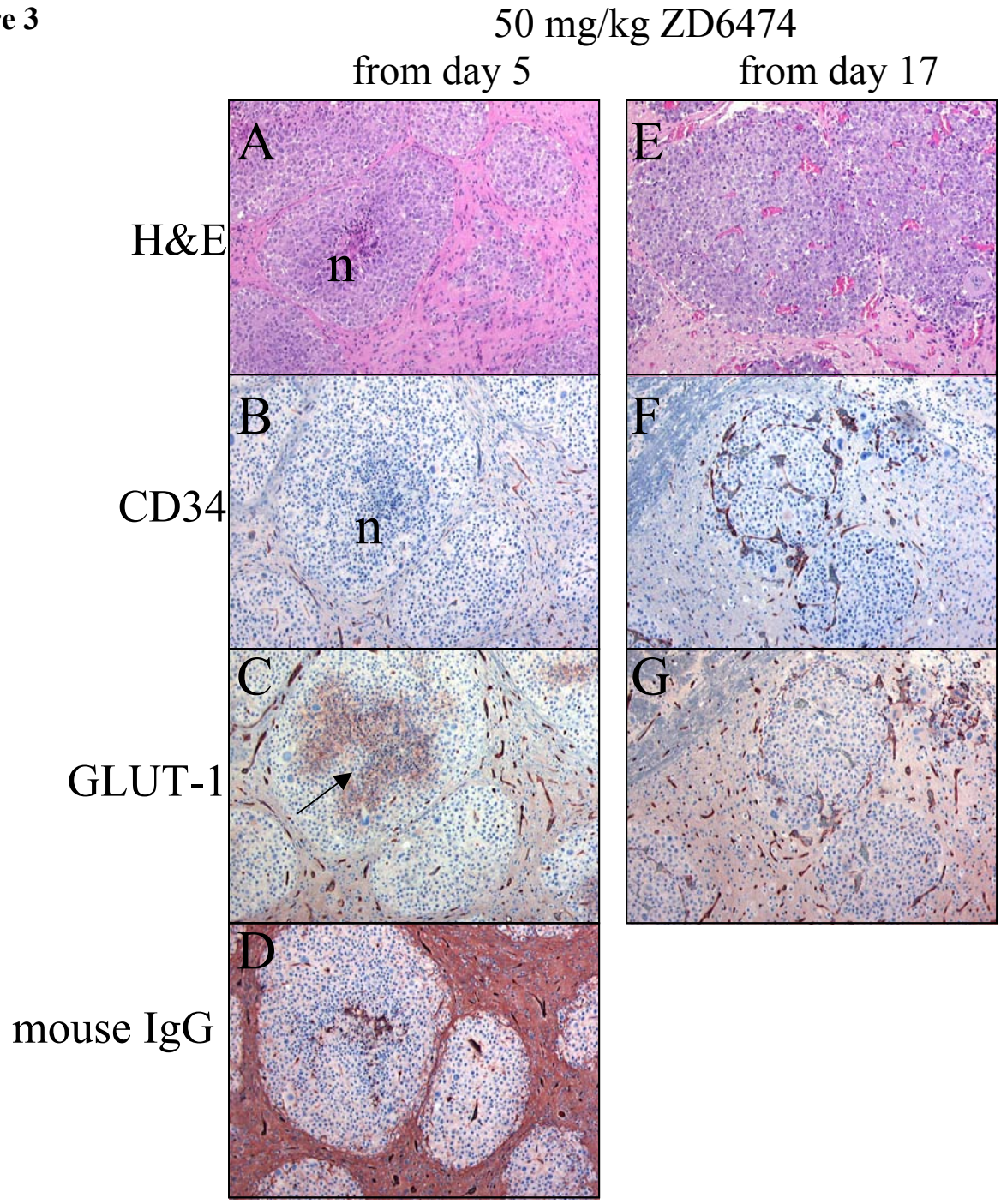

Fig 3 – Effects of 50 mg/kg ZD6474 on Mel57-VEGF-A brain lesions.
ZD6474 (50 mg/kg) was administered daily to nude mice carrying Mel57-VEGF-A_{165} tumors in their brains. Treatment was initiated at day 5 (A-D) or day 17 (E-G) post-injection of tumor cells, and mice were sacrificed 20 days after tumor inoculation. Intratumoral vessel density was low (B) and almost no proliferating endothelial cells could be detected within treated tumors (not shown), resulting in large areas of central necrosis (n) in approximately 70% of lesions. Tumor cells surrounding the necrosis stained positive for GLUT-1, indicating that local hypoxia due to insufficient neovascularization resulted in necrosis (C). Despite effective inhibition of neovascularization, vessels were still leaky as indicated by the presence of extravasated IgG (D). When treatment was initiated at day 17 post injection of tumor cells, a high vessel density still could be observed (E and F) and no necrosis was observed. Intratumoral vessels were glut-1 negative (G) indicating that these were newly formed. See also colour display page 156.

Figure 4

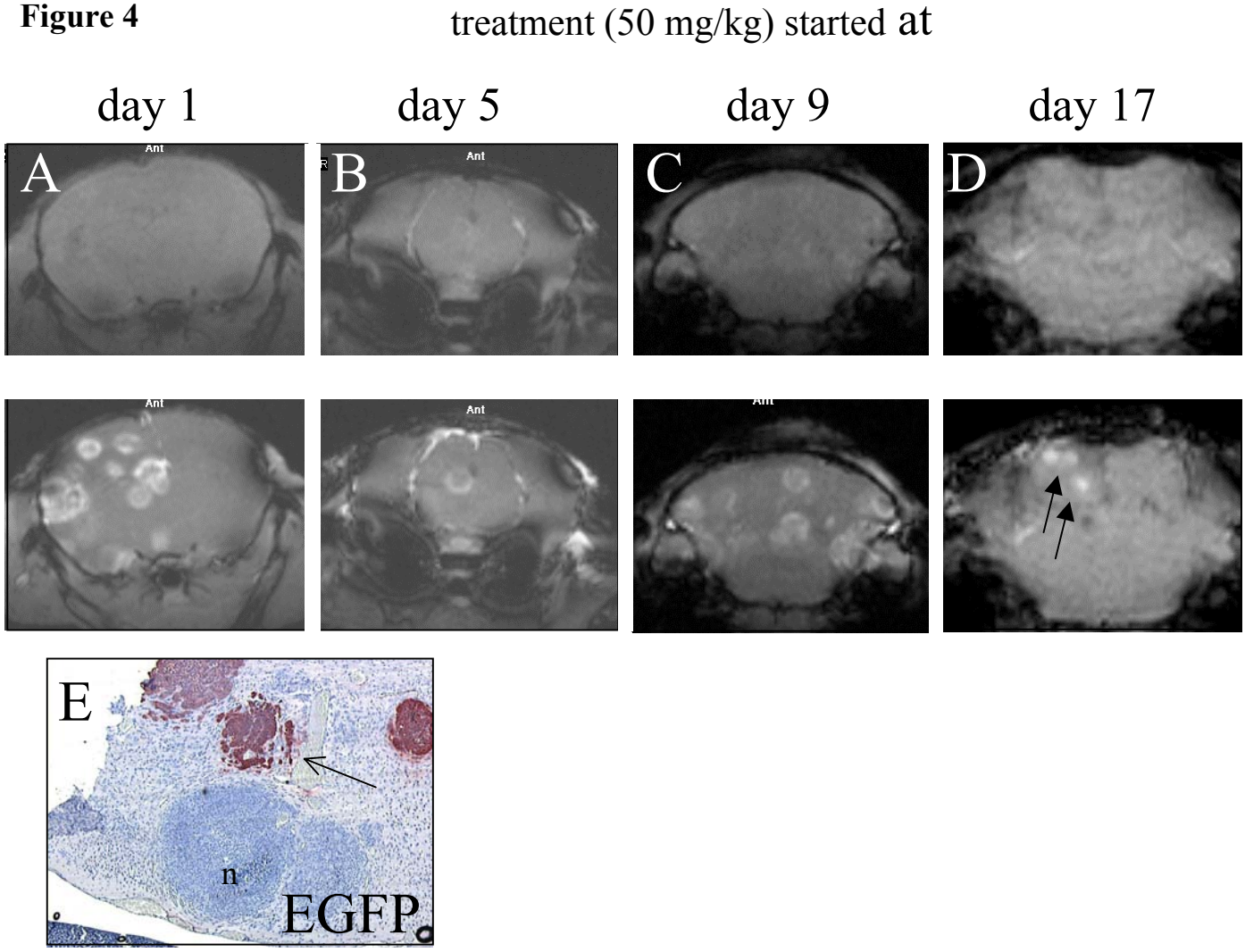

Fig 4 – Brain MRI of tumor-bearing mice treated with 50 mg/kg ZD6474 from day 1, 5 , 9 or 17 post-inoculation of tumor cells as indicated. T1-weighted Gd-DTPA-enhanced images were acquired at day 20, before (upper panels) and directly after intravenous injection of the contrast agent. Clearly, at this dose of ZD6474, VEGF-induced vessel leakage is not inhibited. Note the ring enhancement of the tumors when treatment is started at earlier time points, while bulky enhancement was observed in the group treated from day 17 to 19. The enhancement patterns correlate with the histology of the lesions (see figure 3), where tumor centers are very poorly vascularized and often necrotic leading to poor enhancement.
Panel (E) EGFP immunostaining on brain of a mouse, carrying both EGFP and VEGF-A-expressing Mel57 tumors, and treated with 25 mg/kg ZD6474. Note that co-opting Mel57-EGFP tumors were not affected by ZD6474 treatment (arrow) whereas the VEGF-expressing tumors display central necrosis (n). See also colour display page 157.

Discussion

ZD6474 has been shown to be a promising anti-angiogenic agent, which inhibits VEGFR-2 tyrosine kinase activity and has additional activity against EGFR tyrosine kinase [21]. It prevents tumor growth in a wide range of histologically diverse tumor models, and is currently being evaluated in Phase II clinical trials. It is generally accepted that tumor growth is heavily dependent on angiogenesis, but a number of reports have been published that now suggest that angiogenesis is not always a prerequisite for tumor growth, as tumor cells may

exploit pre-existent vasculature, a process known as vascular co-option [25-28,33]. In this report we investigated the effects of ZD6474 on tumor behavior in a mouse model of brain colonization by the human melanoma cell line Mel57. This cell line homes to brain parenchyma [31] where it grows rapidly to relatively large, vital infiltrative tumors by co-option of pre-existent vessels. Blood supply from these brain vessels was adequate for tumor growth, as no hypoxia developed in the lesions [27]. Consequently, the trigger for upregulation of VEGF-A expression and the angiogenic switch did not occur. Furthermore, co-opted blood vessels were not notably affected by the tumor, as the blood-brain barrier remained intact [30]. In contrast, stably transfected Mel57 cells expressing human $VEGF_{165}$, evoked a fulminant angiogenic response in which the conceptual hallmarks of angiogenesis were present: tumor vessels were dilated and tortuous, and contained numerous proliferating endothelial cells. Furthermore, the blood-brain barrier was disrupted, enabling Gd-DTPA-enhanced detection in MRI. Importantly, the fact that these tumors induce angiogenesis does not preclude co-option: in fact, at the tumor rim co-option of vessels can be observed.

When treatment with 100 mg/kg ZD6474 was initiated 2 days post-carotid injection, VEGF-A effects were completely abrogated, whereupon the tumor adopted the pre-existing vessel co-opting phenotype in which the blood-brain barrier remained intact. Accordingly, treated tumors were invisible in Gd-DTPA-enhanced MRI. Importantly, these co-opting tumors still expressed high levels of VEGF-A, excluding the possibility that the development of this phenotype was due to loss of VEGF-A expression.

These results were anticipated, as abrogation of VEGF-A effects in Mel57-VEGF-A cells would indeed be expected to result in a parental Mel57-tumor-like phenotype. However, Mel57-VEGF-A tumors were also invisible in Gd-DTPA-enhanced MRI when mice were treated from day 10-17 post injection of tumor cells. This illustrates that ZD6474 not only prevents, but probably also reverts VEGF-A-induced vascular changes. This is in accordance with previous observations that ZD6474 led to regression of certain established subcutaneous tumors [21]. We did not perform Kaplan-Mayer analysis, and therefore we cannot make definite conclusions about effects of treatment on survival. It appeared however that ZD6474 treatment, despite significant inhibition of tumor angiogenesis and vessel permeability, did not delay the appearance of neurological symptoms, presumably because in this experimental model Mel57 tumor cells co-opt normal vasculature.

In a rat model of intracranial glioma it has also been reported that anti-VEGF treatment led to conversion of an angiogenic to a co-option phenotype [34]. This conversion, brought about by treatment with an anti-VEGF antibody, was accompanied by slower tumor growth and

prolonged survival. The apparent discrepancy between these results and those reported here may be related to the fact that upon injection of tumor cells in the internal carotid artery numerous lesions develop, whereas stereotactic tumor cell implantation will give rise to one tumor. In the latter case, the effects of anti-VEGF therapy are predicted to result in slower growth of one single lesion, since only the tumor-rim has the possibility of outgrowth via infiltration/co-option. In our model, all lesions may grow via vessel co-option since upon extravasation, tumor cells can directly take profit from the vessels from which they extravasated. Therefore, although individual tumors in our brain colonization model are smaller in the ZD6474 treated groups, the overall number of lesions is not different between treatment and placebo groups. This may explain our finding that 100 mg/kg ZD6474 treatment did not delay the onset of neurological symptoms.

At lower doses, ZD6474 potently inhibited new vessel formation, but did not prevent VEGF-A-induced vascular leakage. Consequently, tumors treated with 25 or 50 mg/kg of ZD6474 were still visible by Gd-DTPA-enhanced MRI. Thus, at lower doses ZD6474 appears to have differential effects on two VEGF-A-induced effects: increased vascular permeability and endothelial proliferation, both activities that are mediated by VEGFR-2 [13]. This suggests that endothelial cell proliferation and vascular permeability are the result of a divergence in cell signaling pathways downstream of VEGFR-2. Such a divergence has indeed recently been described [35]. Permeability depends on a Rac-dependent pathway, while proliferation is mediated by Erk1/2. Our data suggest that the Erk1/2 pathway requires a stronger signal from VEGFR-2 than the Rac-pathway.

An intriguing observation from this study was that ZD6474 treatment at 100 mg/kg resulted in tumor progression via co-option of pre-existent brain vessels, a process that appears efficient since no hypoxia or necrosis develops in the tumor. In contrast, tumors treated with lower doses of ZD6474 often showed central necrosis, while in the same animals necrosis in co-opting Mel57-EGFP tumors was never observed. These data support the following interpretation: ZD6474 at 25 or 50 mg/kg inhibits new vessel formation, but does not prevent vascular leakage. Increased vessel permeability presents a potential benefit to the tumor as it leads to increased supply of nutrients to the tumor cells, and consequently increased and expansive tumor growth. However, because compensating angiogenesis does not occur, due to a lack of endothelial cell proliferation, central hypoxia and eventually necrosis develop. Interestingly, we found that on the morphological and MRI level there was little or no difference between brain tumors in the different groups of mice in which treatment was

started from day 1 or day 13 onwards. Possibly this is due to both potent anti-vascular and anti-angiogenic activity of ZD6474.

Differential effects on angiogenesis and vascular permeability have the potential to be exploited in brain tumor therapy since it creates the possibility of manipulating the blood-brain barrier for therapeutic benefit. For instance, by creating a situation where VEGF-dependent angiogenesis, but not vascular leakage, is inhibited, combination treatment with chemotherapeutic agents may be more effective. Where both processes are inhibited, leading to restoration of the blood brain barrier, reduced accessibility of chemotherapy for the tumor cells may occur. This subject is currently under investigation in our laboratory.

ZD6474 has potent activity against VEGFR-2 signaling and has additional activity against EGFR. EGFR is upregulated on endothelium and is involved in angiogenesis [36]. Since the particular vascular phenotype in Mel57-VEGF-A brain tumors is an unambiguous VEGF-A effect [29], the ZD6474 effects are likely due to VEGFR-2 antagonism rather than EGFR antagonism.

In animals treated with 100 mg/kg ZD6474, tumor cells still had a high proliferation rate (more than 50% of the cells were positive for the proliferation antigen Ki67), while endothelial cell proliferation was completely abolished. This provides strong evidence that the effects of ZD6474 on the tumor phenotype might be entirely attributed to effects on the vasculature and not on the tumor cells. This is in agreement with the fact that Mel57 cells *in vitro* do not respond to VEGF-A, although they express VEGFR-2 similar to other melanoma cell lines (data not shown).

At present in clinical practice, the best non-invasive way to diagnose brain tumors is by CE-MRI. Our model system indicates that tumors that adopt a vessel co-opting phenotype would be invisible by Gd-DTPA-enhanced MRI. If a switch to this phenotype occurred while VEGFR-2 was fully antagonized by a treatment regimen, it may falsely suggest tumor regression had been induced. However, it is not known if switching to a vessel co-option phenotype, as seen in the Mel57-VEGF-A tumor model, will translate widely to the human clinical situation. Based on our findings, the use of a low dose treatment regimen of ZD6474 would allow for a more reliable MRI follow-up.

Acknowledgements – This work was supported by the Dutch Cancer Society, grant 2000-2304. The authors are grateful to AstraZeneca for providing ZD6474. Debby Smits is acknowledged for her help with intracarotid injections. We also thank Huib Croes (dept. of Cell Biology, UMC Nijmegen) for providing us with the anti-GFP antibody.

References

1. Neufeld G, Cohen T, Gengrinovitch S, Poltorak Z. Vascular endothelial growth factor (VEGF) and its receptors. Faseb J, 1999; 13: 9-22.

2. Hamano Y, Zeisberg M, Sugimoto H, et al. Physiological levels of tumstatin, a fragment of collagen IV alpha3 chain, are generated by MMP-9 proteolysis and suppress angiogenesis via alphaVbeta3 integrin. Cancer Cell, 2003; 3: 589-601.

3. Sudhakar A, Sugimoto H, Yang C, et al. Human tumstatin and human endostatin exhibit distinct antiangiogenic activities mediated by alpha vbeta 3 and alpha 5beta 1 integrins. Proc Natl Acad Sci U S A, 2003; 100: 4766-4771.

4. Gorski DH, Mauceri HJ, Salloum RM, et al. Prolonged Treatment with Angiostatin Reduces Metastatic Burden during Radiation Therapy. Cancer Res, 2003; 63: 308-311.

5. Kim YM, Hwang S, Pyun BJ, et al. Endostatin blocks vascular endothelial growth factor-mediated signaling via direct interaction with KDR/Flk-1. J Biol Chem, 2002; 277: 27872-27879.

6. Rehn M, Veikkola T, Kukk-Valdre E, et al. Interaction of endostatin with integrins implicated in angiogenesis. Proc Natl Acad Sci U S A, 2001; 98: 1024-1029.

7. Kuroi K, Toi M. Circulating angiogenesis regulators in cancer patients. Int J Biol Markers, 2001; 16: 5-26.

8. Soff GA. Angiostatin and angiostatin-related proteins. Cancer Metastasis Rev, 2000; 19: 97-107.

9. Maeshima Y, Sudhakar A, Lively JC, et al. Tumstatin, an endothelial cell-specific inhibitor of protein synthesis. Science, 2002; 295: 140-143.

10. Wang M, Liu YE, Greene J, et al. Inhibition of tumor growth and metastasis of human breast cancer cells transfected with tissue inhibitor of metalloproteinase 4. Oncogene, 1997; 14: 2767-2774.

11. Kumar CC. Integrin alpha v beta 3 as a therapeutic target for blocking tumor-induced angiogenesis. Curr Drug Targets, 2003; 4: 123-131.

12. Schraa AJ, Kok RJ, Moorlag HE, et al. Targeting of RGD-modified proteins to tumor vasculature: a pharmacokinetic and cellular distribution study. Int J Cancer, 2002; 102: 469-475.

13. Leenders W, Lubsen N, van Altena M, et al. Design of a variant of vascular endothelial growth factor-A (VEGF-A) antagonizing KDR/Flk-1 and Flt-1. Lab Invest, 2002; 82: 473-481.

14. Siemeister G, Schirner M, Reusch P, et al. An antagonistic vascular endothelial growth factor (VEGF) variant inhibits VEGF-stimulated receptor autophosphorylation and proliferation of human endothelial cells. Proc Natl Acad Sci U S A, 1998; 95: 4625-4629.

15. Athanassiades A, Hamilton GS, Lala PK. Vascular endothelial growth factor stimulates proliferation but not migration or invasiveness in human extravillous trophoblast. Biol Reprod, 1998; 59: 643-654.

16. Borgstrom P, Bourdon MA, Hillan KJ, Sriramarao P, Ferrara N. Neutralizing anti-vascular endothelial growth factor antibody completely inhibits angiogenesis and growth of human prostate carcinoma micro tumors in vivo. Prostate, 1998; 35: 1-10.

17. Sweeney P, Karashima T, Kim SJ, et al. Anti-vascular endothelial growth factor receptor 2 antibody reduces tumorigenicity and metastasis in orthotopic prostate cancer xenografts via induction of endothelial cell apoptosis and reduction of endothelial cell matrix metalloproteinase type 9 production. Clin Cancer Res, 2002; 8: 2714-2724.
18. Kunkel P, Ulbricht U, Bohlen P, et al. Inhibition of Glioma Angiogenesis and Growth in Vivo by Systemic Treatment with a Monoclonal Antibody against Vascular Endothelial Growth Factor Receptor-2. Cancer Res, 2001; 61: 6624-6628.
19. Holash J, Davis S, Papadopoulos N, et al. VEGF-Trap: A VEGF blocker with potent antitumor effects. Proc Natl Acad Sci U S A, 2002; 12: 12.
20. Kim ES, Serur A, Huang J, et al. Potent VEGF blockade causes regression of coopted vessels in a model of neuroblastoma. Proc Natl Acad Sci U S A, 2002; 12: 12.
21. Wedge SR, Ogilvie DJ, Dukes M, et al. ZD6474 Inhibits Vascular Endothelial Growth Factor Signaling, Angiogenesis, and Tumor Growth following Oral Administration. Cancer Res, 2002; 62: 4645-4655.
22. Fong TA, Shawver LK, Sun L, et al. SU5416 is a potent and selective inhibitor of the vascular endothelial growth factor receptor (Flk-1/KDR) that inhibits tyrosine kinase catalysis, tumor vascularization, and growth of multiple tumor types. Cancer Res, 1999; 59: 99-106.
23. Drevs J, Hofmann I, Hugenschmidt H, et al. Effects of PTK787/ZK 222584, a specific inhibitor of vascular endothelial growth factor receptor tyrosine kinases, on primary tumor, metastasis, vessel density, and blood flow in a murine renal cell carcinoma model. Cancer Res, 2000; 60: 4819-4824.
24. Bergers G, Song S, Meyer-Morse N, Bergsland E, Hanahan D. Benefits of targeting both pericytes and endothelial cells in the tumor vasculature with kinase inhibitors. J Clin Invest, 2003; 111: 1287-1295.
25. Leenders W, Kusters B, De Waal R. Vessel co-option: How tumors obtain blood supply in the absence of sprouting angiogenesis. Endothelium, 2002; 9: 83-87.
26. Vermeulen PB, Colpaert C, Salgado R, et al. Liver metastases from colorectal adenocarcinomas grow in three patterns with different angiogenesis and desmoplasia. J Pathol, 2001; 195: 336-342.
27. Kusters B, Leenders WP, Wesseling P, et al. Vascular endothelial growthfactor-A(165) induces progression of melanoma brain metastases without induction of sprouting angiogenesis. Cancer Res, 2002; 62: 341-345.
28. Wesseling P, Ruiter DJ, Burger PC. Angiogenesis in brain tumors; pathobiological and clinical aspects. J Neurooncol, 1997; 32: 253-265.
29. Kusters B, de Waal RM, Wesseling P, et al. Differential effects of vascular endothelial growth factor A isoforms in a mouse brain metastasis model of human melanoma. Cancer Res, 2003; 63: 5408-5413.

30. Leenders W, Küsters B, Pikkemaat J, et al. Vascular endothelial growth factor-A determines detectability of experimental melanoma brain metastasis in Gd-DTPA-enhanced MRI. Int J Cancer, 2003; 105: 437-443.
31. Kusters B, Westphal JR, Smits D, et al. The pattern of metastasis of human melanoma to the central nervous system is not influenced by integrin alpha(v)beta(3) expression. Int J Cancer, 2001; 92: 176-180.
32. Yamamoto N, Yang M, Jiang P, et al. Determination of clonality of metastasis by cell-specific color-coded fluorescent-protein imaging. Cancer Res, 2003; 63: 7785-7790.
33. Dome B, Paku S, Somlai B, Timar J. Vascularization of cutaneous melanoma involves vessel co-option and has clinical significance. J Pathol, 2002; 197: 355-362.
34. Rubenstein JL, Kim J, Ozawa T, et al. Anti-VEGF antibody treatment of glioblastoma prolongs survival but results in increased vascular cooption. Neoplasia, 2000; 2: 306-314.
35. Eriksson A, Cao R, Roy J, et al. Small GTP-binding protein Rac is an essential mediator of vascular endothelial growth factor-induced endothelial fenestrations and vascular permeability. Circulation, 2003; 107: 1532-1538.
36. Hirata A, Ogawa S, Kometani T, et al. ZD1839 (Iressa) induces antiangiogenic effects through inhibition of epidermal growth factor receptor tyrosine kinase. Cancer Res, 2002; 62: 2554-2560.

Chapter 7

Micronodular transformation as a novel mechanism of VEGF-A-induced metastasis

Benno Küsters
Robert MW de Waal
Pieter Wesseling
Cathy Maass
Kiek Verrijp
Dirk J Ruiter
William PJ Leenders

submitted

Abstract

Expression by a tumor of the angiogenic factor Vascular Endothelial Growth Factor-A (VEGF-A) correlates with high vascular density and increased metastasis, but how these latter two relate mechanistically is unclear. We here report that spontaneous metastasis from subcutaneous xenografts is dramatically enhanced when these express recombinant VEGF-A. This effect was attributed to the early stage of tumor cell intravasation as VEGF-A expression did not result in increased tumor burden after hematogeneous delivery to target organs in colonization assays. In contrast to the commonly accepted concept of increased shedding of single cells into a condensed vascular bed, the metastatic potential was enhanced by a distinct architectural transformation of tumors: VEGF-A-expressing tumors, but not VEGF-A-negative xenografts, were characterized by a micronodular growth pattern. Multicellular micronodules budded into vessel lumina, were covered by endothelial cells and generated metastatic tissue embolisms in pulmonary arteries. From mixed xenografts, consisting of both VEGF-A-positive and negative cells, polyclonal lung metastases developed, indicating that it is VEGF-A-induced organized tumor cell clusters, and not single cells, that are responsible for metastasis. This mechanism of metastasis has clinical relevance, as intravascular tumor fragments, covered by an endothelial cell layer, were also observed in renal clear cell carcinomas, tumors that often express high levels of VEGF.

These results challenge the hypothesis that metastasis is restricted to a subpopuplation of aggressive tumor cells, since angiogenically impotent cells can travel along with VEGF-A-expressing cells.

Introduction

Development of metastasis in cancer patients and its treatment is a major problem in oncology. Metastasis is a complex multistep process. The current view is that by a micro-evolutionary process, tumor cells in a primary tumor acquire a metastatic phenotype, characterized by the capacity to invade blood vessels and, after transport via the blood stream, extravasate and grow to clinically relevant lesions at distant sites. As spontaneous metastasis models are rare, most investigations in the field have been performed using colonization approaches in which tumor cells are hematogenously delivered to the organs of interest [1,2]. These colonization models, however, lack the initial event of tumor cell entry into the blood stream, an important and possibly rate-limiting step.

The generally accepted concept of intravasation of tumor cells is that they leave the primary tumor as single cells by degrading stromal matrix and vascular basement membranes, using a repertoire of matrix degradation enzymes and adhesion molecules (for review [3]), followed by entry into the blood or lymphatic vascular bed. This model predicts that the probability of tumor cell entry into the blood increases with tumor vessel density. Indeed, for a number of tumor types a correlation between vessel density and poor prognosis was found (for review see [4-6]). After intravasation, tumor cells may circulate until they adhere to endothelium in distant organs, extravasate and grow out. Alternatively, adhering cells may grow initially intravascularly [7]. Clinical and preclinical data suggest, however, that not the amount of circulating single tumor cells but rather that of circulating tumor cell clusters correlate with development of metastases [8-11]. At this moment it is not clear whether these clusters have a single cell origin or are derived from tumor cell aggregates that dissociated from the primary tumor and intravasated as such. Support for the latter hypothesis comes from studies showing that spontaneous metastases derived from genetically polyclonal tumors were, at least in part, also polyclonal [12].

Angiogenesis in tumors has been recognized as a prognostic feature for tumor progression and development of metastases. As discussed before, increased vessel density in tumors expressing the angiogenic factor Vascular Endothelial Growth Factor-A (VEGF-A) (for review [13]) may simply augment the chance that a tumor cell encounters a vessel. Also, a tumor that has acquired the capacity to induce angiogenesis will be more successful in outgrowing its dormant state after metastatic deposition. These explanations might be somewhat oversimplified, however. First, recent reports demonstrated the presence of intravascular endothelium-covered tumor cell clusters in the primary tumor as origin of metastasis, suggesting that more complex phenomena play a role [14-16] . Secondly, clinical [17-19]

and animal [20,21] data show that for part of the metastatic tumors, induction of angiogenesis is not a prerequisite as for these tumors co-option of the pre-existent vascular bed can be sufficient for tumor blood supply. We previously described that in a mouse model of brain colonization, the human melanoma cell line Mel57 efficiently co-opts pre-existent blood vessels without induction of an angiogenic switch, consistent with minimal expression of angiogenic factors by this cell line [20-22].

It has been suggested by others that VEGF-A-expression is essential, though not sufficient, for metastasis formation in a similar animal tumor model [23]. In preliminary experiments, we found that expression of transgenic VEGF-A by Mel57 cells did not result in increased brain colonization potential, but rather to a change in tumor morphology which was characterized by the presence of dilated and leaky vessels [24]. This led to increased supply of oxygen and nutrients to the tumor cells and consistently to enhanced tumor growth.

As the exact relationship between VEGF-A expression and metastasis is still not clear, we have addressed this issue by investigating the mechanisms of metastasis formation by Mel57 cell lines in the absence or presence of VEGF-A expression.

Materials and Methods

Animals

Specific pathogen-free male (SPF), 6 to 8 weeks old BALB/c nu/nu mice were housed under SPF conditions (5 mice/cage, temperature 20-24 °C; relative humidity 50-60%; 15 air changes per hour; light-dark periods 14 h/10 h). Water and food were available to the animals ad libitum. Experiments were carried out in accordance with the national animal protection laws.

Cell lines and transfections

pIRESneo vector and pEGFP-IRESneo (EGFP=enhanced green fluorescent protein) were obtained from Clontech (Palo Alto, CA). VEGF-A_{165} cDNA was cloned in the EcoR1-BamH1 site of pIRESneo (pVEGF-IRESneo) as described [20]. Mel57 melanoma cells were transfected using Fugene reagent (Roche, Mannheim, Germany) with plasmid pEGFP-IRESneo or pVEGF-IRESneo and stable treansfectants were selected by culturing in 400 µg/ml G418. VEGF-A expression levels in conditioned media were determined by ELISA as described previously [25] and were 30-50ng/10^6 cells/24h. Consistent with the fact that neomycin resistance was linked via the IRES to expression of the cDNA of interest, close to 100% of Mel57-EGFP cells expressed EGFP as determined by fluorescence microscopy *in vitro*, and *in vivo* by immunohistochemistry on brain sections of mice, carrying Mel57-EGFP brain lesions

(see below). Conversely, using in situ hybridization for VEGF-A on Mel57-VEGF-A brain lesions, we could demonstrate that all of these cells, but not parental or EGFP expressing Mel57 cells, expressed VEGF-A. There was no difference between growth rates of the different cell lines *in vivo*.

Colonization and metastasis models

Colonization models:

Equal numbers ($5x10^4$) of Mel57-VEGF-A and Mel57-EGFP cells were co-injected into the internal carotid artery for induction of brain metastases as described previously (*n*=11) [20,26] . Similarly, $6x10^6$ Mel57-VEGF and Mel57-EGFP cells (in a 1:1 ratio) were injected into the tail vein of nude mice (*n*=7) to examine homing to lung and brain. Animals were sacrificed after two to three weeks when mice developed cachexia or acute neurological defects.

Spontaneous metastasis

To examine spontaneous lung metastasis, two sets of experiments were performed. Subcutaneous tumors were induced in nude mice by injection of a mixture of Mel57-VEGF-A and Mel57-EGFP cells into the flank ($1x10^6$ cells for each cell line, *n*=9). Otherwise, two separate tumors were induced on the right (Mel57-EGFP) and the left (Mel57-VEGF-A) flank ($2x10^6$ cells per flank)(*n*=5). Because VEGF-A-expressing tumors grew faster than Mel57-EGFP tumors, we injected the Mel57-EGFP cells 5 weeks prior to VEGF-A expressing cells. Thus, Mel57-VEGF-A and Mel57-EGFP tumors were of comparable size at the time of analysis.

Mice were sacrificed after development of severe cachexia due to tumor load. In two out of five animals carrying tumors on both flanks, Mel57-EGFP tumors had to be removed because of severe ulceration after 6 weeks of tumor growth. These mice were still included in the analysis of metastatic composition.

Histological and immunohistochemical analysis

For (immuno)histochemistry, tissues (subcutaneous tumor, heart, lung, liver, kidney and brain) were snap-frozen in liquid nitrogen or fixed in buffered formalin. Brains were sectioned in six coronal slices. All six slices of each brain were placed side by side in one cassette, and embedded in paraffin. To examine lung metastases, right and left lungs were separated from each other and subsequently each lung side was dissected in individual lobes.

These lobes were placed side by side in one cassette, and embedded in paraffin. Using this protocol a representative overview of each organ in each section is obtained. Sections of 4 μm underwent conventional H&E staining or immunohistochemical staining as described before [20,27] . Antibodies used were anti-EGFP (a kind gift of Dr. E. Cuppen, Dept. of Cell Biology, UMCN) to detect Mel57-EGFP cells, anti-murine CD31 and CD34 (Hycult Biotechnology, Uden, The Netherlands) and 9F1 [20,27] to detect endothelial cells, rabbit anti-mouse Ki-67 (Dianova, Hamburg, Germany) to identify proliferating murine cells (this antibody does not cross-react with human Ki67), mouse anti- α-smooth muscle actin (α-Sm1, Sigma, Zwijndrecht, The Netherlands) to detect pericytes and vascular smooth muscle cells, and rabbit anti-laminin (Dako, Glostrup, Denmark) to detect basement membranes. To detect Mel57-VEGF-A cells, we performed in situ hybridization (ISH) on 10 μm sections using a digoxigenin-labelled VEGF-A antisense RNA as probe and the corresponding sense RNA as a control, using standard techniques.
Sections of human renal cell carcinomas or melanoma that had previously been eveluated on H&E staining as having intravascular localization, were stained with anti-CD31 to detect endothelial cells.

Statistical analysis

In each mouse, the number of microscopic lesions consisting of EGFP- or VEGF-A-expressing cells and mixed lesions were counted. From these numbers, ratios of monoclonal/polyclonal lesions were calculated. For subcutaneous tumors, volumes were determined by multiplying hight x width x depth. The softwareprogram SPSS (SPSS 9.0 for Windows, SPSS Inc., Chicago, Illinois, USA) was used for statistical analysis. Differences were considered significant when $p<0.05$, as determined by Wilcoxon signed rank test. Analyses were performed both on absolute numbers and ratios, where appropriate.

Results

VEGF-A does not increase metastatic burden in colonization assays

To investigate whether VEGF-A increased the rate of brain colonization, we injected a mixture of equal numbers of Mel57 cells expressing VEGF-A or EGFP (serving as VEGF-A negative, readily detectable control cells) into the internal carotid artery of nude mice and analyzed distribution and numbers of Mel57-EGFP and Mel57-VEGF-A lesions by anti-EGFP immunostaining and in situ hybridization (ISH) for VEGF-A, respectively. More than 85% of the lesions grew by clonal expansion as they consisted of either Mel57-EGFP cells or Mel57-VEGF-A cells (p=0.002, Fig. 1A, upper two panels and Fig. 1B; Table 1a). There was no significant difference between numbers of EGFP- and VEGF-A expressing lesions (Fig. 1B; Table 1a), implying that in this colonization model VEGF-A did not enhance metastasis formation. To confirm these data in a second colonization assay, we injected a similar mixture of Mel57-VEGF-A and Mel57-EGFP cells into the tail vein of nude mice and analyzed tumor formation in various organs. Apart from lung, brain was the only organ in which tumor growth could be detected. Again, brain lesions were predominantly formed by clonal expansion of single tumor cells (p=0.016) and VEGF-A did not confer a colonization advantage upon the tumor cells (Fig. 1C ; Table 1b). Remarkably, while in the brains of these animals multiple lesions were always present (Table 1b), no or only few lung lesions were detected, indicating a strong preference for the melanoma cells to grow in brain parenchyma. To be able to still analyze lung lesions after intravenous injection, we had to inject an uncommonly high number of tumor cells (6 million). Intriguingly, in contrast to the brain lesions which were monoclonal, 50% of the lung lesions in these same animals had a mixed tumor phenotype (Fig. 1D; Table 1b). The polyclonal character of these lung lesions could be attributed to outgrowth of cell aggregates that were present in the highly concentrated cell suspension that was injected, an observation which was similar to that previously described by Yamamoto et al.[28]. Thus, upon intravenous injection, tumor cell aggregrates were captured in the lungs while single cells passed the lung capillary filter and homed to the brain.

Figure 1

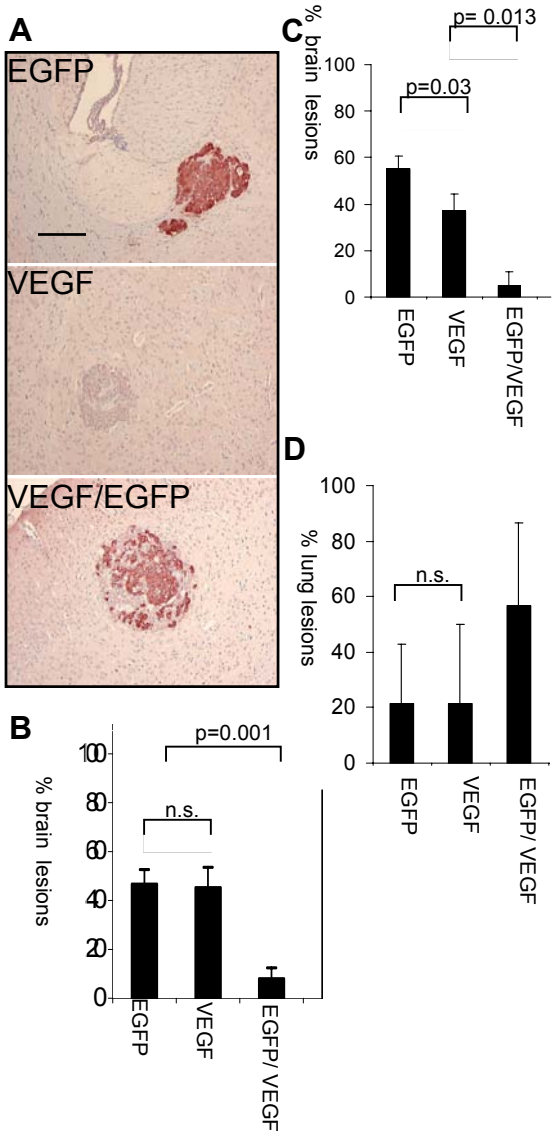

Fig 1. VEGF-A expression does not facilitate colonization potential in brain upon intracarotid or intravenous injection. A: EGFP immunostaining of brain lesions consisting of Mel57-EGFP, Mel57-VEGF-A or a mixture as indicated. Bar represents 0.2 mm. B: Quantification of monoclonal and polyclonal lesions in brain after intracarotid injection of a 1:1 mixture of VEGF-A and EGFP cells . Note that VEGF-A did not enhance homing to brain (n=11; see also Table 1a). More than 85% of the lesions were homogeneous and thus were likely to have a monoclonal origin. C: Quantification of tumor types in brain after intravenous injection into the tail vein (n=7; see also Table 1b). Again, brain lesions had a predominantly monoclonal origin. D: Analysis of lung lesions after intravenous injection . See also colour display page 158.

Table 1

a) Composition of brain metastases in mice, injected with a 1:1 mixture of Mel57-VEGF-A and Mel57-EGFP cells into the internal carotid artery.

mouse#	days p.i	# VEGF- lesions (%)	# EGFP- lesions (%)	# sum of monoclonal lesions (%)	# mixed lesions (%)	# all brain lesions
1	15	38 (36.9)	53 (51.5)	91 (88.4)	12 (11.6)	103
2	15	60 (37.3)	81 (50.3)	141 (87.6)	20 (12.4)	161
3	15	72 (43.4)	81 (48.8)	153 (92.2)	13 (7.8)	166
4	15	63 (47.0)	63 (47.0)	126 (94.0)	8 (6.0)	134
5	20	17 (54.8)	14 (45.2)	31 (100)	0 (0)	31
6	18	26 (40.0)	33 (50.8)	59 (90.8)	6 (9.2)	65
7	18	23 (54.7)	17 (40.5)	40 (95.2)	2 (4.8)	42
8	18	16 (43.3)	15 (40.5)	31 (83.8)	6 (16.2)	37
9	18	38 (59.4)	24 (37.5)	62 (96.9)	2 (3.1)	64
10	18	48 (47.1)	45 (44.1)	93 (91.2)	9 (8.8)	102
11	16	33 (34.0)	56 (57.7)	89 (91.7)	8 (8.2)	97
	mean	39.5	43.8	83.3	7.8	
		P=0.3 (n.s.)		P=0.002		

b) Composition of lung and brain metastases in mice, injected with 6 million cells into the tail vein.

Mouse #	days p.i	# VEGF- lesions in lung (%)	# EGFP- lesions in lung (%)	# sum of monoclonal lung lesions (%)	# mixed lesions in lung(%)	# all lung lesions	# VEGF- lesions in brain (%)	# EGFP- lesions in brain (%)	# all monoclonal brain lesions (%)	# mixed lesions in brain (%)	# all brain lesions
1	16	2 (66,7)	0 (0)	2 (66,7)	1 (33,3)	3	88 (36,6)	141 (58,5)	229 (95,0)	12 (5)	241
2	16	0	0	0	0	0	1 (50)	1 (50)	2 (100)	0 (0)	2
3	16	0 (0)	4 (44,4)	4 (44,4)	5 (55,6)	9	37 (39,4)	55 (58,5)	92 (97,9)	2 (2,1)	94
4	16	6 (31,6)	8 (42,1)	14 (73,7)	5 (26,3)	19	7 (29,2)	17 (70,8)	24 (100)	0 (0)	24
5	16	6 (9,7)	13 (21,0)	19 (30,7)	43 (69,3)	62	69 (32,4)	129 (60,4)	198 (93,0)	15 (7)	213
6	23	0	0	0	0	0	2 (33,3)	3 (50)	5 (83,3)	1 (16,7)	6
7	20	0 (0)	0 (0)	0 (0)	1 (100)	1	27 (42,8)	33 (52,4)	60 (95,2)	3 (4,8)	63
	mean	2	3,5	5,6	7,9		33	54	87	5	
		P=0.13		P=0.81			P=0.03		P=0.016		

c) Composition of lung lesions in mice, carrying subcutaneous ipsilateral Mel57-EGFP tumor and contralateral Mel57-VEGF-A tumor.

mouse #	day post first inoculation	# VEGF- lesions in lung (%)	# EGFP- lesions in lung (%)	# mixed VEGF/EGFP lesions	# all lung lesions
1	67	31 (75,6)	10 (24,4)	0	41
2	67	13 (76,5)	4 (23,5)	0	17
3	67	15 (93,8)	1 (6,2)	0	16
4	67	24 (100)	0 (0)	0	24
5	67	17 (100)	0 (0)	0	17
	mean	18	3	0	21
		P=0.043			

d) Composition of lung lesions in mice, carrying subcutaneous Mel57-EGFP/Mel57-VEGF mixed tumors.

mouse #	days post tumor injection	# VEGF- lesions in lung (%)	# EGFP-lesions in lung (%)	# sum of monoclonal lung lesions (%)	# mixed VEGF/EGFP lesions (%)	# all lung lesions
1	26	0 (0)	2 (20,0)	2 (20,0)	8 (80,0)	10
2	26	0 (0)	3 (18,8)	3 (18,8)	13 (81,2)	16
3	39	1 (4,35)	1 (4,35)	2 (8,7)	21 (91,3)	23
4	38	1 (4,8)	2 (9,5)	3 (14,3)	18 (85,7)	21
5	26	0 (0)	0 (0)	0 (0)	15 (100,0)	15
6	49	0 (0)	0 (0)	0 (0)	1 (100,0)	1
7	49	0 (0)	0 (0)	0 (0)	2 (100,0)	2
8	49	0 (0)	1 (10,0)	1 (10,0)	9 (90,0)	10
9	49	0 (0)	0 (0)	0 (0)	2 (100,0)	2
	mean	0.2	1	1.2	9.9	
		P=0.13 (n.s.)		P=0.003		

e) Composition of lung lesions in mice, carrying subcutaneous Mel57-EGFP/Mel57-VEGF mixed tumors.
P-values were calculated via Wilcoxon-signed rank test based on absolute numbers. When comparing ratio's, similar p-values result (see corresponding figure 1).

mouse #	days post tumor injection	# parental- lesions in lung (%)	# EGFP- lesions in lung (%)	# sum of monoclonal lung lesions (%)	# mixed parental/EGFP lesions (%)	# all lung lesions
1	81	0 (0)	1 (25,0)	1 (25,0)	3 (75,0)	4
2	81	1 (7,1)	4 (28,6)	5 (35,7)	9 (64,3)	14
3	81	5 (20,0)	2 (8,0)	7 (28,0)	18 (72,0)	25
4	81	10 (34,5)	4 (13,8)	14 (48,3)	15 (51,7)	29
5	81	0 (0)	1 (20,0)	1 (20,0)	4 (80,0)	5
	mean	3.2	2.4	5.6	9.8	
		P=0.94		P=0.06 (n.s.)		

Morphology of subcutaneous tumors: VEGF-A induced micronodular transformation

Subcutaneous tumors from either Mel57-EGFP or Mel57-VEGF-A cells were grown and characterized on the morphological and immunohistochemical level in at least three independent experiments using groups of 5 mice for each tumor type. Parental Mel57 and Mel57–EGFP tumors behaved similarly with respect to growth rate (not shown) and had comparable phenotypes. They developed relatively slowly and were highly necrotic (Fig. 2A), leaving a small rim of viable tumor tissue which was sparsely vascularised as was shown by anti-CD31 staining (Fig. 2D). A completely different growth rate and architecture was observed with Mel57-VEGF-A xenografts. These grew rapidly to large, histologically viable-appearing tumors with a distinct morphology (Fig. 2B,C, E-J). Tumors were composed of multiple micronodules which were surrounded by a network of endothelial cells and pericytes (Fig. 2E-J, see also Fig. 4G). Some of these (smaller) nodules were protruding in large sinusoidal vessels (Fig. 2C, E, G and respective insets). Stainings for αSMA and CD34 on serial sections revealed a composition in which the endothelial cells were localized at the outer edge, while pericytes were on the inside (Figure 2I and J). This is consistent with a model of bulging of micronodules into dilated vessels during which process nodules become gradually covered by vessel wall elements as previously suggested [15]. Sometimes, small nodules in the tumor periphery appeared only loosely, if at all, attached to the vessel wall and impressed as tumor emboli. The notion that these nodules were not attached to the vessel wall was strengthened by further stainings of the same nodule at different levels (not shown). Such loose nodules were encountered only occasionally, presumably because these will be carried away rapidly by the circulation. Instead of widespread central necrosis, the larger individual tumor nodules in the tumor centre showed small areas of central necrosis (compare Fig. 2B and 2A).

Figure 2

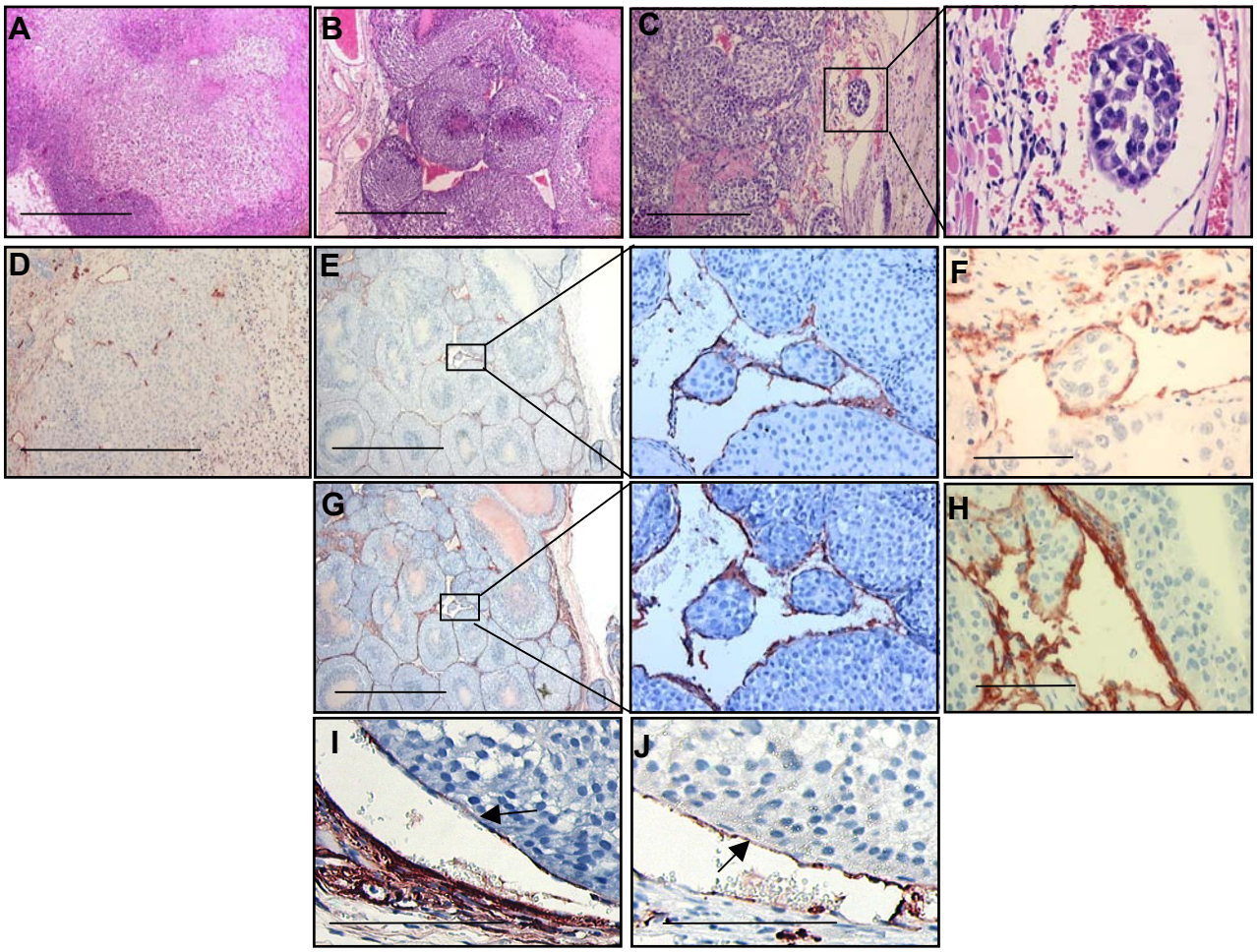

Fig 2. Histological architecture of Mel57-EGFP (A, D) and Mel57-VEGF-A (B, C, E-J).
A, B and C: H&E staining. D, E and J: anti-CD34 staining. Note the micronodular structure of the VEGF-A tumor and the coverage of these nodules by pericytes and endothelial cells (αSMA-staining in (G) and (I) and CD34 staining in (E) and (J)); endothelial identity was confirmed by 9F1 staining (F) and CD31 (H). Note in figures I and J, which are stainings on serial sections, that endothelial cells were localized primarily at the outer side of the nodules, whereas pericytes were on the inside (arrows in (I) and (J)). Frequently, loose nodules were observed in dilated sinusoidal vessels (C,E and G and inset). In contrast, Mel57 tumors were highly necrotic in the tumor center (A). Only the tumor rim consisted of viable cells with few vessels (A,D). Bars represent: 1 mm in A-E,G; 0.1 mm in F,H and 0.2 mm in I,J. See also colour display page 159.

VEGF-A increases metastatic capacity in a spontaneous metastasis model

To examine whether VEGF-A increased the efficiency of metastasis, we grew both tumor types (Mel57-EGFP and Mel57-VEGF-A) on opposite flanks of the same mouse. Based on growth curves of individual tumors obtained from previous experiments (not shown), we injected the Mel57-EGFP tumors in groups of mice five weeks prior to injection of Mel57-VEGF-A tumors to compensate for the difference in tumor growth rates. Metastatic burden and the composition of the metastases were examined by anti-EGFP immunostaining and VEGF-A mRNA in situ hybridization after nine weeks, when EGFP and VEGF-A tumors had

reached similar sizes (Fig. 3A). In striking contrast to the results obtained in the colonization assays, we now found that VEGF-A expression significantly increased the probability of lung metastasis formation (p=0.043, Fig. 3B; Table 1c). At least 90% of the lesions consisted of Mel57-VEGF-A cells only, despite the fact that Mel57-EGFP tumors had been growing for 5 weeks longer. No mixed lung lesions were found in this group. In two mice in which the EGFP tumors had to be resected due to severe ulceration (at a size of approximately 700 mm^3) and in which consequently EGFP tumors had been growing for 6 weeks instead of 9, exclusively VEGF-A lesions were found. Tumors were localized in the larger branches of pulmonary arteries (Fig. 3C, arrows), strongly suggesting that these originated from tumor embolisms. Brain metastases were never detected in mice carrying subcutaneous xenografts.

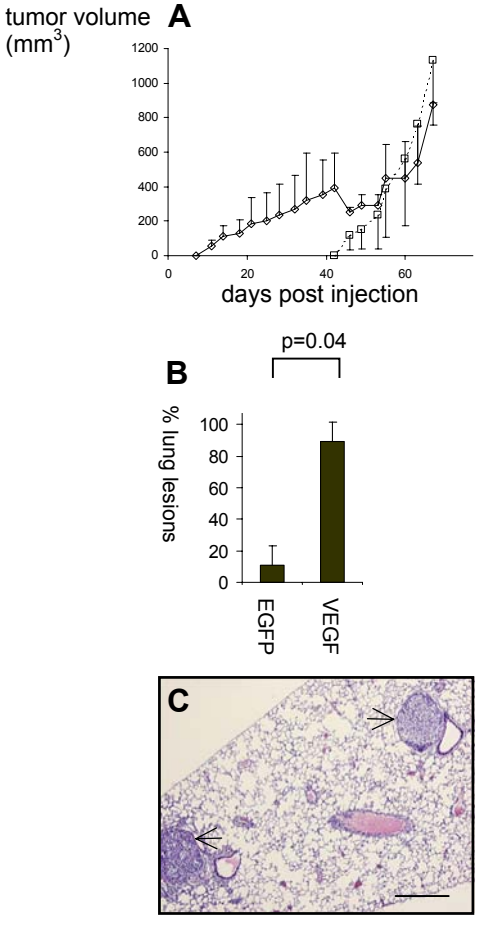

Figure 3. VEGF-A enhances spontaneous metastasis from subcutaneous tumors.
A: Growth curves of EGFP (-o-) and VEGF-A (…□…) expressing Mel57 tumors, grown on the opposite flanks of mice (*n*=5). After 9 weeks, when tumors had reached similar sizes, mice were sacrificed (see text). Tumor growth was measured weekly using calipers. Tumor volumes are expressed as h x w x d. The dip in the growth curve at day 45 is caused by the excision of Mel57-EGFP tumors in two mice due to ulceration. These mice were included in the analysis of composition of metastasis. B: Lung lesions, consisting of Mel57-VEGF-A or Mel57-EGFP cells were counted after EGFP immunostaining (see also Table 1c). To confirm identity of VEGF-A lesions, VEGF mRNA-ISH was performed (not shown). C: Representative H&E staining, showing tumor emboli located in the larger branches of the pulmonary arteries (arrows). Bar represents 0.3 mm. See also colour display page 158.

VEGF-A-induced micronodular growth facilitates the formation of multicellular tumor emboli

To examine in more detail the composition of the tumor emboli in the lungs, we performed the following experiment: Mel57-EGFP and Mel57-VEGF-A cells were mixed in a 1:1 ratio and injected into the flank of nude mice to establish mixed subcutaneous tumors. The resulting tumors had comparable growth profiles and phenotypes as Mel57-VEGF-A xenografts (see H&E staining in the inset in figure 4A), consistent with the paracrine activity of VEGF-A. Also, polyclonal intravascular loose nodules could be observed in these xenografts (see EGFP staining in figure 4M). Analysis of the primary tumors and lung metastases thereof by EGFP staining revealed that the composition of lung deposits was very similar to that of the micronodules in the primary tumor (compare Fig. 4A and B), which was confirmed by VEGF-A-mRNA in situ hybridization (Fig. 4H). Analysis of serial sections revealed that VEGF-A in situ hybridization and EGFP stainings were complementary (not shown), indicating that transgenic proteins were stably expressed and that no confounding loss of expression had occurred. Most lesions were polyclonal, as they were composed of both Mel57-EGFP and Mel57-VEGF-A (Fig. 4L; Table 1d). Only a small fraction of the lesions was clonal, containing either Mel57-EGFP or Mel57-VEGF-A cells (Fig. 4L; Table 1d). This reflected the composition of the primary tumors where occasionally nodules were found that consisted of a single cell type, probably also arising by clonal expansion within the primary tumor (Fig. 4C, arrowheads). Interestingly, in the right ventricle of the heart of one tumor-bearing animal we found tumor micronodules of the same mosaic composition as the primary tumor and the lung metastases (Fig. 4D and inset). Again, these nodules had tissue characteristics as they contained laminin (Fig. 4E) and were covered by proliferating murine cells (Fig. 4F: Ki67-staining, Fig. 4G: α-SM staining). From the location of the Ki67-positive cells we conclude that these cells consist of both pericytes and endothelial cells (see also figures 2I and 2J), although it is difficult to accurately identify each proliferating cell in these stainings.

If generation of tumor emboli augments metastasis formation, the question arises how the parental or EGFP-expressing tumors metastasize. To answer this, we generated subcutaneous tumors containing equal numbers of parental Mel57 and Mel57-EGFP cells, and analyzed the composition of lung deposits using anti-EGFP immunohistochemistry (Fig. 5A). Most lung metastases examined were composed of both EGFP and parental Mel57 cells (Fig. 5B; Table 1e), implying that these tumors may also metastasize by shedding of tumor cell aggregates into the circulation. Although we could not resolve whether these aggregates were also

accompanied by primary tumor-derived murine endothelial cells and pericytes, the architecture and composition of these primary tumors suggest otherwise.

Figure 4

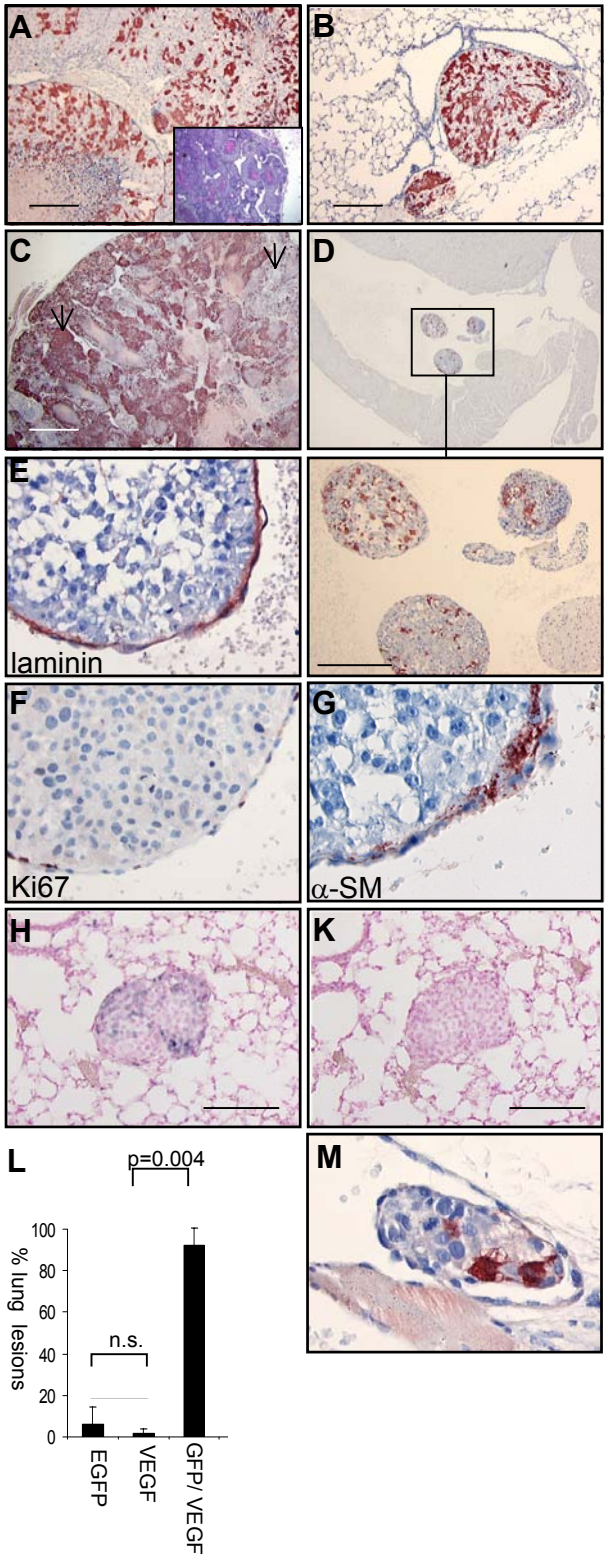

Analysis of VEGF-A-induced metastatic tissue. Subcutaneous mixed tumors containing equal numbers of Mel57-EGFP and Mel57-VEGF-A cells were grown on the flanks of nude mice (*n*=9). A: EGFP staining of a subcutaneous mixed tumor and (B) a lung lesion from the same animal. The inset in (A) shows an H&E overview field (x25) of the same tumor, showing the nodular phenotype that is characteristic of Mel57-VEGF-A tumors. Note the similar composition of lung lesions in (B) and subcutaneous tumor micronodules. C: In the primary tumor, regions with a homogeneous composition could be identified (arrow), consistent with the occurrence of small numbers of homogenous lung lesions (L). D: EGFP staining of tumor micronodules in the right ventricle of the heart. Immunostaining showed that nodules were covered by laminin (E), proliferating (F) endothelial cells and pericytes (G), giving these nodules tissue characteristics. Note that in figure F only murine proliferating cells are detected with our antibody. To confirm VEGF-A identity of EGFP-negative Mel57 cells, VEGF-A *in situ* hybridisations on lung lesions were performed (H); sense control hynbridization (K). Bars represent 0.2 mm. L: Quantification in lungs of mono- and polyclonal metastases, derived from mixed subcutaeneous xenografts (see also Table 1d). M: intravascular nodule, derived from a VEGF-A/EGFP mixed tumor with a polyclonal composition, as illustrated by EGFP-immunostaining. See also colour display page 160.

Intravascular endothelial cell-covered tumor fragments are observed in clinical tumors

To evaluate whether intravascular micronoduli have clinical relevance, we looked in detail at renal cell carcinomas, tumors that often have high constitutive expression of VEGF-A due to mutations of the Von Hippel Lindau (VHL) protein [29]. We found that in tumors that were designated by pathologists to have intravascular localization, such endothelium-covered nodules could indeed be observed. Figure 5D shows an example of such a nodule, laying within a dilated blood vessel which is at some distance of the main tumor mass (arrow). These results confirm those obtained by Sugino et al. [16] who recently reported on this phenotype in a number of clinical tumor types. The relation of this phenotype to VEGF-A expression is currently under investigation in our laboratory.

Figure 5

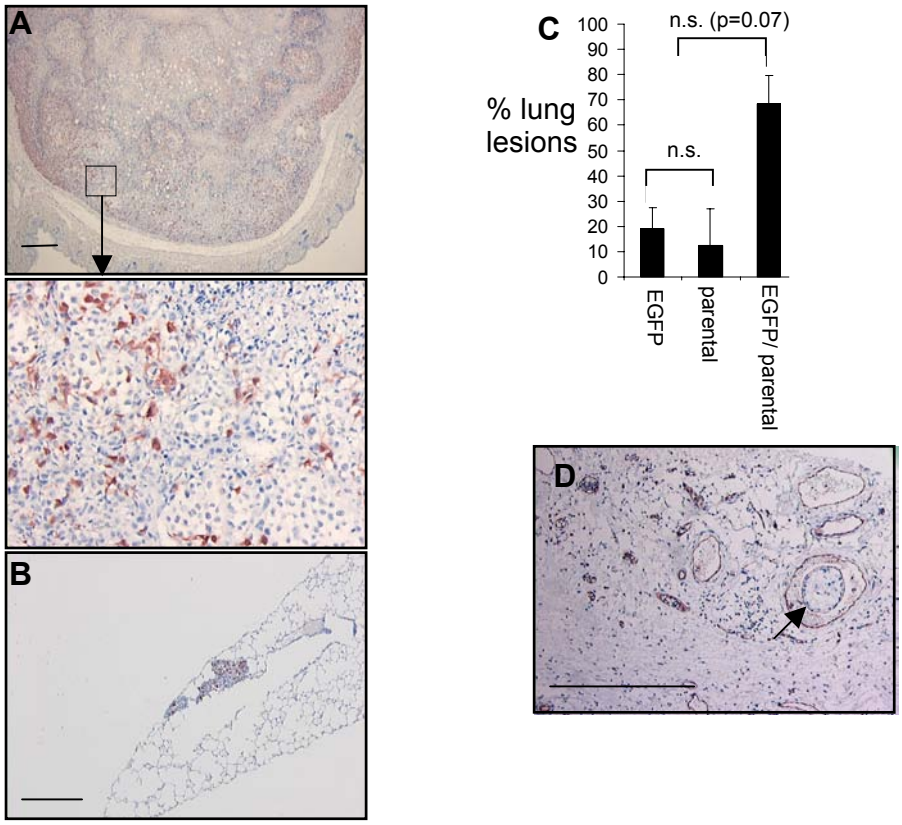

Fig 5. Analysis of metastasis from mixed parental and EGFP-expressing Mel57 subcutaenous tumors.
A and B: EGFP immunostaining of a subcutaneous mixed tumor containing equal numbers of Mel57-EGFP and parental Mel57 cells (*n*=5) (A) and a derived lung lesion (B). Note that lung metastases are predominantly composed of both cell types. C: Distribution in lungs of mono- and polyclonal lesions (see also Table 1e). The low number of homogenously appearing lesions may be due to the existence of homogenous areas in the primary tumor, like in Figure 4.
D: CD31 staining of a section of a clinical renal clear cell carcinoma, showing the presence of an intravascular tumor fragment, covered by endothelial cells (arrow). Bars represents 0.3 mm. See also colour display page 158.

Discussion

Metastasis of tumors is a complex multistep process, requiring intravasation, transport, extravasation and outgrowth. Expression of VEGF-A by tumors and concomitant high tumor vessel densities have been associated with poor prognosis in a number of cancer types (for review see [4,13]). This correlation has been attributed to an increasing probability of tumor cell intravasation. Obviously, other factors must play a role too, since a correlation between numbers of circulating tumor cells and prognosis is lacking (for review see [11]). For instance, the angiogenic potential of a tumor cell might determine part of its metastatic properties, as an angiogenic phenotype will fuel outgrowth of distant metastases beyond a dormant stage [3,30]. However, we and others recently demonstrated that especially in vessel-dense organs like brain, lung, kidney and liver, tumors can grow by vessel co-option in an angiogenesis-independent fashion [18-21,31,32].

In our brain colonization models in which mixed populations of tumor cells were injected intravenously or into the internal carotid artery, metastases developed predominantly by clonal outgrowth of single cells, which is in agreement with observations by others [33]. Interestingly, upon injection of Mel57 cells into the tail vein, multiple brain lesions but only few lung lesions developed, indicating a clear preference of this cell line to colonize brain (compatible with the 'seed and soil' hypothesis [34]). The low preference of Mel57 cells to colonize lungs forced us to inject high numbers of tumor cells to establish lung lesions in a colonization assay. Unavoidably, tumor cell aggregates were formed in these high-density cell suspensions, leading to embolism in the lungs. Therefore, we consider this result as an artefact with little or no relevance for the human situation. In fact, this finding was confirmed in a recent publication by Yamamoto et al., who showed that intravenous injection of relatively small numbers of tumor cells resulted in predominantly monoclonal lung lesions, whereas injection of high numbers of cells resulted in polyclonal lesions [28].

In our colonization models, VEGF-A did not increase tumor burden in brains. In a previous report, Yano et al. also described that overexpression of VEGF-A in a panel of carcinoma cell lines, did not lead to enhanced metastasis formation in a similar brain colonization model [23]. However, downregulation of VEGF-A by antisense transfection led to a significantly attenuated brain colonization potential, suggesting that a basal level of VEGF-A expression by tumor cells was necessary for brain colonization. In contrast, our results showed that the parental Mel57 and Mel57-EGFP lines were able to generate brain metastases in the absence of significant VEGF-A expression. Apparently, Mel57 melanoma metastases were more

successful in incorporating pre-existent brain vessels in the absence of VEGF-A than the cell lines used by Yano et al.

The heterogeneity in numbers of lung lesions in metastasis experiments within groups (see also tables 3-5) made it hard to make solid statements about differences in metastatic efficacies by just comparing absolute numbers of lung lesions in mice carrying EGFP- or VEGF xenografts. The differences in growth rate between EGFP and VEGF-expressing tumors would make interpretation even more difficult. Therefore, to compare metastatic capacities of VEGF-A and EGFP-expressing xenografts, we chose to establish the respective xenografts in the same mice. This enabled us to determine the ratio of EGFP and VEGF-lesions in the lungs, which is far more reliable than absolute numbers. We found that, in striking contrast with the colonization assays, Mel57-VEGF-A tumors metastasized to lungs much more efficiently than Mel57-EGFP tumors in mice carrying contralateral EGFP- and VEGF-A-expressing tumors. The study of metastatic properties of these tumor cell lines with such different growth profiles may seem cumbersome also in this experimental setup. However, our data suggest that in this instance the comparison is justified. First, volumes of the respective tumors were comparable in each mouse at the end point of analysis. Secondly, Mel57-VEGF-A tumors had much less time to metastasize than the Mel57-EGFP tumors, evenmore suggesting that VEGF-A expression is the crucial determinant for efficient metastasis in this model.

Our morphological data show that tumor cells did not detach from the primary tumor as single cells but rather as tissue fragments, at least partly covered by a basal lamina, endothelium and pericytes. These tissue fragments enter the circulation, are captured by the filter of the lung capillary bed and grow out. This hypothesis is consistent with the fact that in the primary tumors, tumor nodules that ly loose within vasculature are encountered only occasionally. Indeed, such nodules will be carried away by the circulation instantly, similar to the model proposed by Sugino et al.[15].

It is unclear how the architecture of the VEGF-A-expressing tumors evolves. Because Mel57 cells secrete laminin, endothelial cells lining dilated vasculature may be induced by tumor-derived VEGF-A to proliferate and migrate, using tumor cell-associated laminin as a matrix. Indeed, endothelial cells and/or pericytes were in a proliferative state on the surfaces of the tumor nodules. VEGF-A expression may also lead to higher laminin expression levels and the formation of matrix layers [35]. Like angiogenic endothelial cells, Mel57 cells also express VEGFR2 (data not shown), leaving open the possibility that an autocrine VEGF/VEGFR2 loop is involved in the development of this phenotype. Which target genes of VEGF-A, either

in stromal cells or tumor cells, are involved in development of metastatic tumor tissue nodules, is currently under investigation in our lab.

Interestingly, brain metastases were never observed in animals carrying subcutaneous tumors, favoring the hypothesis that the tumor emboli within the circulation cannot pass the lungs efficiently. Our findings with mixed parental/EGFP tumors show that these may also metastasize via a mechanism of tumor cell cluster embolism, although much less efficient than Mel57-VEGF-A tumors. Importantly, in these tumors we did not detect intravascular endothelium-covered nodules, suggesting a potential correlation between endothelial coverage and metastatic efficiency.

Based on our observations, VEGF-A may facilitate the metastatic process by induction of irregular vasodilatation, allowing for protrusion of micronodular tumor cell aggregates into the vessel lumen. This scheme of events would indeed predict that endothelial cells form the outer, and pericytes the inner layer of the nodular cover, just as we demonstrated via stainings with anti-CD34 and anti-α-SMA on serial sections. Nodules within the main tumor mass that, during tumor growth, become localized suboptimally for intravasation, will remain there and grow to large nodules, ultimately making up the main tumor mass.

Our data may also provide an explanation for the lack of correlation between circulating tumor cells and poor prognosis: PCR-based techniques on whole blood samples do not distinguish between tumor cell clusters with metastastic capacity and single circulating tumor cells that may not be able to survive because they are not in a 'tumor-tissue' context. This tissue context, especially the endothelial coverage, may mask tissue factor exposure by tumor cells and thereby prevent clot formation in the microenvironment of the primary tumor. It is also tempting to speculate that coverage by endothelial cells leads to protection from the immune system, thus further increasing the chance of successful metastatic deposition.

Our study challenges the prevailing view that metastases arise by clonal outgrowth of single tumor cells that, due to genetic instability and via a micro-evolutionary process, have acquired a metastatic phenotype [1,33,36]. In fact, tumor cells like Mel57-EGFP, that intrinsically metastasize inefficiently, can successfully travel along with VEGF-A-expressing tumor cells. This may explain the occasional presence in cancer patients of metastases that have little angiogenic potential although they originated from highly angiogenic primary tumors [17]. Tumor tissue fragments may have high clinical relevance since these are frequently found in lymph- and blood vessels of cancer patients [37,38] and their presence correlates with poor prognosis (for review [11]). It needs to be established in which human tumors VEGF-A expression contributes to generation of metastatic tissue. Interestingly, Von Hippel Lindau

(VHL)-associated renal clear cell carcinomas (RCCs), cancers with high VEGF-A expression levels, also frequently display intravascular growth, and we indeed could detect intravascular RCC nodules, covered with endothelial cells. To what extent intravascularly growing tumors contain stromal cells and what their characteristics are, is under investigation in our lab.
Yet, not all tumor types experience enhanced metastatic dissemination upon VEGF-A overexpression [39,40], indicating that the effect of VEGF-A that we describe here must be umor type-specific to a certain extent. We consider it unlikely that our observations are the result of artificial VEGF-A overexpression, since the levels of recombinant VEGF-A, expressed by Mel57-VEGF-A cells, are comparable to those found in for example glioma cell lines [41].
Recently, in a murine model of metastatic mammary carcinoma the presence in lung of tumor cell emboli, covered by an endothelial cell layer, was demonstrated [14,15]. Micronodular pattern formation in the corresponding primary tumors was attributed to pleiotrophin expression. An exclusive role for pleiotrophin in the development of the nodular micro-architecture of Mel57-VEGF-A tumors can be excluded since this factor is expressed also in parental Mel57 cells [27]. E-cadherin has been described to be essential for intercellular tumor cell adhesion in circulating tumor cell clusters [42,43]. In our model, however, neither the parental nor the VEGF-A expressing cell lines or the derived tumors expressed E-cadherin (unpublished results).
Anti-VEGF therapy has been considered to be a powerful approach to prevent clinical manifestations of metastatic disease in cancer patients. By inhibiting angiogenesis, minute metastatic deposits should remain dormant, turning cancer into a chronic disease. However, especially in vessel-dense organs the angiogenesis-dependency of tumors is at least questionable, since tumors may (partly) thrive by incorporating pre-existent vasculature. Our results, however, point to a possible novel role for anti-angiogenic therapy: anti-VEGF therapy in patients with primary cancers might decrease the chance of metastatic spread, not simply by decreasing vascular density, but rather by preventing the formation of a micronodular architecture that facilitates intravasation. In this regard, it will be important to further investigate the clinical relevance of a micronodular growth pattern in other types of cancer. An interesting initial study on this has recently been published by Sugino et al who demonstrated intravasation of tumor micronodules in a number of tumor types, among which RCC [16]. Unraveling of the underlying mechanisms will therefore be of potentially high significance in oncology.

Acknowledgements – We thank Debby Smits, Ilona van den Brink and Geert Poelen for excellent technical assistance with the animal experiments.

References

1. Fidler IJ Critical determinants of melanoma metastasis J Investig Dermatol Symp Proc 1996;1:203-208.
2. Killion JJ, Radinsky R, and Fidler IJ Orthotopic models are necessary to predict therapy of transplantable tumors in mice Cancer Metastasis Rev 1998;17:279-284.
3. Ellis LM and Fidler IJ Angiogenesis and metastasis Eur J Cancer 1996;32A:2451-2460.
4. Hasan J, Byers R, and Jayson GC Intra-tumoural microvessel density in human solid tumours Br J Cancer 2002;86:1566-1577.
5. Weidner N Tumoural vascularity as a prognostic factor in cancer patients: the evidence continues to grow J Pathol 1998;184:119-122.
6. Weidner N and Folkman J Tumoral vascularity as a prognostic factor in cancer Important Adv Oncol 1996;167-190.
7. Al-Mehdi AB, Tozawa K, Fisher AB, et al. Intravascular origin of metastasis from the proliferation of endothelium-attached tumor cells: a new model for metastasis Nat Med 2000;6:100-102.
8. Fidler IJ The relationship of embolic homogeneity, number, size and viability to the incidence of experimental metastasis Eur J Cancer 1973;9:223-227.
9. Glaves D Correlation between circulating cancer cells and incidence of metastases Br J Cancer 1983;48:665-673.
10. Liotta LA, Saidel MG, and Kleinerman J The significance of hematogenous tumor cell clumps in the metastatic process Cancer Res 1976;36:889-894.
11. Vlems FA, Ruers TJ, Punt CJ, Wobbes T, and van Muijen GN Relevance of disseminated tumour cells in blood and bone marrow of patients with solid epithelial tumours in perspective Eur J Surg Oncol 2003;29:289-302.
12. Moffett BF, Baban D, Bao L, and Tarin D Fate of clonal lineages during neoplasia and metastasis studied with an incorporated genetic marker Cancer Res 1992;52:1737-1743.
13. Ferrara N VEGF and the quest for tumour angiogenesis factors Nat Rev Cancer 2002;2:795-803.
14. Sugino T, Kawaguchi T, and Suzuki T Sequential process of blood-borne lung metastases of spontaneous mammary carcinoma in C3H mice Int J Cancer 1993;55:141-147.
15. Sugino T, Kusakabe T, Hoshi N, et al. An invasion-independent pathway of blood-borne metastasis: a new murine mammary tumor model Am J Pathol 2002;160:1973-1980.
16. Sugino T, Yamaguchi T, Ogura G, et al. Morphological evidence for an invasion-independent metastasis pathway exists in multiple human cancers BMC Med 2004;2:9.
17. Pezzella F Evidence for novel non-angiogenic pathway in breast-cancer metastasis. Breast Cancer Progression Working Party. Lancet 2000;355:1787-1788.
18. Neves S, Mazal PR, Wanschitz J, et al. Pseudogliomatous growth pattern of anaplastic small cell carcinomas metastatic to the brain Clin Neuropathol 2001;20:38-42.

19. Vermeulen PB, Colpaert C, Salgado R, et al. Liver metastases from colorectal adenocarcinomas grow in three patterns with different angiogenesis and desmoplasia J Pathol 2001;195:336-342.
20. Kusters B, Leenders WP, Wesseling P, et al. Vascular endothelial growth factor-A(165) induces progression of melanoma brain metastases without induction of sprouting angiogenesis Cancer Res 2002;62:341-345.
21. Kim ES, Serur A, Huang J, et al. Potent VEGF blockade causes regression of coopted vessels in a model of neuroblastoma Proc Natl Acad Sci U S A 2002;12:12.
22. Leenders W, Kusters B, and De Waal R Vessel co-option: How tumors obtain blood supply in the absence of sprouting angiogenesis Endothelium 2002;9:83-87.
23. Yano S, Shinohara H, Herbst RS, et al. Expression of vascular endothelial growth factor is necessary but not sufficient for production and growth of brain metastasis Cancer Res 2000;60:4959-4967.
24. Kusters B, de Waal RM, Wesseling P, et al. Differential effects of vascular endothelial growth factor A isoforms in a mouse brain metastasis model of human melanoma Cancer Res 2003;63:5408-5413.
25. Span PN, Grebenchtchikov N, Geurts-Moespot J, et al. EORTC Receptor and Biomarker Study Group Report: a sandwich enzyme-linked immunosorbent assay for vascular endothelial growth factor in blood and tumor tissue extracts Int J Biol Markers 2000;15:184-191.
26. Kusters B, Westphal JR, Smits D, et al. The pattern of metastasis of human melanoma to the central nervous system is not influenced by integrin alpha(v)beta(3) expression Int J Cancer 2001;92:176-180.
27. Westphal JR, Van't Hullenaar R, Peek R, et al. Angiogenic balance in human melanoma: expression of VEGF, bFGF, IL-8, PDGF and angiostatin in relation to vascular density of xenografts in vivo Int J Cancer 2000;86:768-776.
28. Yamamoto N, Yang M, Jiang P, et al. Determination of clonality of metastasis by cell-specific color-coded fluorescent-protein imaging Cancer Res 2003;63:7785-7790.
29. Harris AL von Hippel-Lindau syndrome: target for anti-vascular endothelial growth factor (VEGF) receptor therapy Oncologist 2000;5:32-36.
30. Folkman J What is the evidence that tumors are angiogenesis dependent? J Natl Cancer Inst 1990;82:4-6.
31. Passalidou E, Trivella M, Singh N, et al. Vascular phenotype in angiogenic and non-angiogenic lung non-small cell carcinomas Br J Cancer 2002;86:244-249.
32. Pezzella F, Pastorino U, Tagliabue E, et al. Non-small-cell lung carcinoma tumor growth without morphological evidence of neo-angiogenesis Am J Pathol 1997;151:1417-1423.
33. Fidler IJ and Talmadge JE Evidence that intravenously derived murine pulmonary melanoma metastases can originate from the expansion of a single tumor cell Cancer Res 1986;46:5167-5171.

34. Fidler IJ The pathogenesis of cancer metastasis: the 'seed and soil' hypothesis revisited Nat Rev Cancer 2003;3:453-458.
35. Potgens AJ, van Altena MC, Lubsen NH, Ruiter DJ, and de Waal RM Analysis of the tumor vasculature and metastatic behavior of xenografts of human melanoma cell lines transfected with vascular permeability factor Am J Pathol 1996;148:1203-1217.
36. Fidler IJ, Schackert G, Zhang RD, Radinsky R, and Fujimaki T The biology of melanoma brain metastasis Cancer Metastasis Rev 1999;18:387-400.
37. Ruiter DJ, van Krieken JH, van Muijen GN, and de Waal RM Tumour metastasis: is tissue an issue? Lancet Oncol 2001;2:109-112.
38. Weidner N New paradigm for vessel intravasation by tumor cells Am J Pathol 2002;160:1937-1939.
39. Kanayama H, Yano S, Kim SJ, et al. Expression of vascular endothelial growth factor by human renal cancer cells enhances angiogenesis of primary tumors and production of ascites but not metastasis to the lungs in nude mice Clin Exp Metastasis 1999;17:831-840.
40. Gannon G, Mandriota SJ, Cui L, et al. Overexpression of vascular endothelial growth factor-A165 enhances tumor angiogenesis but not metastasis during beta-cell carcinogenesis Cancer Res 2002;62:603-608.
41. Sonoda Y, Kanamori M, Deen DF, et al. Overexpression of vascular endothelial growth factor isoforms drives oxygenation and growth but not progression to glioblastoma multiforme in a human model of gliomagenesis Cancer Res 2003;63:1962-1968.
42. Alpaugh ML, Tomlinson JS, Kasraeian S, and Barsky SH Cooperative role of E-cadherin and sialyl-Lewis X/A-deficient MUC1 in the passive dissemination of tumor emboli in inflammatory breast carcinoma Oncogene 2002;21:3631-3643.
43. Tomlinson JS, Alpaugh ML, and Barsky SH An intact overexpressed E-cadherin/alpha,beta-catenin axis characterizes the lymphovascular emboli of inflammatory breast carcinoma Cancer Res 2001;61:5231-5241.

Chapter 8

Summarizing discussion

partially adapted from:

Vessel co-option: how tumors obtain blood supply in the absence of sprouting angiogenesis

William PJ Leenders
Benno Küsters
Robert de Waal

Endothelium 2002;9(2):83-7.

In chapters 2 to 7 different studies in animal models have been described followed by a detailed discussion in each chapter. In this last part of the thesis we place the data presented in chapters 2-7 in a broader, partly hypothetical or even speculative context of theories on tumor growth and metastasis by returning to the questions asked in chapter 1.

Do tumors depend on angiogenesis?

As described particularly in chapter 3, tumor growth may occur without angiogenesis. In our studies melanoma cells were able to co-opt the pre-existent vasculature of the brain by infiltrating the brain parenchyma in the perivascular space. In the human situation this growth pattern may be observed in the brain as well; e.g. in melanoma, small cell lung cancer metastasis and in cerebral lymphoma[1]. Macroscopically, brain metastases of epithelial tumors often show an expanding (pushing) border, sometimes with central necrosis and viable tumor tissue at the rim. This central necrosis indicates the absence of a sufficient (neo)vascular bed in the cores of these lesions. Indeed, in this situation the tumoral vessels are often located in the remnants of the brain tissue in and around the periphery of the tumor. Morphologically, this vasculature often differs from normal brain vessels: it may show a delicate branching with the formation of new vessels, that may be embedded in a desmoplastic stroma. In addition, these peritumoral microvessels frequently show the pattern that we described with Mel57 melanoma cells expressing the VEGF-isoforms 121 (chapters 4 and 5) and VEGF165gly-ser (chapter 3): vasodilation with occasional glomeruloid microvascular proliferation (mvp). Vasodilation may just be the result of morphological modulation of the pre-existing vessels without the formation of a neovascular bed, while glomeruloid mvp may be considered as aberrant in situ proliferation of endothelial cells and pericytes, without formation of a tubular structure; some studies have already described the patho-physiological and anatomical background of such vessels[2,3]. However, we have to realize that vasodilation and mvp are not sprouting or intussuceptive angiogenesis[4,5] and may only facilitate sufficient blood supply to tumor tissue over short distances. Why is the center of many metastatic and primary tumor lesions necrotic? We offer the following hypothesis: tumor cells are thought to induce angiogenesis because of hypoxia[6], but the upregulation of angiogenic factors apparently is too late or otherwise insufficient, to prevent necrosis to occur. The peritumoral rim frequently shows dilated (pre-existing?) vessels. Recent findings (own unpublished results) indicate that probably only VEGF-isoforms that do not exhibit a strong matrix binding capacity can reach more distant (e.g. peritumoral) vessels, while larger VEGF isoforms, that

in itself are able to induce angiogenesis (chapter 5) are not able to reach more distant vessels because of matrix binding in the direct neighborhood of the VEGF secreting cells.
The VEGF165gly-ser isoform we used in studies in chapter 3 differs from the wild type isoform 165 in its amino terminal end (i.e. exon 8): gly-ser instead of arg-arg. To date, this amino terminus, has not been described to be relevant in the VEGF-receptor interaction and the VEGF-effect in angiogenesis[7]. However, we found that differences in the VEGF amino terminus do seem to have consequences for the receptor activation program: the 165gly-ser isoform of VEGF shows induction of a comparable vasculature as VEGF121, while the vasculature induced by VEGF165arg-arg is different. This implicates that presumably not only VEGFR2 and NRP-1 play a role as receptor for VEGF, but that other receptors may be involved as well to initiate the complete program of induction of a neovascular bed.

Is vascular co-option a phenomenon that is limited to the brain?
In 1999 Holash et al. reported on the phenomenon of vessel co-option[8] using an animal glioma model. The authors described that in this model initial co-option of pre-existent vessels occurred, followed by vessel regression and finally a neo-angiogenic response. Malignant tumors are often characterized by infiltrative growth. Should such infiltration be accompanied by complete destruction of the infiltrated healthy tissue, for tumor growth angiogenesis would be necessary to replace the pre-existing vessels that are destroyed by the tumor. Does this scenario occur in tumors? Sometimes it does, but more frequently the tumor border of most types of tumors shows infiltration of tumor cells into the pre-existing tissue without complete destruction of its anatomy. Rather, tumors grow along anatomical structures such as vessels or nerves. In the last years, vessel co-option has gained a lot attention. The phenomenon has now been described in human tumors in different organs (lung, liver, kidney and brain) and in different animal models[9-15]. The phenomenon of vessel co-option itself is of course not new. Pathologists are confronted with it in everyday practice while examining microscopy slides of infiltrating tumors.

What are the consequences of co-option for the diagnosis and treatment of cancer?
As described in chapters 4 and 6, infiltrative tumor cells that co-opt/incorporate the pre-existing vasculature may escape detection with modern radiological imaging techniques. Besides a insensitivity of such cells to anti-angiogenic treatment, this situation will hamper correct diagnosis of tumor size and tissue involvement in human cancer. For example, glioblastoma multiforme is a tumor in which it is difficult to demarcate the tumor margins

because of diffuse infiltrative growth in the surrounding brain tissue. However, in chapter 6 it is described that contrast-enhanced MRI, although it fails to detect co-opting tumors with conventional contrast agents, may be a suitable instrument to monitor the response to anti-angiogenic therapy by evaluating the attenuation or complete loss of contrast enhancement during therapy.

Why is increased angiogenesis correlated with worse prognosis for most of the malignancies[17-19]?

For some tumors the simple explanation mentioned in chapter 7 would probably suffice: more vessels increase the chance that a tumor cell hits a vessel. Furthermore, an angiogenic phenotype of metastatic tumor cells will enhance the growth rate of metastases.
The data presented in chapter 7 show another aspect of how the angiogenic phenotype of tumors facilitates the development of metastases: the microarchitecture in angiogenic tumors leads to the formation of multicellular tumor emboli that escape from the primary tumor. This phenomenon may well be the explanation for the pathologist's experience of the occurrence of multicellular tumor emboli within (peri)tumoral vessels and at metastatic sites.

A crucial finding in this respect is that tumor emboli may be polyclonal (chapter 7). Non-angiogenic tumor cells can thus travel along with angiogenic ones, resulting in polyclonal metastases (consisting of angiogenic and non-angiogenic tumor cells).
In Darwinian terms, this does not fully fit. It is not the selection of the angiogenic fittest clone. Some might even speculate about 'tumoral altruism' in terms of Darwinian social-biology (see also later in this chapter for more discussion on this topic).

Is the center of the tumor history and the rim the future?

In contrast to the tumor rim the tumor center may show both extremes of morphology: on the one hand, vital highly vascularized tumor tissue without any recognizable pre-existent healthy tissue and, on the other hand, extensive tumor necrosis. The majority of tumors exhibit both, reflecting the ability to induce sufficient functional angiogenesis in some areas and failing to do so in others. Therefore one could also ask if there are differences between the tumor rim and the tumor center in tumor progression. More specifically, are there clonal differences between rim and center? Or are the histological differences only the result of different tumor micro-environment interactions?

If the tumor rim is infiltrative and the center probably expansive and angiogenic, which part of the tumor will then be the most dangerous for the patient? We can envisage some hypothetical scenarios:
If there are different subclones with regard to angiogenic phenotype in the tumor center versus the rim, it would be more plausible that tumor cells from the center disseminate, because they are angiogenic. If, on the other hand one tumor is a single clone, tumor cells may disseminate from the rim and the center at random, because tumor cells at the rim are as angiogenic as those in the center of the tumor.
But what about co-opting metastases? These exist as is shown in studies described in chapters 3-7. Several other groups have also confirmed their presence in the human liver and lung[11,15,16]. Based on these findings one can therefore not conclude that only the angiogenic tumor part will successfully metastasize, and the answer to the question which part of the tumor (center or rim) will kill the patient still remains open (although for tumors with extensive necrosis, the rim of course is the "tumor's future").

Is the concept of Darwinian tumor evolution and metastasis right?
Autonomic growth of a primary tumor can clearly be described as an evolutionary cascade. All genetic events that enhance mitotic rate, inhibit apoptosis and increase nutrition supply by angiogenesis or infiltration and co-option of pre-existing vessels will select the fittest clones in this respect. Bernards and Weinberg have published an interesting letter in which they mentioned that there is a conceptual mistake in the current metastasis model[20]. The question is: what is the selective pressure in the primary tumor for developing a metastatic subclone? There is no selective pressure for tumor cells to leave the primary tumor. Selection of tumor cell clones on their capacity to form a metastasis takes place at the site of metastasis: can tumor cells settle there and cope with the micro-environment[21]. Bernards and Weinberg, therefore, hypothesize that metastasis must occur at random in tumor progression and can be an early event in patient tumor history. Both authors state that there are no genes in the tumor that are solely involved in the creation of a metastatic phenotype, as there is no selective pressure for such an event. The capacity of tumor cells to leave the primary tumor can then be considered as an epiphenomenon in neoplastic evolution: the same genes that initiate autonomous growth, including that of invasive behavior, are responsible for the fact that tumor cells leave the primary tumor and form metastases. Recent findings in microarray tests comparing the genetic profile of metastases and their primary tumors revealed that they were identical[22,23]. This means that no definite clonal differences between metastasis and primary

tumor were detectable. Thus, no additional metastasis gene was identifiable in the metastasis that would qualify the metastasis as a more malignant subclone of the primary tumor. The data presented in chapter 7 fit in very well with this point of view on the development of metastasis: The genetic event creating an angiogenic phenotype (mimicked by VEGF gene transfection) obviously increases the growth rate of the primary tumor but is simultaneously accompanied by an increased rate of metastasis. In evolutionary perspective, cells with such an angiogenesis gene can be selected in the primary tumor because it enhances tumor growth, but not because it enhances metastatic rate. In fact, the latter phenomenon can be considered as an epiphenomenon caused by a different vascular architecture!
The discussion by Bernards and Weinberg still continues among researchers[24-29] and the dogma of evolutionary selection of a metastatic phenotype in primary tumor growth[30,31] is still a sensitive spot in the Darwinian cancer concept.

What about the seed and soil hypothesis?
This hypothesis describes that a metastatic tumor cell is selected by its capacity to settle at a metastatic site and to grow out[32]. As already mentioned in chapter 1, many tumor types are known for their tendency to spread preferentially to particular organs, a phenomenon which is partially independent of the anatomical situation defined by vascular supply and delivery. Dissemination of melanoma frequently results in brain metastasis[33]. Our data clearly illustrate this phenomenon: when injected intravenously, melanoma cells showed a preference for CNS metastasis and not lung metastasis, while the lung is the first organ which is reached by the tumor cells after i.v. injection (chapter 7). This phenomenon might (partially) be explained by the embryological, i.e. neuroectodermal background of these cells, which may provide them with a phenotype that makes them "feel at home"in the CNS micro-environment.
Interestingly, the metastatic patterns can be different between different melanoma cell lines not only in organ preference[21,34] , but also in subregions of a certain organ. As described in chapter 2, some cell lines show a preference for metastases in the meninges, whereas others show preferential parenchymal involvement. This must be dependent on selective adhesion between tumor cells and local vasculature, as a pure anatomical (embolism!) or micro-environmental background could be ruled out (chapter 2). The successful outgrowth of metastatic tumors in particular organs can thus be considered as evolutionary selective step in line with the seed and soil hypothesis.

Some final remarks on animal models

In this thesis, studies are presented in which human tumor cells are investigated in mouse models. The question is how relevant these data are for clinical practice. As mentioned in chapter 1, we have to bear in mind the sentence: 'mice tell lies'. Investigators must have a clear idea about what they want to investigate. In studies on tumors this background implicates the use of an animal model that on the one hand mimics the human situation as closely as possible, while at the other hand the harm done to the animals is limited as much as possible. Profound knowledge of pathology, biochemistry and patho-physiology in humans and animals are therefore essential prerequisites.

Many disappointing results with anti-angiogenic therapies in patient trials could probably have been avoided when 'relevant' animal models were used from the start instead of 'a priori' biased tumor models in which tumors were in fact selected for their angiogenesis dependency (see also discussion chapter 3).

References

1. Nakanishi, H., Hosoda, S., Takahashi, Y., Goto, S., and Tamura, J. Alteration of tumour cell arrangement related to connective tissue stroma in metastatic brain tumours. Histological and immunohistochemical studies of 68 autopsy cases. Virchows Arch.A Pathol.Anat.Histopathol., *414*: 485-495, 1989.

2. Wesseling, P., Vandersteenhoven, J. J., Downey, B. T., Ruiter, D. J., and Burger, P. C. Cellular components of microvascular proliferation in human glial and metastatic brain neoplasms. A light microscopic and immunohistochemical study of formalin-fixed, routinely processed material. Acta Neuropathol.(Berl), *85*: 508-514, 1993.

3. Wesseling, P., Schlingemann, R. O., Rietveld, F. J., Link, M., Burger, P. C., and Ruiter, D. J. Early and extensive contribution of pericytes/vascular smooth muscle cells to microvascular proliferation in glioblastoma multiforme: an immuno-light and immuno-electron microscopic study. J.Neuropathol.Exp.Neurol., *54*: 304-310, 1995.

4. Burri, P. H., Hlushchuk, R., and Djonov, V. Intussusceptive angiogenesis: its emergence, its characteristics, and its significance. Dev.Dyn., *231*: 474-488, 2004.

5. Patan, S. Vasculogenesis and angiogenesis. Cancer Treat.Res., *117*: 3-32, 2004.

6. Acker, T. and Plate, K. H. Hypoxia and hypoxia inducible factors (HIF) as important regulators of tumor physiology. Cancer Treat.Res., *117*: 219-248, 2004.

7. Holmes, D. I. and Zachary, I. The vascular endothelial growth factor (VEGF) family: angiogenic factors in health and disease. Genome Biol., *6*: 209, 2005.
8. Holash, J., Maisonpierre, P. C., Compton, D., Boland, P., Alexander, C. R., Zagzag, D., Yancopoulos, G. D., and Wiegand, S. J. Vessel cooption, regression, and growth in tumors mediated by angiopoietins and VEGF. Science, *284*: 1994-1998, 1999.
9. Kim, E. S., Serur, A., Huang, J., Manley, C. A., McCrudden, K. W., Frischer, J. S., Soffer, S. Z., Ring, L., New, T., Zabski, S., Rudge, J. S., Holash, J., Yancopoulos, G. D., Kandel, J. J., and Yamashiro, D. J. Potent VEGF blockade causes regression of coopted vessels in a model of neuroblastoma. Proc.Natl.Acad.Sci.U.S.A, *99*: 11399-11404, 2002.
10. Rubenstein, J. L., Kim, J., Ozawa, T., Zhang, M., Westphal, M., Deen, D. F., and Shuman, M. A. Anti-VEGF antibody treatment of glioblastoma prolongs survival but results in increased vascular cooption. Neoplasia., *2*: 306-314, 2000.
11. Passalidou, E., Trivella, M., Singh, N., Ferguson, M., Hu, J., Cesario, A., Granone, P., Nicholson, A. G., Goldstraw, P., Ratcliffe, C., Tetlow, M., Leigh, I., Harris, A. L., Gatter, K. C., and Pezzella, F. Vascular phenotype in angiogenic and non-angiogenic lung non-small cell carcinomas. Br.J.Cancer, *86*: 244-249, 2002.
12. Pezzella, F., Pastorino, U., Tagliabue, E., Andreola, S., Sozzi, G., Gasparini, G., Menard, S., Gatter, K. C., Harris, A. L., Fox, S., Buyse, M., Pilotti, S., Pierotti, M., and Rilke, F. Non-small-cell lung carcinoma tumor growth without morphological evidence of neo-angiogenesis. Am.J.Pathol., *151*: 1417-1423, 1997.
13. Vermeulen, P. B., Colpaert, C., Salgado, R., Royers, R., Hellemans, H., Van Den, H. E., Goovaerts, G., Dirix, L. Y., and Van Marck, E. Liver metastases from colorectal adenocarcinomas grow in three patterns with different angiogenesis and desmoplasia. J.Pathol., *195*: 336-342, 2001.
14. Stessels, F., Van den, E. G., Van, d. A., I, Salgado, R., Van Den, H. E., Harris, A. L., Jackson, D. G., Colpaert, C. G., Van Marck, E. A., Dirix, L. Y., and Vermeulen, P. B. Breast adenocarcinoma liver metastases, in contrast to colorectal cancer liver metastases, display a non-angiogenic growth pattern that preserves the stroma and lacks hypoxia. Br.J.Cancer, *90*: 1429-1436, 2004.
15. Pezzella, F. Evidence for novel non-angiogenic pathway in breast-cancer metastasis. Breast Cancer Progression Working Party. Lancet, *355*: 1787-1788, 2000.
16. Vermeulen, P. B., Colpaert, C., Salgado, R., Royers, R., Hellemans, H., Van Den, H. E., Goovaerts, G., Dirix, L. Y., and Van Marck, E. Liver metastases from colorectal adenocarcinomas grow in three patterns with different angiogenesis and desmoplasia. J.Pathol., *195*: 336-342, 2001.
17. Weidner, N. Intratumor microvessel density as a prognostic factor in cancer. Am.J.Pathol., *147*: 9-19, 1995.
18. Weidner, N. Tumoural vascularity as a prognostic factor in cancer patients: the evidence continues to grow. J.Pathol., *184*: 119-122, 1998.

19. Weidner, N. Intratumor microvessel density as a prognostic factor in cancer. Am.J.Pathol., *147*: 9-19, 1995.
20. Bernards, R. and Weinberg, R. A. A progression puzzle. Nature, *418*: 823, 2002.
21. Fidler, I. J. Critical determinants of cancer metastasis: rationale for therapy. Cancer Chemother.Pharmacol., *43 Suppl*: S3-10, 1999.
22. Weigelt, B., Glas, A. M., Wessels, L. F., Witteveen, A. T., Peterse, J. L., and van't Veer, L. J. Gene expression profiles of primary breast tumors maintained in distant metastases. Proc.Natl.Acad.Sci.U.S.A, *100*: 15901-15905, 2003.
23. Ramaswamy, S., Ross, K. N., Lander, E. S., and Golub, T. R. A molecular signature of metastasis in primary solid tumors. Nat.Genet., *33*: 49-54, 2003.
24. Gatenby, R. A. and Maini, P. Modelling a new angle on understanding cancer. Nature, *420*: 462, 2002.
25. Edwards, P. A. Metastasis: the role of chance in malignancy. Nature, *419*: 559-560, 2002.
26. Sherley, J. L. Metastasis: objections to the same-gene model. Nature, *419*: 560, 2002.
27. Hunter, K., Welch, D. R., and Liu, E. T. Genetic background is an important determinant of metastatic potential. Nat.Genet., *34*: 23-24, 2003.
28. Liotta, L. A. and Kohn, E. C. Cancer's deadly signature. Nat.Genet., *33*: 10-11, 2003.
29. Fidler, I. J. and Kripke, M. L. Genomic analysis of primary tumors does not address the prevalence of metastatic cells in the population. Nat.Genet., *34*: 23, 2003.
30. Fidler, I. J. and Kripke, M. L. Metastasis results from preexisting variant cells within a malignant tumor. Science, *197*: 893-895, 1977.
31. Poste, G. and Fidler, I. J. The pathogenesis of cancer metastasis. Nature, *283*: 139-146, 1980.
32. Fidler, I. J. The pathogenesis of cancer metastasis: the 'seed and soil' hypothesis revisited. Nat.Rev.Cancer, *3*: 453-458, 2003.
33. Bafaloukos, D. and Gogas, H. The treatment of brain metastases in melanoma patients. Cancer Treat.Rev., *30*: 515-520, 2004.
34. Zhang, R. D., Price, J. E., Schackert, G., Itoh, K., and Fidler, I. J. Malignant potential of cells isolated from lymph node or brain metastases of melanoma patients and implications for prognosis. Cancer Res., *51*: 2029-2035, 1991.

Samenvatting

Kanker is een levensbedreigende ziekte en in westerse landen een frequente en (o.a. vanwege de “vergrijzing” van de bevolking) zelfs toenemende oorzaak van ziekte en overlijden. Vooral de behandeling van gemetastaseerde (uitgezaaide) kanker vormt een groot probleem. De gebruikelijke chirurgische, chemotherapeutische en radiotherapeutische behandelingen schieten in zo’n situatie uiteindelijk vaak te kort. Een nieuwe benadering ter bestrijding van kankergezwellen is er op gericht om de bloedvoorziening van het gezwelweefsel te onderbreken en zo de tumor als het ware “uit te drogen”. Een gezwel heeft, net als normaal weefsel, een functionerend vaatbed nodig om vitaal te blijven en te kunnen groeien. Hiertoe vormen veel gezwellen nieuwe vaatjes, een proces dat angiogenese wordt genoemd. De belangrijkste angiogene factor is Vascular Endothelial Growth Factor (VEGF). Anti-angiogene therapie zou door het remmen van angiogenese de tumor mogelijk verhinderen verder te groeien of zelfs kunnen doen krimpen. Een bijkomend voordeel van deze benadering zou kunnen zijn dat tumorcellen minder makkelijk de bloedbaan bereiken en daardoor minder uitzwermen in het lichaam. De toepassing van anti-angiogene therapie bevindt zich tot nu toe nog in experimenteel stadium.

Het melanoom van de huid is een van de meest kwaadaardige tumoren bij de mens. Genezing van deze tumor is vaak slechts mogelijk als het gezwel wordt verwijderd in een vroeg stadium waarin de tumor nog niet dieper in de huid is gegroeid. Bij dieper groeiende melanomen is de kans namelijk groot dat reeds tumorcellen zijn uitgezaaid naar andere organen. De metastasen worden in eerste instantie vaak aangetroffen in lymfklieren in de buurt van de tumor, maar vervolgens ook meer op afstand in organen als longen, lever en hersenen. Hersenmetastasen komen bij patienten met maligne melanoom relatief frequent voor, mogelijk heeft dit te maken met het feit dat melanoomcellen wat betreft herkomst verwantschap tonen met hersenweefsel.

Om het biologisch gedrag van tumoren te kunnen bestuderen en nieuwe therapeutische en diagnostische mogelijkheden te ontwikkelen en te testen is wetenschappelijk onderzoek noodzakelijk. Voor meer basale of onrijpe klinische vraagstellingen wordt vaak dierexperimenteel onderzoek verricht, al dan niet met met gebruik making van patientenmateriaal (bijv. weefsel dat o.a. is verkregen voor pathologisch onderzoek). De meer uitgewerkte onderzoeksvragen kunnen vervolgens in klinische trials worden onderzocht. Een

groot voordeel van dierexperimenten is dat hierbij een zeer gestandaardiseerde opzet mogelijk is met nauwkeurige manipulatie van verschillende facetten van het te onderzoeken fenomeen. Ook diagnostische technieken kunnen in principe vaak in dierexperimentele setting worden getest.

In dit proefschrift wordt dierexperimenteel onderzoek in zogenaamde “naakte muizen” beschreven. Deze muizen heten zo omdat zij nauwelijks behaard zijn, samenhangend met een gestoorde immuunafweer. Deze gestoorde immuunafweer maakt het ook mogelijk om in dergelijke muizen tumoren van de mens te laten groeien zonder dat deze worden afgestoten. In hoofdstuk 2 wordt de ontwikkeling van een geschikt diermodel voor hersenmetastasering beschreven. In dit model wordt gebruik gemaakt van humane melanoomcellijn(en). De invloed van de aanwezigheid van het eiwit $\alpha_v ß_3$ integrine (dat o.a. binding bewerkstelligt tussen cellen onderling en hun omgeving) op tumorcellen en de rol van individuele tumorcellen versus groepen van tumorcellen op het metastase-gedrag in de hersenen werden onderzocht. Wij vonden dat het patroon van metastasering (in hersenvliezen versus in het hersenweefsel zelf) niet werd beinvloed wordt door de aanwezigheid van $\alpha_v ß_3$ integrine op melanoomcellen. Ook maakte het voor het metastaserings-patroon niet uit of individuele tumorcellen of tumorcelclusters in de bloedstroom van de proefdieren gebracht werden.

Hoofdstuk 3 vermeldt onderzoek (met behulp van het in hoofdstuk 2 ontwikkeld model) naar de groeiwijze van metastasen in het eigenlijke hersenweefsel. Wij tonen aan dat metastasen van melanoomcellen die de angiogene factor VEGF niet produceren in hersenweefsel kunnen groeien zonder nieuwe vaten aan te maken. Dergelijke tumoren maken gebruik van reeds bestaande bloedvaten in de hersenen (zogenaamde vaat-coöptie). Als dezelfde tumorcellen echter kunstmatig zo worden veranderd dat ze wel VEGF gaan produceren dan leidt dit tot vorming van nieuwe vaten en tot vaatverwijding en verhoogde permeabiliteit van pre-existente bloedvaten (hoofdstukken 3 en 5). Verschillende isovormen van VEGF bleken hierbij verschillende effecten te hebben op het vaatpatroon in en rond de tumoren.

De diagnostische consequenties van vaat-coöptie in hersentumoren worden in hoofdstuk 4 besproken: tumoren zonder angiogenese en zonder VEGF-productie zijn niet goed te herkennen op basis van MRI onderzoek met conventionele contrastmiddelen. Het gebruik van nieuwe, op ijzeroxide gebaseerde contrastmiddelen kan in zo’n geval van nut zijn. Deze laatste contrastmiddelen blijven in het vaatstelsel van normaal en door tumor ingenomen

hersenweefsel, maar ter plaatse van de tumor zijn de preexistente vaten vaak uiteengedrukt en wordt daardoor minder contrast gevonden dan in normaal hersenweefsel.

Hoofdstuk 6 beschrijft onderzoek waarbij wordt aangetoond dat antiangiogene behandeling van tumoren die VEGF maken inderdaad leidt tot het sterk verminderen of ontbreken van angiogenese en vaatlekkage. Deze tumoren blijven echter wel groeien, maar dan door preexistente vaten te incorporeren. Omdat deze groeiwijze niet goed meer zichtbaar is te maken met behulp van de conventionele MRI diagnostiek bestaat het gevaar dat de anti-angiogene behandeling ten onrechte als zeer succesvol wordt beschouwd.

VEGF productie door tumorcellen leidt ertoe dat metastasen sneller groeien (hoofdstukken 3 en 5). De vraag is of zulke tumoren ook eerder metastasen geven als tumoren die niet angiogeen zijn. In hoofdstuk 7 wordt onderzoek beschreven waarbij in verschillende diermodellen wordt gekeken naar de kans op metastasering van melanoomcellen in relatie hun VEGF-productie. Uit dit onderzoek bleek dat de kans dat melanoomcellen in de bloedbaan geraken vanuit de oorspronkelijke tumor duidelijk hoger is wanneer de tumor VEGF maakt. Het “landen” van melanoomcellen in diverse organen (de kolonisatie) werd echter niet beinvloed wordt door de aan- of afwezigheid van VEGF op tumorcellen. De grotere kans op uitzwermen van tumorcellen in de bloedbaan in VEGF producerende tumoren lijkt niet alleen te verklaren door een relatief hoge vaatdichtheid en daardoor een hogere trefkans voor tumorcellen om in een bloedvat te geraken. Wij menen dat ook andere, door VEGF geinduceerde miro-architecturele veranderingen in de tumor hierbij een rol spelen: in VEGF producerende tumoren werden regelmatig tumorcel-clusters gevonden die deels uitpuilden in het lumen van bloedvaatjes en soms zelfs als multicellulaire emboli op afstand in de bloedbaan werden aangetroffen. Hierbij bleek binnen deze tumoremboli een heterogene populatie van (o.a. meer en minder VEGF producerende) tumorcellen aanwezig te zijn, hetgeen begrijpelijk maakt dat vanuit dergelijke emboli zelfs niet-angiogene metastasen kunnen ontstaan.

Samenvattend komen in dit proefschrift nieuwe inzichten naar voren in de mogelijkheid van tumoren om in hun bloedvoorziening te voorzien door middel van vaat-coöptie en in de consequenties van een dergelijke groeiwijze voor radiologische beoordeling van bijv. het effect van anti-angiogene behandeling. Daarnaast bevat het dierexperimenteel werk beschreven in dit proefschrift aanwijzingen dat de door VEGF productie in tumoren teweeg

gebrachte microarchitecturele veranderingen o.a. aanleiding kunnen geven tot vorming van in vaatlumina uitpuilende, multicellulaire tumorcel-aggregaten die vervolgens los geraken en tot metastasen op afstand aanleiding geven. Verder onderzoek in humaan tumorweefsel is inmiddels gestart om na te gaan of, en zo ja, hoe vaak dit fenomeen bij de mens voorkomt. De eerste indruk hierbij is dat dit fenomeen bij bijv. heldercellig niercelcarcinoom relevant is.

Zusammenfassung

Krebs ist eine lebensbedrohliche Krankheit und ist eine häufige Ursache für Krankheit und Tod in westlichen Ländern. Gerade die Behandlung von Krebsmetastasen stellt ein großes Problem dar. Die gängigen chirurgischen, chemotherapeutischen und radiotherapeutischen Behandlungsschemata sind in diesen Fällen häufig nicht effizient genug. Deshalb wird versucht, neue Wege zur Behandlung zu finden: ein neuer Ansatzpunkt zur Krebsbehandlung zielt darauf die Gefäßversorgung der Krebsgeschwulst zu unterbinden und somit den Tumor „auszuhungern". Das Konzept dahinter ist die Hypothese, daß Krebsgeschwülste, wie normales Gewebe auch, zur Aufrechterhaltung eines vitalen Status eine Blutgefäßversorgung nötig haben, die Tumoren durch den Prozeß von Angiogenese (Gefäßneuformung) selbst induzieren. Eine Antiangiogene Therapie würde damit das Wachstum eines Tumors verhindern und vielleicht sogar die Metastasierung hemmen, da Tumorzellen den primären Tumor häufig via die Blutbahn verlassen und damit der Ursprung von Metastasen sind. Die Erprobung van antiangiogener Therapie befindet sich zurzeit noch in experimentellen Studien und ist noch nicht etablierte Standardtherapie innerhalb der Onkolgie.

Das Melanom der Haut ist eines der bösartigsten Krebserkrankungen des Menschen, dessen Heilung nur möglich ist, wenn der Tumor in einem frühen Stadium vollständig exzidiert wird. Ist das Melanom tiefer in die Haut infiltriert, ist die Wahrscheinlichkeit auf Metastasenformung deutlich erhöht. Erste Metastasen werden häufig in regionalen Lymphknoten, später auch in anderen Organen wie Lunge, Leber und Gehirn angetroffen. Hirnmetastasen sind beim metastasierten Melanom im Vergleich zu anderen Tumoren relativ häufig.

Um die biologische Eigenschaften und neue therapeutische und diagnostische Ansätze zu entwickeln, ist weitere Forschung von Nöten. Basale und noch präklinische Fragestellungen werden hierbei in erster Linie durch tierexperimentelle Studien, flankiert durch Analyse von Patientenmaterial (Material aus pathologischen Archiven) angegangen. Bei schon ausgereiften Konzepten werden klinische Studien an Patienten durchgeführt. Der Vorteil tierexperimenteller Studien ist die Möglichkeit der Standardisierung der Versuchsbedingungen und die Möglichkeit bestimmte Mechanismen der Tumorbiologie durch Manipulation in definierten Stoffwechsel/Gen-Mechanismen zu verändern und damit Einsichten zu Wirkmechanismen zu erlangen.

In dieser Dissertation werden tierexperimentelle Studien mit „nackten Mäusen“ beschrieben. Diesen Mäusen fehlt neben einer regulären Behaarung auch ein kompetentes zelluläres Immunsystem, sodaß es möglich ist, in diese Mäuse menschliche Tumorzellen zu transplantieren, ohne daß diese durch eine Immunreaktion abgestoßen werden.

In Kapitel 2 wird die Entwicklung eines Tiermodells von Hirnmetastasen beschrieben; hierbei werden humane Melanomzellen verwendet. Die Rolle der Integrin $\alpha_v ß_3$ -Expression durch die Tumorzellen und die Rolle von individuellen Tumorzellen versus Tumorzellaggregaten bei der Metastasierung wurden untersucht. Unsere Ergebnisse zeigten, daß das Metastasierungsmuster (Gehirnparenchym versus Hirnhäute) ebenso wenig beeinflußt wird durch die Integrin $\alpha_v ß_3$ -Expression wie durch die An- bzw. Abwesenheit von Tumorzellaggregaten.

Kapitel 3 untersucht das Wachstumsverhalten der Melanomzellen im Hirngewebe. Wir zeigen, daß Melanomzellen, die den Blutgefäßwachstumsfaktor VEGF (Vascular Endothelial Growth Factor) nicht produzieren, im Hirngewebe wachsen ohne überhaupt neue Blutgefäße zu induzieren, da diese Tumorzellen vom preexistenten Gefäßsystem Gebrauch machen (engl. co-option). Produzieren diese Tumorzellen jedoch einen der verschiedenen Isoformen von VEGF (dies kann durch genetische Manipulation der Tumorzellen erreicht werden), so können neben Gefäßdilatation und erhöhte Permeabilität auch Gefäßneubildungen beobachtet werden (Kapitel 3 und 5); hierbei zeigt sich jedoch ein Unterschied zwischen den einzelnen VEGF-Isoformen.

Die diagnostischen Konsequenzen der Gefäß-cooption von Hirntumoren wird in Kapitel 4 beschrieben: Tumore die keine Gefäßneubildung zeigen bzw. kein VEGF produzieren sind fast unsichtbar in kernspintomographischer Bildgebung (MRI) mit gewöhnlichen Kontrastmitteln. Neuere Kontrastmittel, basierend auf kleinen Eisenoxidpartikeln und in erster Linie im Gefäß verbleibend, können aber solche Tumoren demarkieren, da diese durch eine relative Abnahme der Gefäßdichte innerhalb des Tumors weniger Kontrastanreicherung zeigen als das vergleichbare umgebende Hirngewebe.

In Kapitel 6 wird gezeigt, daß eine anti-angiogene Behandlung von VEGF-produzierenden Tumoren tatsächlich einhergeht mit einer Hemmung der Angiogenese und der Gefäßleckage. Tumore können aber dennoch weiter wachsen durch den Gebrauch preexistenter Gefäße, ohne daß diese Tumoren noch sichtbar sind im MRI. Hierin liegt dann auch die Gefahr, daß bei antiangiogener Therapie zu unrecht eine Tumoreradikation angenommen wird.

Die Sekretion von VEGF durch Tumorzellen erhöht die Wachstumsrate der Tumoren (Kapitel 3 und 5). Die Frage ist, ob VEGF-produzierende Tumorzellen nicht nur schneller wachsende Metastasen formen können, sondern auch die tatsächliche Anzahl der Metastasen erhöhen kann. In Kapitel 7 konnten wir mit Hilfe unterschiedlicher Tumormodelle zeigen, daß eine VEGF-Sekretion durch Tumorzellen auch die Inzidenz von Metastasen erhöht. Dies wird verursacht durch einen mikroanatomischen Umbau des primären Tumors, der zu einer Gefäßarchitektur führt, in der innerhalb der Gefäße (intravaskulär) Tumorfragmente/Tumornoduli gelegen sein, die in der Blutbahn weiter verschleppt und so zu Metastasen werden können. Diese Tumornuduli können heterogen sein bezüglich der VEGF-Produktion, was dazu führen kann, daß selbst Tumorzellen metastasieren können, die kein VEGF sekretieren.

Zusammenfassend beschreibt diese Dissertation neue Einsichten über die Möglichkeiten der Gefäßversorgung von Tumoren, hierbei zu nennen die Gefäß-cooption. Die radiologischen und therapeutischen Konsequenzen derartiger Tumorcharakteristiken werden aufgezeigt. Daneben wird in dieser Arbeit ein alternatives Konzept zur Entstehung van Metastasen beschrieben, dessen Ursache die angiogene Eigenschaft eines Tumors ist. Hierbei spielt die Entstehung van intravaskulären Tumornoduli/Tumoremboli eine entscheidende Rolle. Erste Untersuchungen in humanem Patientenmaterial zeigen, daß dieses Phänomen auch beim Menschen zu beobachten ist, z.B. beim klarzelligen Nierenzellkarzinom.

Dankwoord

Allen die bij het tot standkomen van dit proefschrift betrokken zijn geweest wil ik van harte bedanken. Ik wil echter diegenen die bijzonder hebben bijgedragen aan dit werk nadrukkelijk bedanken:

William Leenders, jij en ik vormden een ideaal duo door het wederzijds inbrengen van kennis en kunnen: jij de moleculair bioloog met ook kennis van het MRI-onderzoek, en ik met mijn medische opleiding. In vele discussies, m.n. ook tijdens de vaak langdurige MRI-sessies, hebben we samen toch menig idee vergaard. Zonder jouw inbreng in dit werk was het onderzoek zoals het in dit boekje is beschreven, niet mogelijk geweest. Het onderzoek verliep dan ook zo productief dat zelfs een nieuw project gebaseerd op de data uit hoofdstuk 7 door het KWF gehonoreerd werd.

Prof. Ruiter, u hebt me door ideeën en discussies tijdens mijn onderzoek en ook tijdens mijn opleiding nieuwe impulsen gegeven. Door u ben ik überhaupt in Nijmegen terechtgekomen en waarschijnlijk bent u het geweest die uiteindelijk de beslissing vergemakkelijkt heeft in plaats van medisch oncoloog toch patholoog te worden.

Rob de Waal, jij hebt vanaf het begin het onderzoek begeleid en gesteund. Je gaf me alle vrijheid en kansen, hoewel deze ook vaak duur waren. Gelukkig maar dat door zowel KWF als NWO steun is gegeven voor dit onderzoek.

Pieter Wesseling, jij bent altijd mijn aanspreekpunt geweest, niet alleen voor vragen met betrekking tot het neuropathologie gedeelte van dit onderzoek, maar ook daarbuiten. Jij hebt me gesteund in de ambitie mij te subspecialiseren in de neuropathologie.

Debby Smits, jouw gouden handen, je snel begrip en je nauwkeurigheid maakten het opzetten van het dierexperimenteel werk mogelijk. We waren bij dit werk een goed afgestemd team.

Cathy Maass en Kiek Verrijp, jullie technische inbreng was van groot belang. De illustraties van ons werk zijn niet alleen wetenschappelijk interessant, maar hebben ook een grote esthetische waarde door jullie deskundigheid.

Hans Westphal, jij hebt me in het begin begeleid bij het opzetten van het onderzoek en hier en daar mijn handjes vastgehouden in het lab- en schrijfwerk.

Prof. Keilholz, u hebt me gemotiveerd eerst onderzoek te doen in het begin van mijn medische carrière. Helaas moest ik u teleurstellen met mijn keuze in plaats van medisch oncoloog toch maar patholoog te worden.

Verder wil ik alle collegae onderzoekers, analisten en arts-assistenten binnen en buiten de afdeling pathologie danken voor de prettige werksfeer, ideeënuitwisseling en het altijd beschikbaar zijn voor vragen en antwoorden. Hierbij wil ik in het bijzonder noemen: Geert Poelen, Ilona van den Brink, Jeroen Pikkemaat, Iris Lamers-Elemans, Bianca Lemmers-van de Weem, Alex Hanssen, Ruud Clarijs, Arno van Leenders, Marcory van Dijk, Iris Nagtegaal, Ine Cornelissen, Lia Schalkwijk, Henry Dijkman, Irene Otte-Höller, Goos van Muijen, Arie Maat, Coos Diepenbroek, Timo ten Hagen, Bert van der Kogel, Hans Peters, Olaf van Tellingen, Arend Heerschap, Jelle Barentsz, Riki Willems, Hans Beck, Jeroen van der Laak, Peter de Wilde, Han van Krieken en Martin Lammens.

Tenslotte Heidi, je hebt altijd een luisterend oor gehad, je hebt dit manuscript mee gecorrigeerd, en je hebt samen met mij de inhoud van hoofdstuk 7 al in een deel van Europa op diversen bijeenkomsten “verkocht”, zodat dit eigenlijk inofficieel reeds gepubliceerd is.

Curriculum vitae

Benno Küsters werd geboren op 29 oktober 1970 te Dülmen (Duitsland). De in Duitsland dertienjarige schoolopleiding voltooide hij met het afleggen van het Abitur in 1990 in het Gymnasium en Internaat Collegium Augustinianum Gaesdonck bij Goch. Tot 1991 deed hij vervangende dienstplicht (15 maanden) in de verpleging in het St. Irmgardis ziekenhuis in Viersen-Süchteln. In oktober 1991 begon hij zijn studie geneeskunde aan de Rheinisch-Westfälische Technische Hochschule in Aken. Die zette hij vanaf 1992 voort in de Westfälische Wilhelms Universität te Münster en voltooide de studie in juni 1998. Tijdens zijn studie werkte hij als student-onderzoeker in het Fysiologische Instituut van de faculteit geneeskunde van de Westfälische Wilhelms Universität met het doel tot promotie tot Dr. med. (doctor medicinae). In oktober 1998 promoveerde hij aan de Westfälische Wilhelms Universität tot Dr. med. met zijn proefschrift getiteld: „PAR-2 Expression in Endothelzellen und dessen Einfluss auf die von Willebrand-Faktor Freisetzung". In oktober 1998 begon hij als arts-onderzoeker te werken in een samenwerkingsverband tussen de Afdeling Hematologie van het Benjamin Franklin ziekenhuis van de Freie Universität Berlijn en de Afdeling Pathologie van het Radboudziekenhuis in Nijmegen met het doel de biologie van hersenmetastasen van het melanoom nader te onderzoeken. Hij ontwikkelde hierbij diermodellen, om vraagstellingen nader te bestuderen. Met de basis van eerste resultaten kon hij onderzoeksstipendia van de NWO en KWF in kader van een AGIKO-constructie verwerven om verder onderzoek te combineren met de opleiding tot patholoog. In april 2006 zal hij zijn opleiding tot patholoog voltooien en zich verder subspecialiseren in de neuropathologie, waarmee hij al tijdens zijn opleiding begon.

List of publications

Leenders WP*, Küsters B *, Verrijp K, Maass C, Wesseling P, Heerschap A, Ruiter DJ, Ryan A, de Waal RM.
Antiangiogenic therapy of cerebral melanoma metastases results in sustained tumor progression via vessel co-option.
Clin Cancer Res. 2004 Sep 15;10(18 Pt 1):6222-30.
(*shared first authorship)

Küsters B, de Waal RM, Wesseling P, Verrijp K, Maass C, Heerschap A, Barentsz JO, Sweep F, Ruiter DJ, Leenders WP.
Differential effects of vascular endothelial growth factor A isoforms in a mouse brain metastasis model of human melanoma.
Cancer Res. 2003 Sep 1;63(17):5408-13.

Leenders W*, Küsters B *, Pikkemaat J, Wesseling P, Ruiter D, Heerschap A, Barentsz J, de Waal RM.
Vascular endothelial growth factor-A determines detectability of experimental melanoma brain metastasis in GD-DTPA-enhanced MRI.
Int J Cancer. 2003 Jul 1;105(4):437-43.
(*shared first authorship)

Küsters B*, Leenders WP*, Wesseling P, Smits D, Verrijp K, Ruiter DJ, Peters JP, van der Kogel AJ, de Waal RM.
Vascular endothelial growth factor-A(165) induces progression of melanoma brain metastases without induction of sprouting angiogenesis.
Cancer Res. 2002 Jan 15;62(2):341-5.
(*shared first authorship)

Küsters B, Westphal JR, Smits D, Ruiter DJ, Wesseling P, Keilholz U, de Waal RM.
The pattern of metastasis of human melanoma to the central nervous system is not influenced by integrin alpha(v)beta(3) expression.
Int J Cancer. 2001 Apr 15;92(2):176-80.

Vance C, Al-Chalabi A, Smith BN, Hu X, Sreedharan J, Siddique T, Schelhaas J, Küsters B, Troost D, Baas F, De Jong V, Shaw CE.
Familial amyotrophic lateral sclerosis with frontotemporal dementia is linked to a locus on Chromosome 9p13.2-21.3.
Brain *accepted*

Bernsen H, Van der Laak J, Küsters B, Van der Ven A, Wesseling P.
Gliomatosis cerebri: quantitative proof of vessel recruitment by cooptation instead of angiogenesis.
J Neurosurg. 2005 Oct;103(4):702-6.

Roodink I, Raats J, van der Zwaag B, Verrijp K, Küsters B, van Bokhoven H, Linkels M, de Waal RM, Leenders WP.
Plexin D1 expression is induced on tumor vasculature and tumor cells: a novel target for diagnosis and therapy?
Cancer Res. 2005 Sep 15;65(18):8317-23.

Ploegmakers MJM, Pruszczynski M, de Rooy J, Küsters B, Veth RPH.
Angiosarcoma with malignant peripheral nerve sheath tumor developing in a patient with Klippel-Trenaunay-Weber syndrome.
Sarcoma. 2005 Sep-Dec; 9(3/4); 137-40

Gijtenbeek J, Jacobs B, Boots-Sprenger S, Bonne A, Lenders J, Küsters B, Wesseling P, Jeuken J.
Molecular analysis as a tool in the differential diagnosis of VHL disease-related tumors.
Diagn Mol Pathol. 2005 Jun;14(2):115-20.

te Velde EA, Küsters B, Maass C, de Waal R, Borel Rinkes IH.
Histological analysis of defective colonic healing as a result of angiostatin treatment.
Exp Mol Pathol. 2003 Oct;75(2):119-23.

Leenders WP, Küsters B, de Waal RM.
Vessel co-option: how tumors obtain blood supply in the absence of sprouting angiogenesis.
Endothelium. 2002;9(2):83-7.

Langer F, Morys-Wortmann C, Küsters B, Storck J.
Endothelial protease-activated receptor-2 induces tissue factor expression and von Willebrand factor release.
Br J Haematol. 1999 May;105(2):542-50.

Storck J, Küsters B, Vahland M, Morys-Wortmann C, Zimmermann ER.
Trypsin induced von Willebrand factor release from human endothelial cells in mediated by PAR-2 activation.
Thromb Res. 1996 Dec 15;84(6):463-73.

Storck J, Küsters B, Zimmermann ER.
The tethered ligand receptor is the responsible receptor for the thrombin induced release of von Willebrand factor from endothelial cells (HUVEC).
Thromb Res. 1995 Feb 1;77(3):249-58.

Submitted:

Küsters B, de Waal RMW, Wesseling P, Maass C, Verrijp K, Ruiter DJ, Leenders WPJ.
Micronodular transformation as a novel mechanism of VEGF-A-induced metastasis.

Wilhelmus MM, Boelens WC, Otte-Höller I, Kamps B, Küsters B, Maat-Schieman MLC, de Waal RMW, Verbeek MM.
Distribution in Alzheimer's disease brains and inhibition of amyloid-β protein aggregation and cerebrovascular amyloid-β toxicity of HspB.

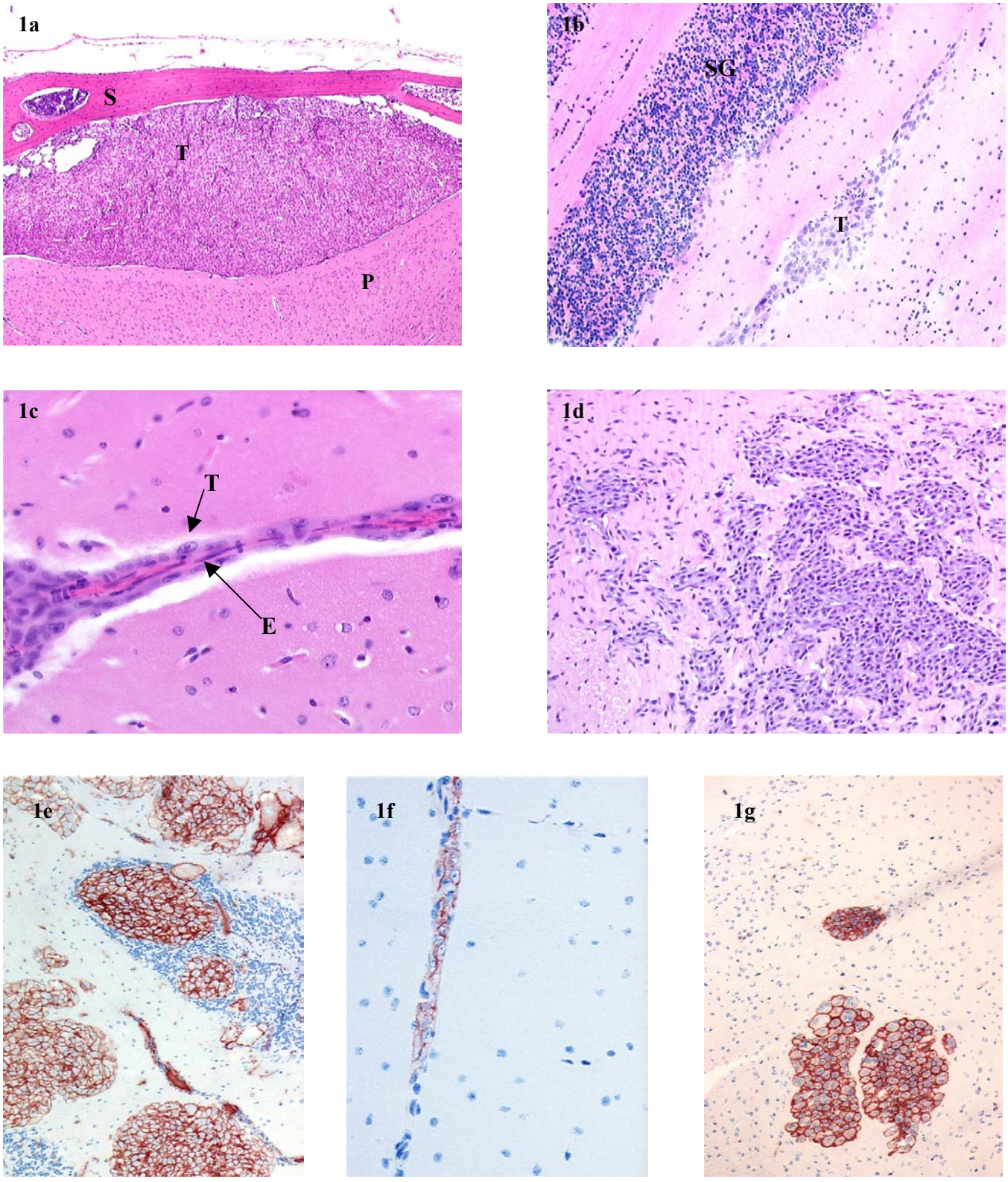

Figure 1, see also page 25

Figure 1, see also page 37

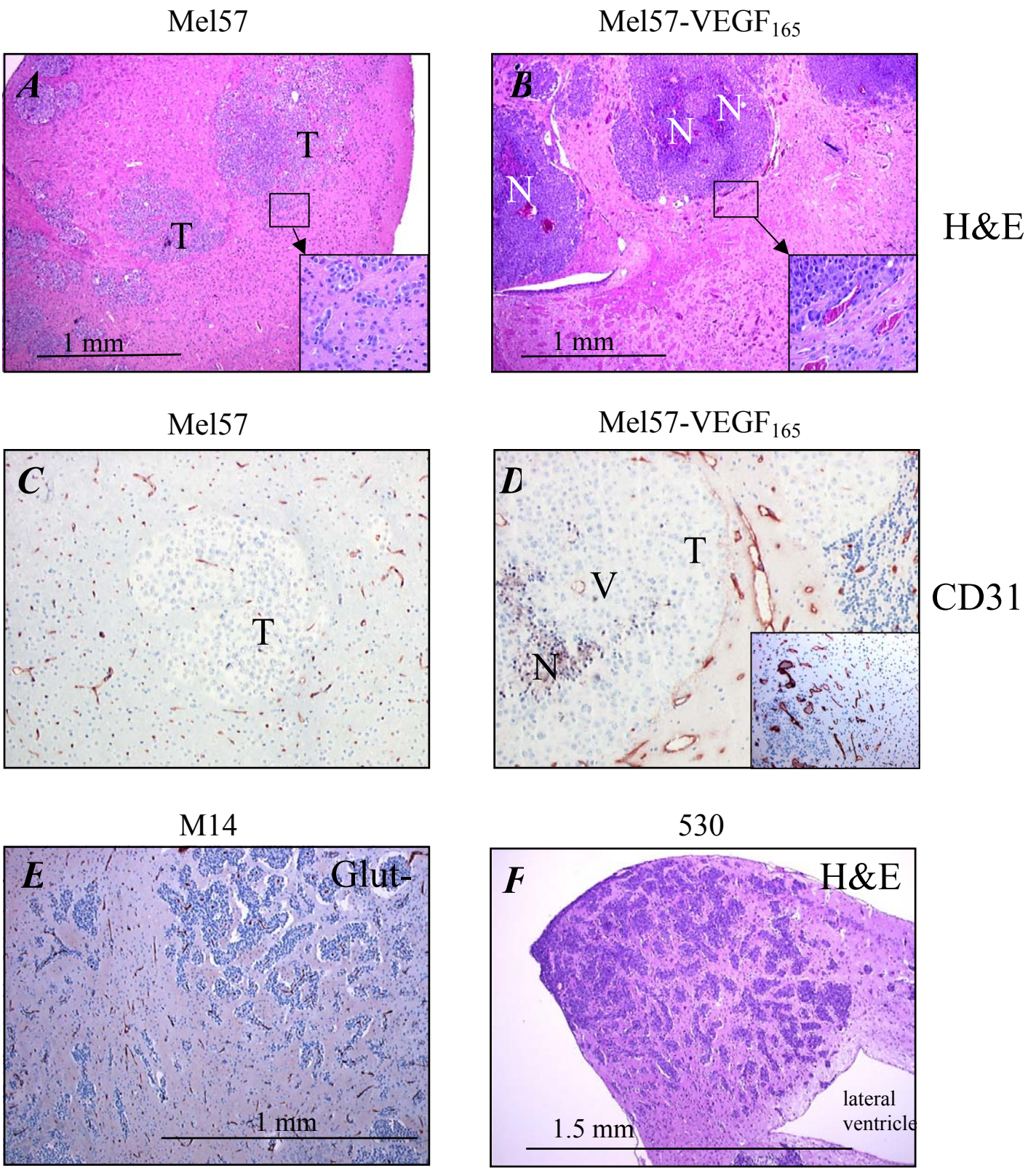

Figure 2, see also page 40

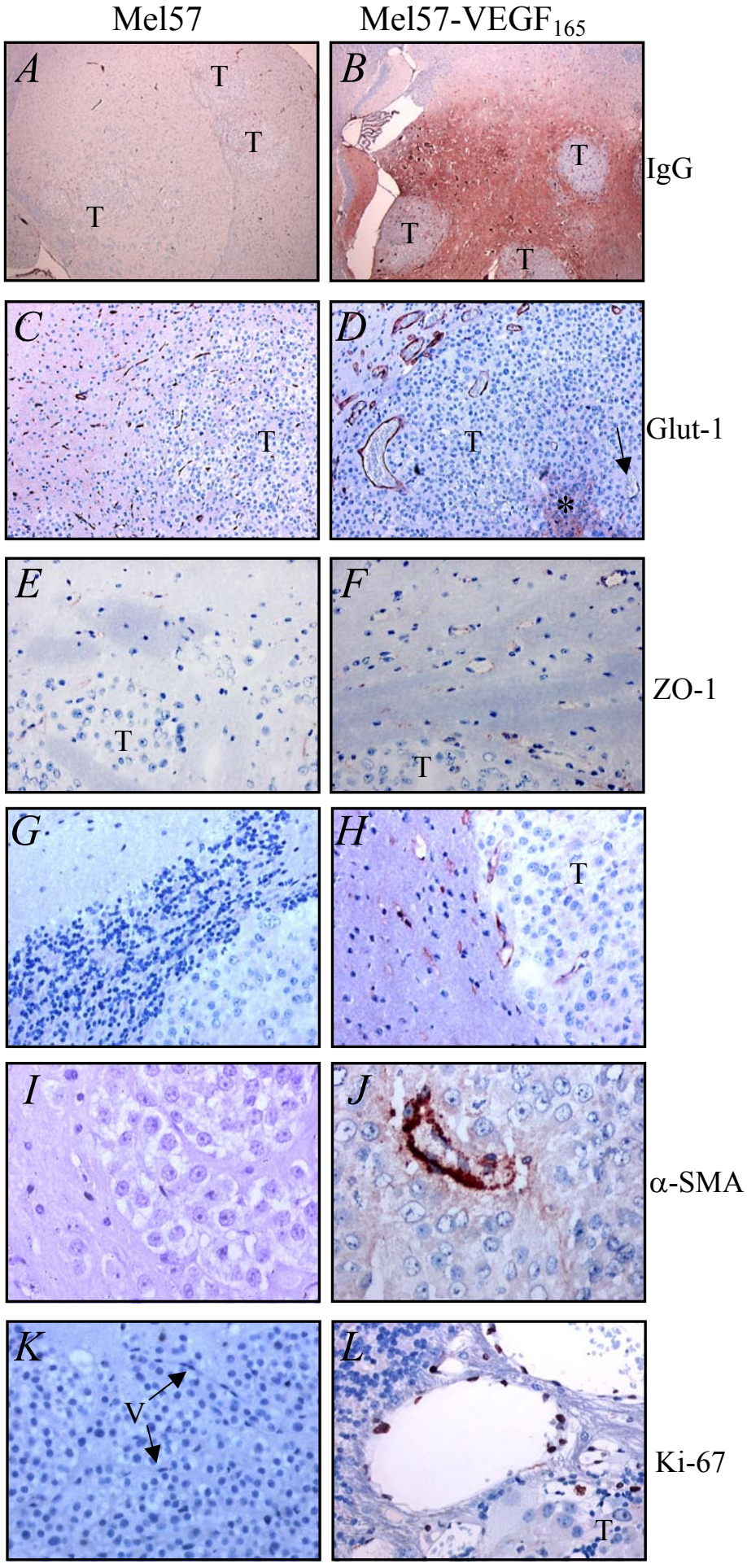

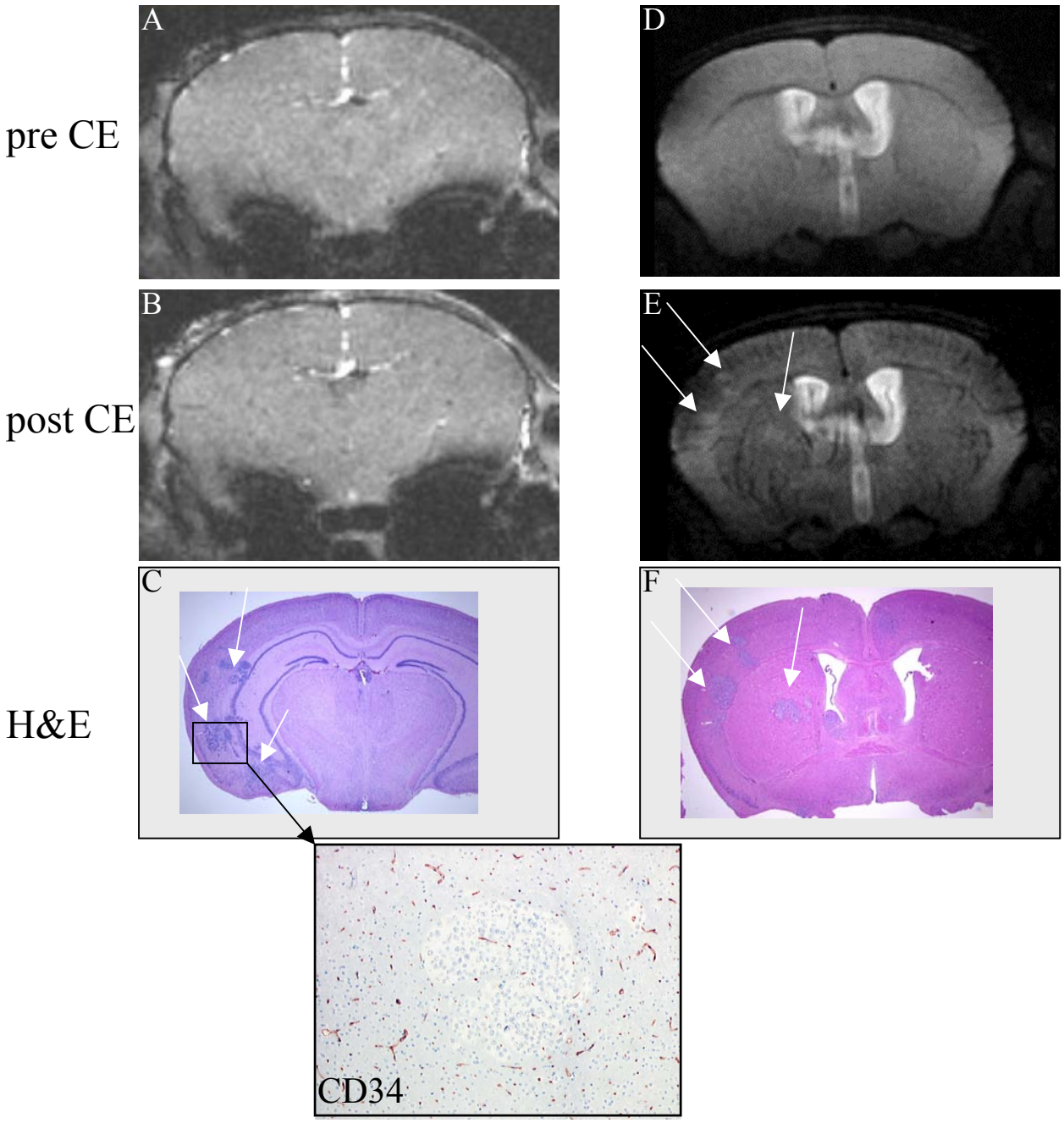

Figure 1, see also page 54

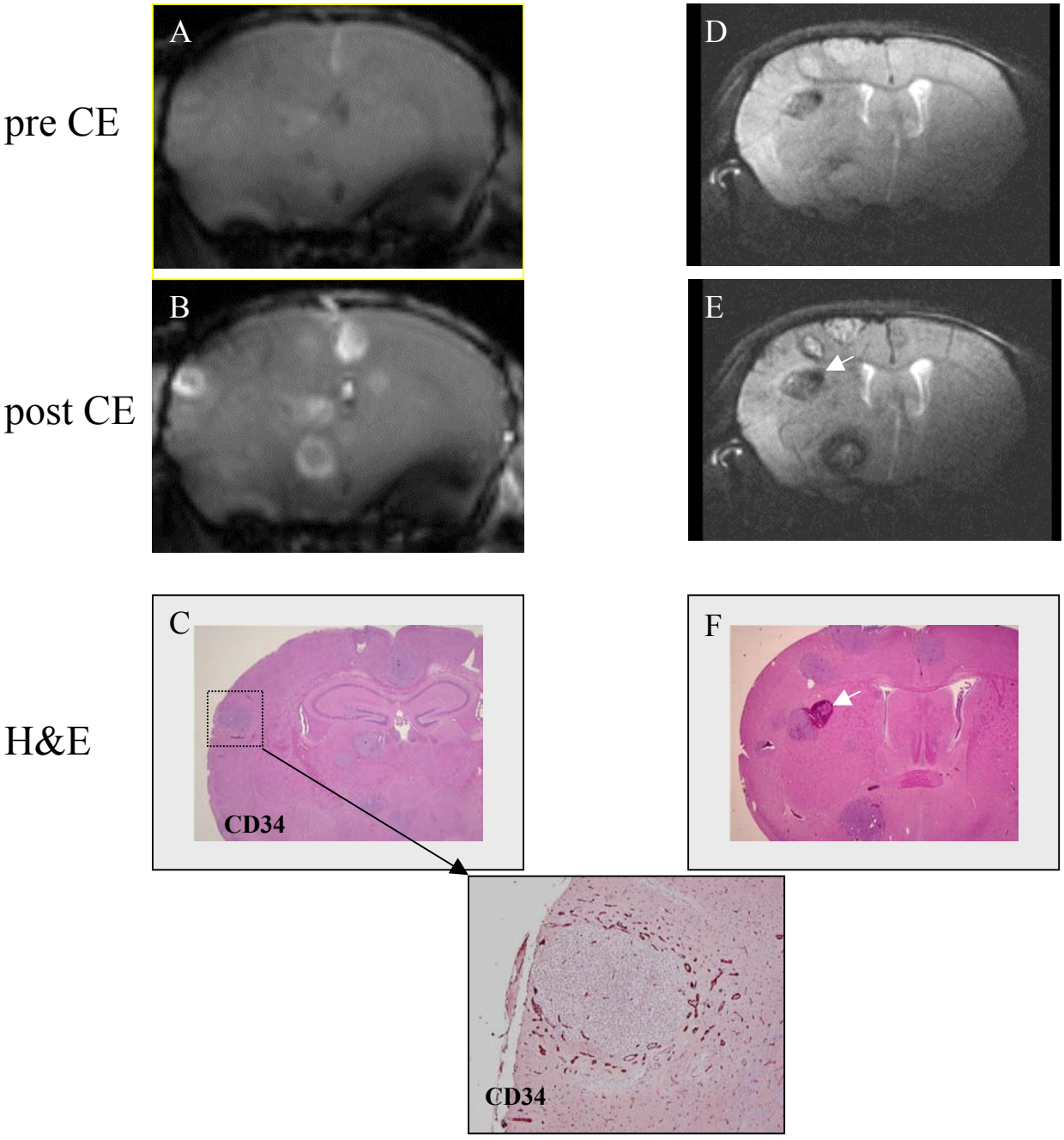

Figure 2, see also page 55

Figure 1, see also page 71

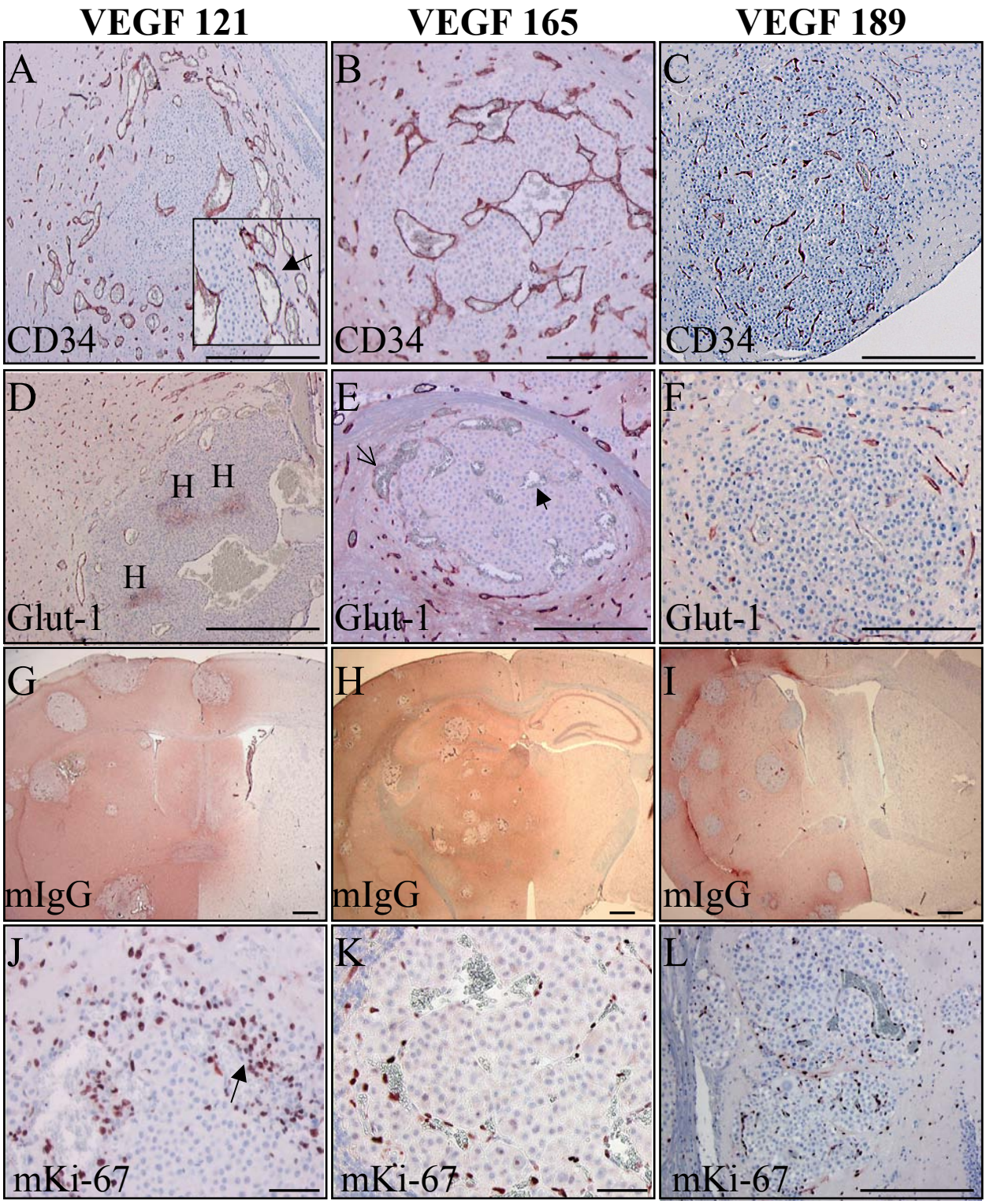

Figure 1, see also page 89

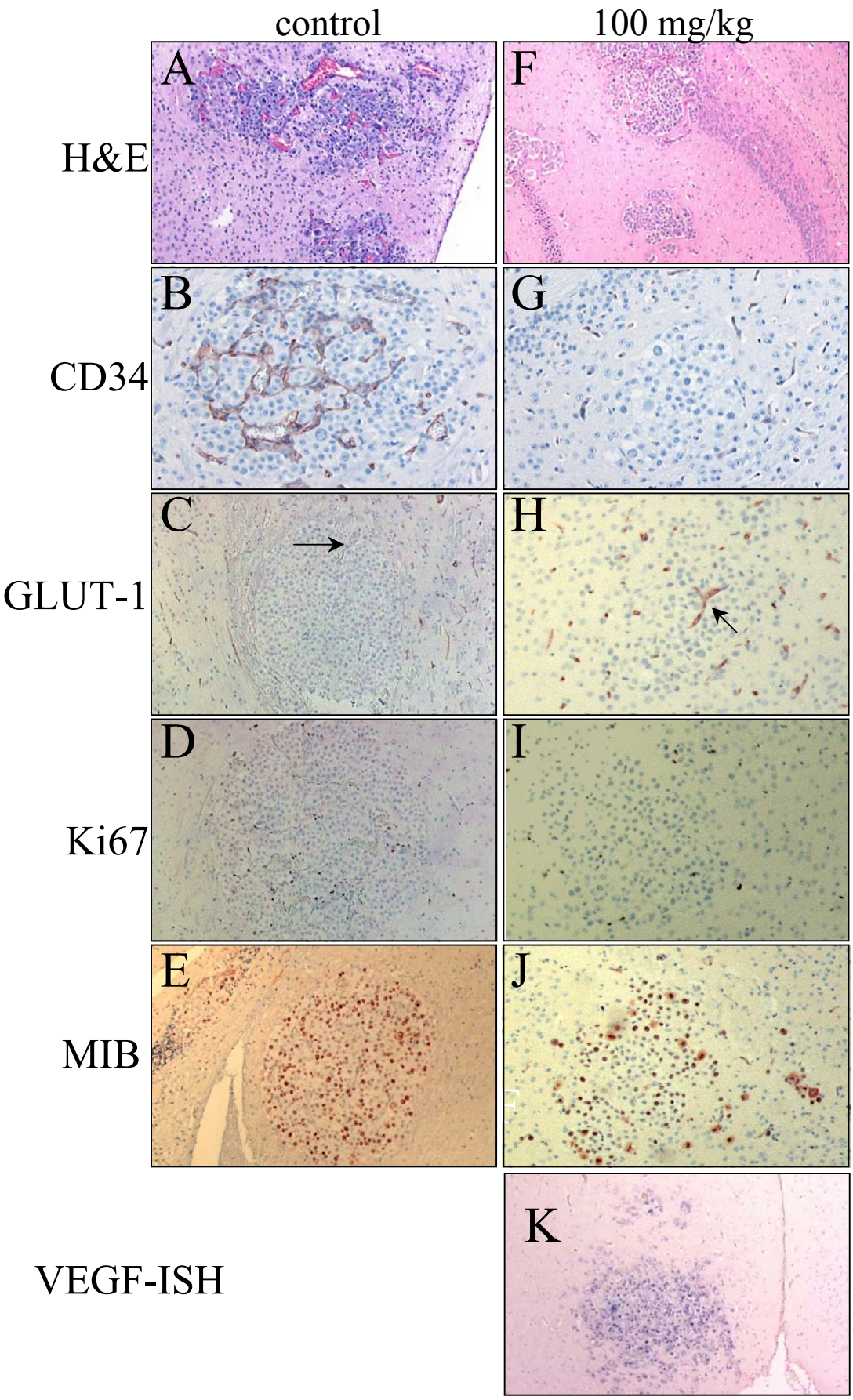

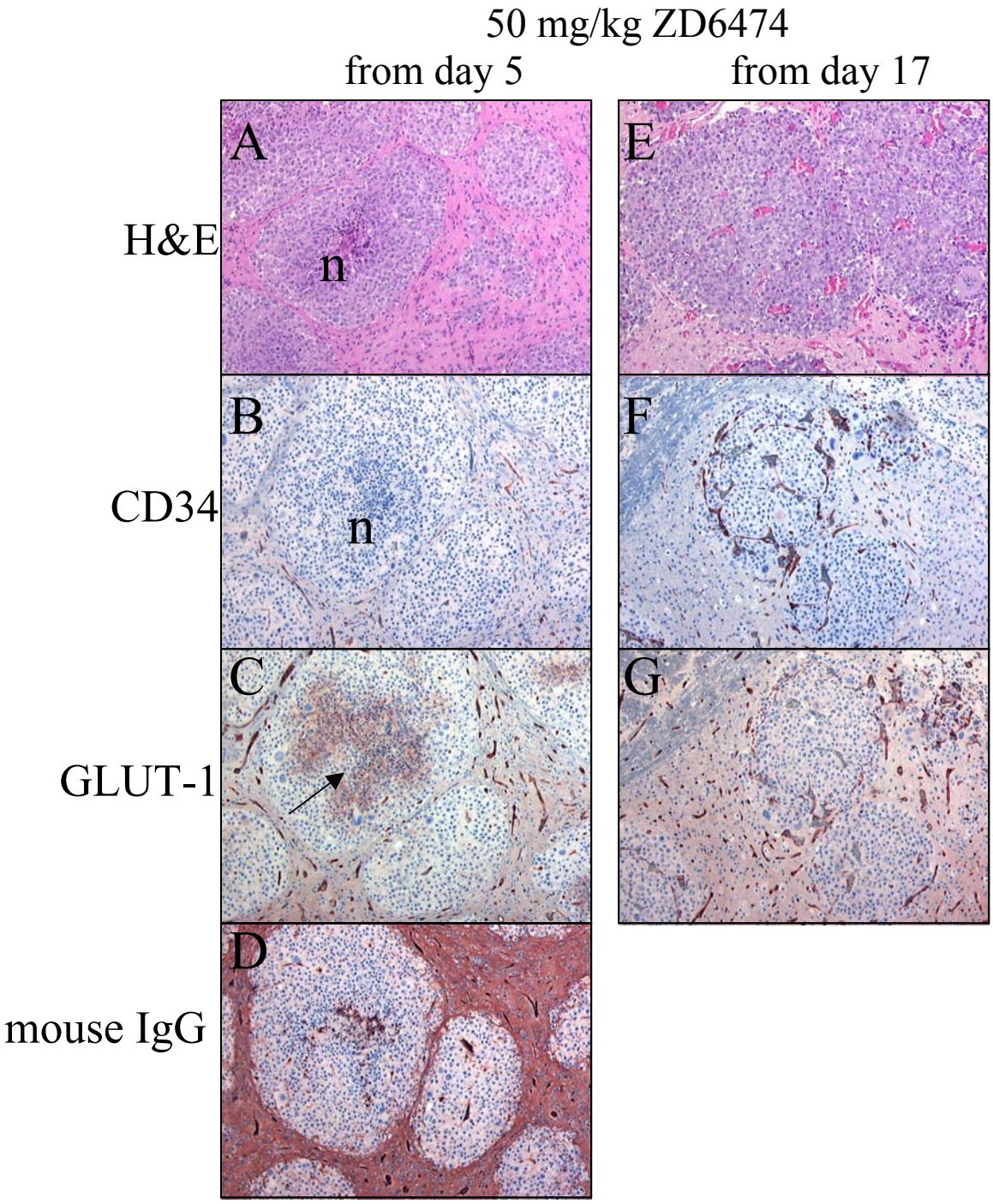

Figure 3, see also page 92

treatment (50 mg/kg) started at

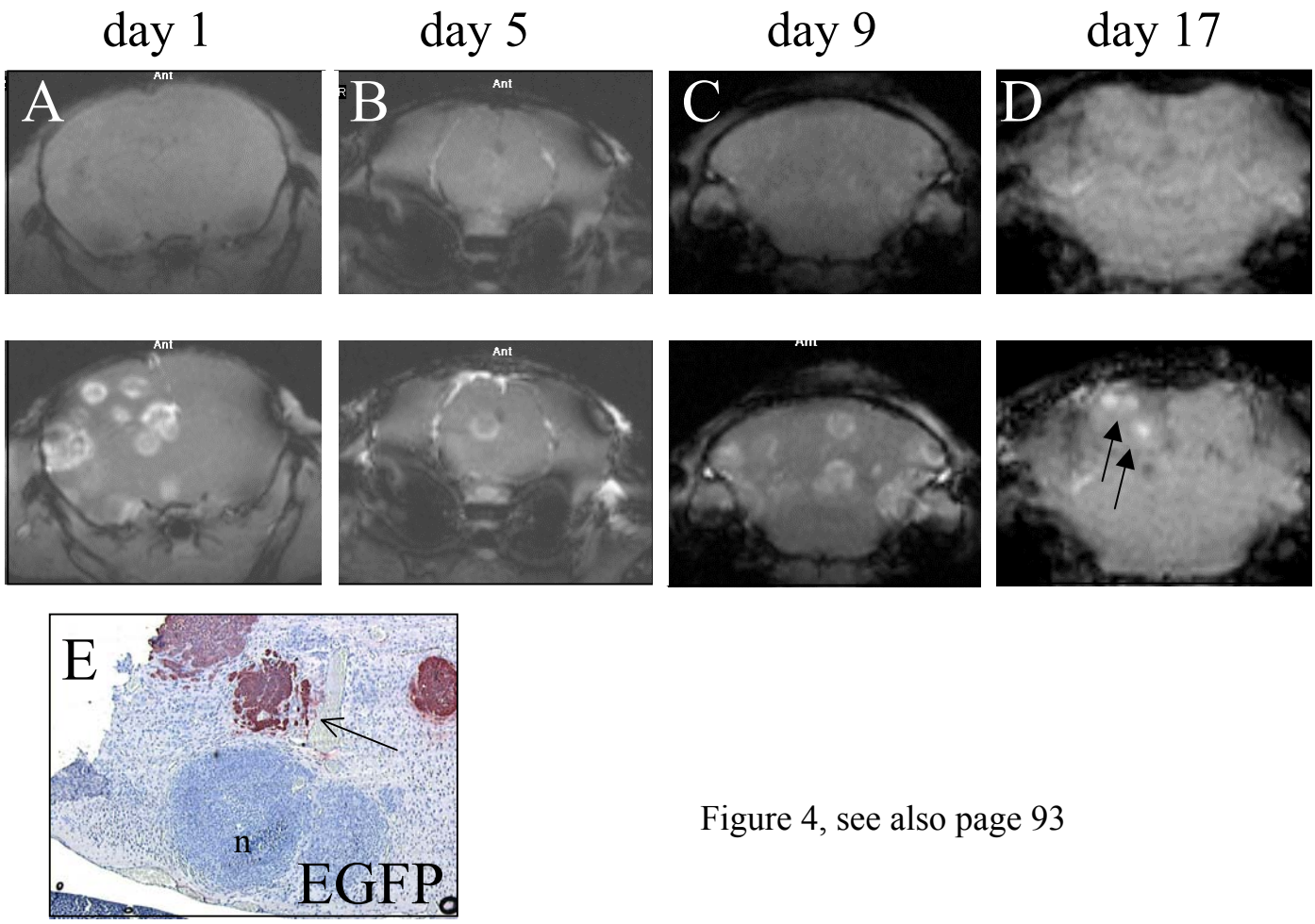

Figure 4, see also page 93

Figure 1, see also page 108

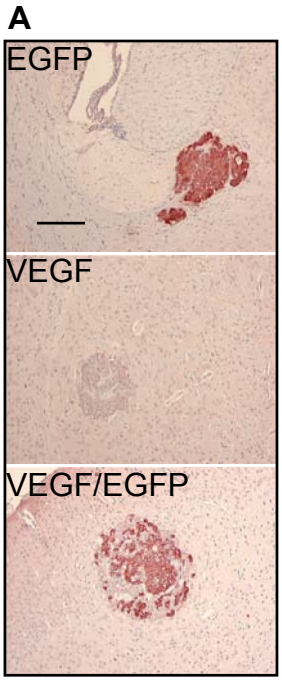

Figure 3, see also page 113

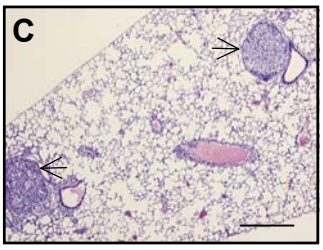

Figure 5, see also page 116

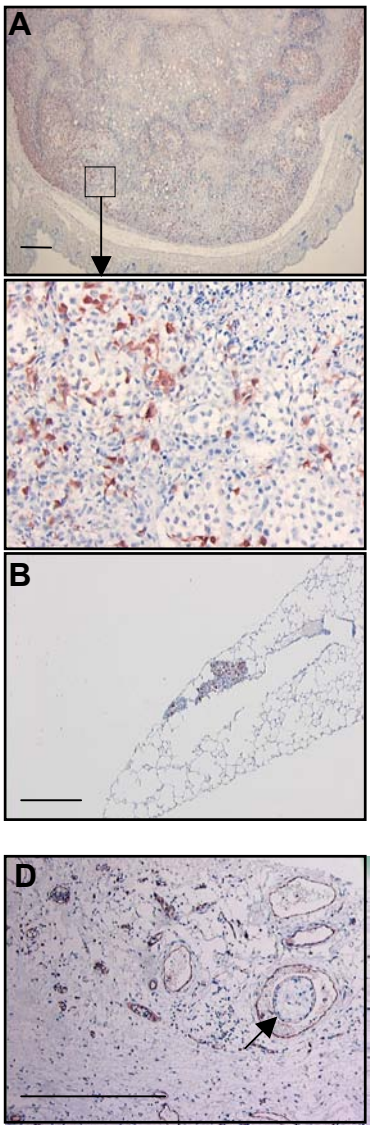

Figure 2, see also page 112

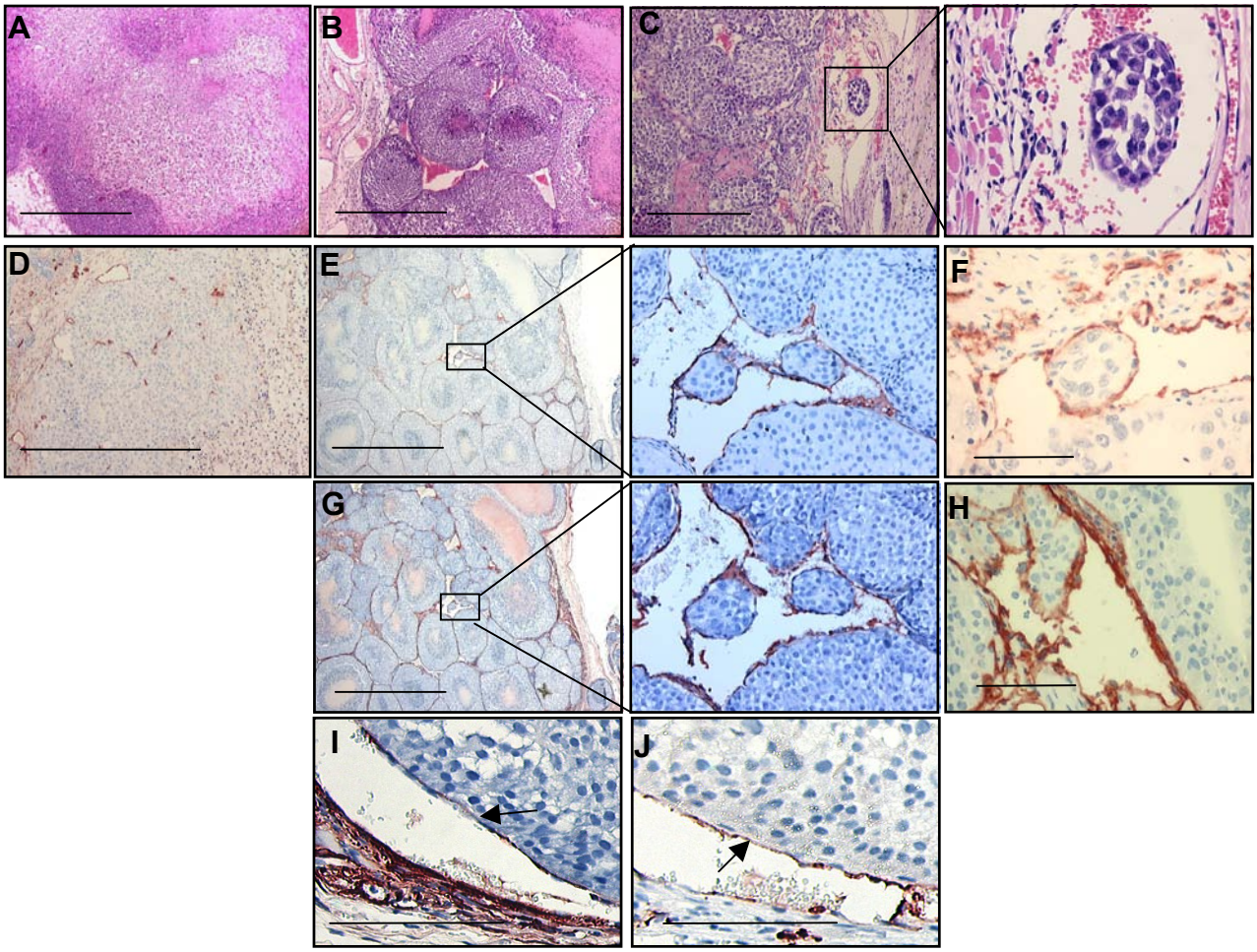

Figure 4, see also page 115